ELECTRON SPIN RESONANCE STUDIES OF MYOGLOBIN AT MILLIMETER WAVELENGTHS

by

E.F. Slade B.Sc.

Being a thesis

submitted to the University of Keele

for the Degree of Doctor of Philosophy

Department of Physics,
University of Keele,
Staffordshire.

May, 1968.

ACKNOWLEDGEMENTS

The author would like to express his thanks to the following:

Professor D.J.E. Ingram for providing laboratory facilities and for his continuous encouragement and supervision of this work.

Dr. D.C. Lainé for his assistance with apparatus in the early part of this work.

Miss K.B. Davies for her care and patience in typing this thesis.

Mrs. E.F. Slade for careful checking and reading the proofs of this thesis.

Dr. R.D. Dowsing for assistance with computation and the loan of his computer programs.

The Technical Staff of the Physics Department and University Workshops for assistance with the fabrication of millimeter components.

Mr. M.W. Johnson for assistance with the photography.

The Royal Society Paul Instrument Fund for financing the development of the millimeter wave spectrometers.

ABSTRACT

The work described in this thesis is concerned with the development of millimeter wave electron spin resonance spectrometers, and the application of such spectrometers to a study of the ferric ion in myoglobin.

Firstly an outline of the basic theory and techniques of electron spin resonance is given, along with a discussion of the theoretical sensitivity of E.S.R. spectrometers. The basic techniques applicable to the design of millimeter wave spectrometers are then reviewed, with particular reference to those which are significantly different to conventional microwave techniques.

A review of the basic theory of the paramagnetic ion in a crystal lattice is given in Chapter III, followed by a discussion of the properties of myoglobin. In these two chapters the basic equations needed for the interpretation of the results obtained are set up.

A detailed description of the 4mm and 2mm spectrometers is given in Chapter VI, together with descriptions of the fabrication of components, and of the superconducting magnet. The sensitivity of the 4mm spectrometer was found to be 2×10^{10} spins per unit linewidth for an integrating time of 1sec. This figure compares favourably with the maximum theoretical sensitivity of 4.3×10^{9} spins.

The final chapter describes measurements at 4mm on acid met myoglobin both in paste and single crystal form. The results are interpreted in terms of an effective Spin Hamiltonian and the parameters of this Hamiltonian have been derived from the experimental results.

CONTENTS

CHAPTER I

INTRODUCTION

The studies reported in this thesis are concerned with the development of millimeter wave electron spin resonance techniques to study further the Ferric ion in acid metmyoglobin. Previous studies have shown that the electron spin resonance spectrum can give detailed structural information on the surroundings of the haem group in the myoglobin molecule, and that a large energy splitting exists between the lowest lying energy levels of the ferric ion. In order to measure this splitting it is necessary to develop techniques for carrying out electron spin resonance measurements at frequencies as high as 70GHz and 140GHz.

1.1 Electron Spin Resonance

When an ion having a resultant angular momentum $\underline{J}$ is placed in an external magnetic field, the energy levels corresponding to the various spatial orientations of the vector J have energies equal to $M_J g\beta H$, where M_J is the electronic magnetic quantum number. Electron spin resonance is the branch of spectroscopy which studies direct transitions between these various levels. The frequency of the radiation involved usually lies in the microwave region of the spectrum and the fields are normally accessible with conventional electromagnets.

The paramagnetic ion is normally under the influence of various internal interactions arising from the lattice in which it resides, and its energy levels will no longer be those of the free ion. A study of the magnetic field dependence and angular dependence of the electron spin resonance spectrum can give considerable information on the immediate surroundings of the ion in question.

There are several instances where the degeneracy of the ground state of the paramagnetic ion is lifted by the action of a crystalline electric field, and in many cases the splitting may be too large to induce transitions between the levels if conventional microwave spectrometers are used. Such a situation occurs for a $^6S_{5/2}$ ground state under the action of a strong axial crystal field, and the ground state is split into three levels, each of which is two fold degenerate. In some cases electron spin resonance spectra may only give information on the lowest of these levels because the splitting is larger than the microwave quantum. In order to obtain information on the magnitude of such splittings it is necessary to increase the frequency of the radiation, and if possible to induce transitions between the various doublets.

This thesis is concerned particularly with the large zero field splittings found for the ferric ion in certain derivatives of myoglobin, and with the construction of high frequency electron spin resonance spectrometers to investigate such large splittings. Previous measurements have indicated that the use of 2 and 4mm radiation would allow a direct measurement of this zero field splitting.

1.2 Haem-Proteins

Electron spin resonance studies of transition metal ions are usually carried out on magnetically dilute materials, where the paramagnetic species is introduced into a diamagnetic host lattice. The haem proteins are large molecules known to contain the transition element, iron, in an octahedral environment. Single crystals can be grown from these proteins but here the magnetic dilution is fixed and the paramagnetic species is not an impurity. At the time of the original electron spin resonance studies on myoglobin and haemoglobin the detailed structure of the proteins was unknown and the early resonance measurements were able to provide structural information on the haem plane orientation which supplemented the X-ray measurements. A detailed determination of the structure of myoglobin is now available, which considerably aids the interpretation of further electron spin resonance results.

The haem-proteins are of considerable interest biologically. Haemoglobin is the pigment responsible for the colour of red blood corpuscles and myoglobin is a constituent of muscle. Both proteins are oxygen carriers and haemoglobin is the material responsible for the transport of oxygen around the body and its exchange for carbon dioxide. The oxygen molecule is carried at the sixth co-ordination point of the haem group and, as yet, no detailed information as to the exact nature of the chemical bond between the oxygen molecule and iron atom is available. A detailed knowledge of the positions of the lowest lying energy levels of the ferric ion is thus of considerable importance as a preliminary to

understanding this important biological function. Unfortunately the oxygenated state is a diamagnetic one and cannot be studied directly by electron spin resonance, but information on the crystal field in other derivatives can be obtained from a study of the high frequency electron spin resonance spectrum. The effects of a variety of reactions with the iron atom can be studied without the effects being obscured by the very much larger diamagnetic part of the molecule.

1.3 Plan of Thesis

An outline of the basic theory and techniques of electron spin resonance is first given and is followed by a discussion of the effects of crystalline electric fields on paramagnetic ions. Particular reference is made to the properties of S state ions in a crystal lattice. In Chapter IV a review is given of the previous electron spin resonance studies of myoglobin since many of the results obtained are relevant to both the spectrometer design and the interpretation of the results obtained. Chapter V contains a review of the techniques available for the production and propagation of the millimeter radiation, and is followed by a description of the millimeter wave spectrometers designed and used for the studies of large zero field splittings in paramagnetic ions. The final chapter contains an account and discussion of the results obtained with the four millimeter spectrometer on acid met myoglobin. This chapter is terminated with a section giving suggestions of how the work might be extended both on met myoglobin and on other derivatives.

CHAPTER II

BASIC THEORY AND TECHNIQUES OF ELECTRON SPIN RESONANCE SPECTROSCOPY

Introduction

This chapter will be concerned with those parts of the basic theory of magnetic resonance which are relevant to the rest of the thesis. A review will also be given of the experimental techniques involved in the detection of electron spin resonance spectra.

An account of the quantum theory of magnetic resonance is given indicating how the resonance condition is derived for an isolated paramagnetic ion. This is followed by a brief mention of the classical theory of magnetic resonance as derived by Bloch. This theory gives considerable insight into the physical processes involved especially with regard to magnetic resonance line shapes and relaxation mechanisms. The studies reported in this thesis are not concerned with line shapes or relaxation mechanisms and so only a brief summary of the classical theory is given.

2.1 The Free Paramagnetic Ion

A classical description of the magnetic resonance phenomenon can be given by considering the vector model of the atom, where the angular momentum is represented by a vector of length $J\hbar$. The associated magnetic moment then precesses about the applied static magnetic field at the Larmor precession frequency. Resonance occurs when the frequency of the applied oscillating field is the same as the precession frequency. Using the classical model the resonance condition can be derived in

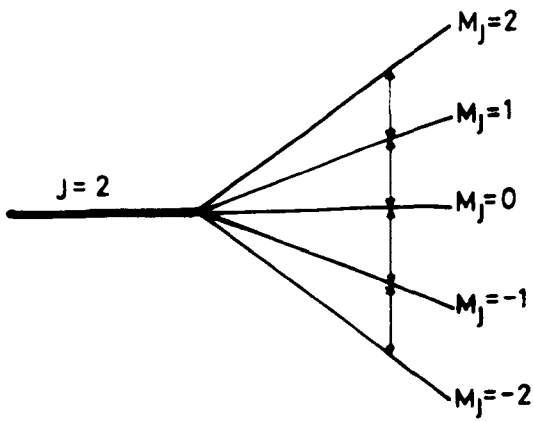

Fig 2·1 SPLITTING OF THE J = 2 LEVEL BY A MAGNETIC FIELD

terms of the Landé splitting factor, g. A detailed account of the classical description of the magnetic resonance phenomenon can be found in the books by Pake (1962) and Slichter (1963).

Quantum Mechanical Treatment

Any ion or atom which possesses a non zero angular momentum $J\hbar$, can be shown to possess a magnetic moment μ. For an ion obeying Russell Saunders coupling this can be shown to be given by:-

$$\underline{\mu} = - g\beta\underline{J} \qquad 2.1$$

where g is the Landé splitting factor and β the Bohr magneton.

In a static magnetic field the interaction of this moment with the magnetic field is given by $-\underline{\mu}.\underline{H}$ and we have a simple Hamiltonian, given by

$$\mathcal{H} = + g\beta\underline{J}.\underline{H} \qquad 2.2$$

Taking the field to be along the z direction we have

$$\mathcal{H} = g\beta J_z\underline{H} \qquad 2.3$$

The eigenvalues of this operator are multiples of the eigenvalues of J_z and the energies are given by

$$E = + g\beta HM_J \qquad 2.4$$

where $M_J = J, J-1, J-2, \ldots -J$

Thus the (2J+1) fold degeneracy of the level in zero field is lifted by the application of the magnetic field $\underline{H}$, and the splitting between the levels is proportional to $\underline{H}$. This interaction, the Zeeman

Effect, is shown in Figure 2.1. In electron spin resonance experiments we are concerned with inducing transitions between the various Zeeman levels by the application of an oscillating magnetic field $h_1 \sin\omega t$ at right angles to H. The energy of this additional interaction is $-\mu_x h_1 \sin\omega t$ where μ_x is the magnetic moment in the x direction.

The Hamiltonian operator for such an interaction is given by

$$' = g\beta h_1 J_x \sin\omega t$$

The probability that such an interaction will cause a transition can be found by using time dependent perturbation theory to compute the matrix elements which link the two states involved. The resulting probability can be shown using standard formulae for magnetic dipole transitions to be:

$$P_{mm'} = g^2\beta^2 h_1^2 |< m'|J_x|m>|^2 \left[\frac{\sin^2\{(\omega_{m'm} - \omega)t/2\}}{(\omega_{m'm} - \omega)}\right] \qquad 2.5$$

where $\omega_{m'm} = \dfrac{E_{m'} - E_m}{\hbar}$

The function in square brackets has a large maximum when $\omega = \omega_{m'm}$, i.e. when $h\nu = E_{m'} - E_m$, ν being the applied frequency $\omega/2\pi$

The matrix element $<m'|J_x|m> = 0$ unless $m' = m \pm 1$.

Thus only transitions between adjacent Zeeman levels are permitted. In Figure 2.1 transitions are allowed as indicated and in the simple case they will all occur at the same frequency.

It should be noted that in the derivation of equation 2.5 only first order perturbation theory is used. Higher order calculations allow other transitions under certain circumstances, particularly for the paramagnetic ion in a crystal lattice.

Combining equations 2.4 and 2.5 leads to the magnetic resonance condition

$$h\nu = E_{m+1} - E_m = g\beta H \qquad 2.6$$

More detailed accounts of the phenomenon of magnetic resonance can be found in the bibliography (see Pake 1962, Slichter 1963).

The magnitude of the Zeeman splittings and hence the g value can be derived quantum mechanically but a better physical insight into the phenomenon of magnetic resonance can be obtained from a classical treatment. The derivation of the g value for an ion in a crystal lattice will be outlined in Chapter III.

2.2 Resonance in an Assembly of Paramagnetic Atoms

In practice magnetic resonance experiments deal with an assembly of paramagnetic centres contained in a solid, liquid or gaseous lattice. The magnetic dipoles will be weakly coupled to the lattice and under the action of a static magnetic field the distribution of electrons amongst the Zeeman levels will be determined by the spin-lattice interaction. Once thermal equilibrium has been attained the populations

of each level will be given by the Boltzmann distribution

$$N_i = N_o e^{-\Delta/kT}$$

where Δ is the splitting between the first and i^{th} levels. The intensity of any absorption will depend on the population difference between the levels concerned.

The behaviour of a bulk assembly of paramagnetic ions has been considered by Bloch (1946) He considers the total magnetisation of the system and defines two relaxation times T_1 and T_2 by which the magnetic system can reach an equilibrium condition.

In order to describe the behaviour of a bulk system under the action of an oscillating magnetic field, Bloch introduces a complex magnetic susceptibility $\chi(\omega)$ given by

$$\chi(\omega) = \chi'(\omega) - j\chi''(\omega) \qquad 2.7$$

The values of χ' and χ'' depend on the values of the oscillating magnetic fields, and on the frequency ω as compared to the relaxation times. Both χ' and χ'' can be shown (Bloch 1946) to undergo a sharp change at the magnetic resonance frequency. From a macroscopic viewpoint magnetic resonance corresponds to a variation in both the real and imaginary parts of the magnetic susceptibility. The imaginary part of $\chi(\omega)$ describes the absorption of energy from the oscillating field on passing through resonance and the real part corresponds to a phase change.
The average rate of energy absorption per unit volume at resonance is given by

$$\overline{P} = \frac{\omega}{2\pi}\int_0^{2\pi/\omega} \underline{H}.\left(\frac{d\underline{M}}{dt}\right)dt = \tfrac{1}{2}\mu_o\omega\chi''h_1^2 \qquad 2.8$$

where $\underline{M}$ is the magnetisation of the bulk material. Substitution in equation 2.8 for χ'' as a function of frequency and the relaxation times T_1 and T_2 gives the characteristic magnetic resonance line shape.

Bloch's classical treatment of an assembly of paramagnetic atoms shows that the two relaxation times play quite distinct roles. The times, T_1 and T_2, are introduced as time constants to describe the exponential return to equilibrium of the longitudinal and transverse components of magnetisation respectively, under the action of the oscillating field. It can be shown that the relaxation time T_1 corresponds to an exchange of energy with the lattice, and determines the degree of saturation. The relaxation time T_2 describes the interaction of the magnetic moment with neighbouring magnetic dipoles and determines the unsaturated linewidth.

2.3 Electron Spin Resonance Linewidths

An assembly of paramagnetic centres obeying the Bloch equations will generally have a characteristic line shape commonly called the "Lorentz" line shape. Such a situation is not usually encountered in paramagnetic solids where the interactions with the surroundings tend to broaden the E.S.R. line. The mechanisms which broaden the line can be divided into two categories:-

(a) Interactions which act by reducing the lifetime in one of the states involved in the transition, thus broadening the line in accordance with the uncertainty principle;

(b) Interactions which produce different local magnetic fields at each paramagnetic centre.

In the absence of any interaction with its surroundings a paramagnetic ion would possess a natural electron spin resonance linewidth determined by the probability of spontaneous emission and the uncertainty principle. In general this probability is so small as to make no contribution to the observed linewidth.

A paramagnetic ion in a crystal lattice will give up its energy to the lattice by way of a mechanism characterised by the spin-lattice relaxation time, T_1. The mechanism responsible for this interaction comes from a fluctuation in the crystalline electric field at the magnetic ion due to the thermal vibrations of the lattice. In a solid, where the paramagnetism is principally due to spin this interaction acts via the spin-orbit coupling. The spin-orbit coupling and hence the relaxation time T_1 varies markedly from sample to sample and in some cases it may be so short as to cause a broadening of the spectral line.

A second broadening process arises because of interactions between neighbouring magnetic dipoles. The dipole moment of each paramagnetic ion will be precessing about its local static magnetic field and will thus produce an oscillating field in the region of its neighbours. If the neighbouring dipoles are identical, this oscillating field may induce

transitions between the two states involved, and thus reduce the lifetime in the excited state. A further broadening of the line will thus be produced, characteristd by the relaxation time T_2. The above two types of broadening are often referred to as homogeneous broadening since any energy is absorbed uniformly by the whole spin system.

The second type of broadening, brought about by local variations in the static magnetic field is often referred to as inhomogeneous broadening. The dipole moment of each paramagnetic ion will produce a static field in the region of its neighbours which will depend on the spatial orientation of the dipoles. This local variation in the magnetic field will produce a slight variation in the resonance condition for each paramagnetic centre and a consequent broadening of the line from the bulk system.

The dipolar broadening can also be caused by interactions between dissimilar magnetic moments, such as those arising from nuclear spins interacting with electronic moments. Such interactions frequently cause a further splitting of the Zeeman levels and the transitions arising within them may produce separate electron spin resonance lines or they may be unresolved (unresolved hyperfine structure).

The magnetic dipole interaction cannot give a complete account of the widths of spectral lines, and Van Vleck (1948) has shown that account must be taken of the exchange interaction between paramagnetic ions. The exchange interaction occurs when there is an overlap between electronic wave functions of neighbouring paramagnetic ions, and its most familiar feature is that it is the interaction which aligns the elementary

magnets within a ferromagnetic or antiferromagnetic domain. It arises because the coulomb interaction between the electrons of two neighbouring ions, leads through the Pauli principle, to an effective interaction between the spins of the two electrons. The effect of the exchange interaction between identical spins is to reduce the electron spin resonance linewidth, whilst the line is broadened when the interaction occurs between dissimilar spins.

Experimental sources of line broadening

An apparent broadening of the electron spin resonance signal will often appear as a result of instabilities in the spectrometer frequency, or more particularly as a result of inhomogeneities in the magnetic field. A further source of broadening often occurs as a result of the field modulation amplitude approaching the linewidth. This point will be discussed further in section 2.4.3.

The detection of an electron spin resonance signal relies on there being a population difference between the two energy levels concerned. If the relaxation time is long compared to the rate at which energy is absorbed, this population difference will be reduced since the spin system will not be able to dissipate its energy to the lattice. In this case an effect known as "saturation" occurs, and the amplitude of the recorded signal falls. The effect is most pronounced at the centre of the absorption curve and a broadening of the line results. Thus if T_1 is comparatively long care must be taken to use low microwave powers.

2.4 Detection of Electron Spin Resonance Signals

As can be seen from the first half of this chapter the basic requirement of any electron spin resonance spectrometer is some means of applying a radio frequency magnetic field to a sample situated in a static magnetic field, such that the two fields are orthogonal. Until recently most spectrometers have operated at frequencies in the X-band region of the spectrum (~10GHz) or the Q-band region (35GHz). The magnetic fields required have usually been obtained from conventional electromagnets. Part of the work described in this thesis is concerned with the construction of electron spin resonance spectrometers for use at higher frequencies up to 140GHz.

The spectrometer must thus have some means of producing the required static magnetic field, some means of generating the required radiation and a method of detecting any resonance absorption which may occur. Specific methods of generating and detecting millimeter radiation will be discussed fully in Chapter V. The resonance can be detected by sweeping either the frequency ν, or the field H, through the resonance condition given in equation 2.6. Since the characteristics of microwave components are usually frequency dependent, it is more convenient to sweep the magnetic field whilst keeping the microwave frequency constant.

The detectors used in the microwave and millimeter wave regions of the spectrum are invariably rather noisy, and the transition probabilities for the magnetic dipole transitions being observed rather low, resulting in a need for very sensitive detection systems.

The need for a sensitive detection system will usually involve some a.c. method. It is more common to amplitude modulate the static magnetic field rather than the radio frequency power, although both methods are feasible. The main reason for this is that the signal observed is directly proportional to the intensity of the radio frequency power, and so if amplitude modulation were to be used the r.f. power level would have to be kept constant to within 10^{-13} Volts R.M.S., which is a typical voltage change from a low intensity electron spin resonance signal. Another consideration affecting the method of modulation is that frequently many detectors used in this region of the spectrum are very sensitive to the power level, and so amplitude modulation of the source would not enable a standing radio frequency bias to be used on the detector.

2.4.1 Basic spectrometer systems

The simplest type of spectrometer would be one in which the paramagnetic sample was placed on one wall of a waveguide passing through a static magnetic field. Power would be fed along the guide from a suitable generator and detected at the other end. The electron spin resonance signal would then appear as a reduction in the power detected as the magnetic field was swept through the resonance condition.

In order to increase the r.f. field intensity at the sample, it is usual to employ some form of resonant structure. The advantage of any such resonant structure is that the standing wave pattern set up within it leads to very large values of h_1, the oscillating magnetic field.

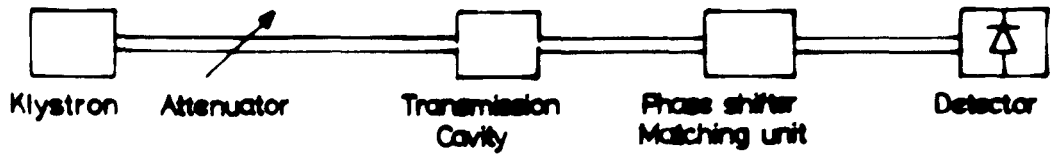

Fig 2·2 TRANSMISSION SPECTROMETER

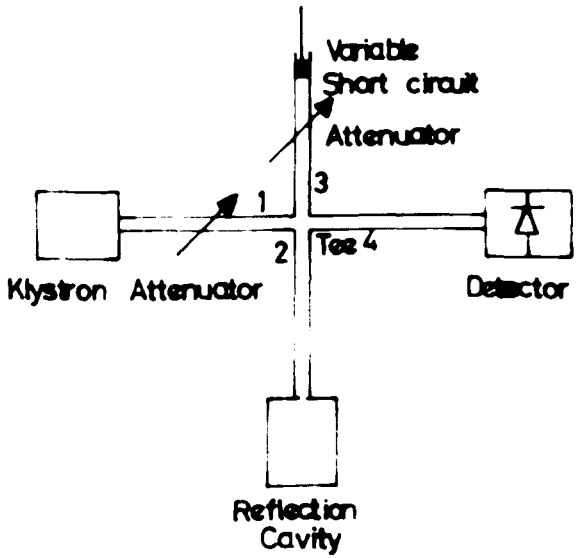

Fig 2·3 REFLECTION SPECTROMETER

In general the signal ultimately observed is increased by the Quality or Q factor of the cavity defined:

$$Q = \frac{\text{(Energy stored at resonance)}}{\text{Energy dissipated per cycle}} \times \omega \qquad 2.9$$

where ω is the resonant frequency.

Typical values of Q for microwave resonators range from 1000 to 20,000. Resonant cavities can be constructed having various modes or standing wave patterns, and the choice of mode depends on the particular application. A detailed account of microwave resonant cavity types and modes can be found in the book by Montgomery (1947), and an account of cavities particularly suited to E.S.R. spectrometers has been given by Ingram (1967) and Poole (1967).

The simplest form of spectrometer, a transmission system, using a resonant cavity, is shown in Figure 2.2. Microwave power is coupled into and out of the cavity via coupling holes or possibly some other conventional coupling technique. The resonance manifests itself as a change in the power transmitted to the detector from the resonator. This type of spectrometer suffers from the disadvantage that it is not possible to vary the microwave power at the sample without varying that at the detector.

A refinement which overcomes this difficulty is shown in Figure 2.3. This type of spectrometer uses a radio frequency bridge and a reflection cavity. Power is fed from the generator to a "magic tee". This component has the property that when arms 2 and 3 are matched and terminated by equal impedances, the input impedance at the first arm is independent of the

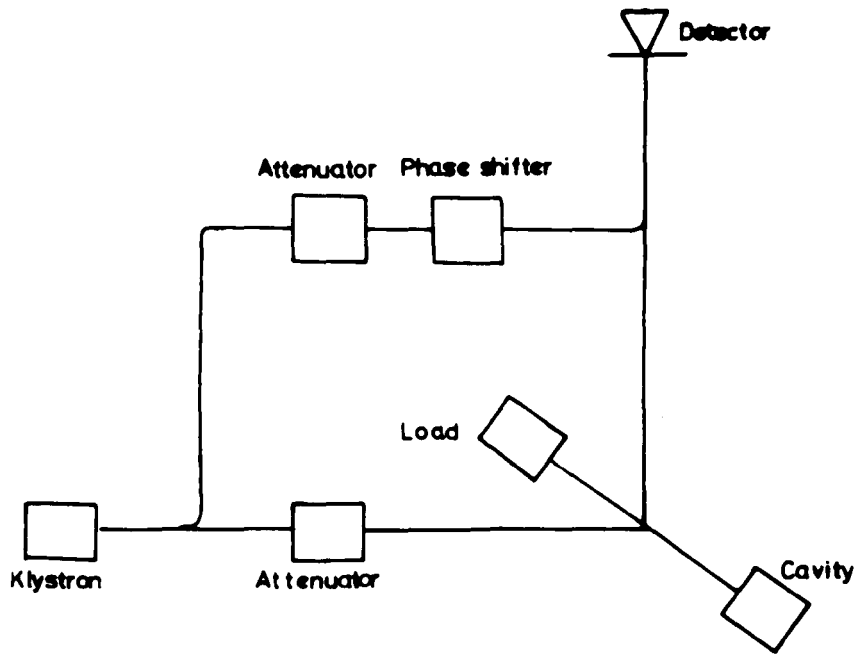

Fig 2·4 SIMPLE SPECTROMETER WITH MICROWAVE BUCKING

output impedance at arm 4. When the Tee is correctly matched power entering at arm 1 is divided equally between arms 2 and 3 and no power enters arm 4. The reflection cavity is placed at arm 2 and a matched load on arm 3. The absorption of power in the cavity now manifests itself as a change in the effective cavity Q factor and causes a mismatch in the bridge. A signal proportional to the degree of mismatching now appears at the detector placed in arm 4. In general the bridge is deliberately mismatched by placing either a slide screw tuner or a short circuit and attenuator in arm 3, to reflect a small amount of power of variable phase and amplitude. This serves both to apply a certain amount of microwave power to the crystal as a bias and to ensure that the signal in arm 4 will be a function of either χ' or χ''. The need for the radio frequency bias on the detector is necessary if a point contact crystal detector is to be used, since the conversion loss and noise output from such crystals are very much dependent on incident power. The noise power increases with incident power whilst the conversion loss decreases, and consequently there occurs an optimum operating point, which in general will be slightly different for every crystal but will usually be around 1mW of bias power.

The principal disadvantage with the bridge system is that it does not permit the spectrometer to be operated at low powers since there would not then be enough power available to bias the detector. This problem has been overcome by the use of microwave bucking techniques where power is coupled from the waveguide run before the bridge and fed separately to bias the crystal as shown in Figure 2.4. A review of the types of microwave circuits available for such spectrometers hasbeen given by Faulkner (1964).

In addition to the range of spectrometers available using microwave bucking, the literature contains many circuits for improving the sensitivity of spectrometers by such techniques as balanced mixing (Vernon 1952) and superheterodyne detection. The balanced mixing technique involves the cancellation of F.M. noise in the power source by mixing the signals from two crystals of opposite polarity. The superheterodyne detection system is a method of reducing the noise output from the crystal by operating at a high intermediate frequency (usually 30MHz). This is done by mixing the microwave signal with a second signal from a separate source whose frequency differs from the experimental frequency by the intermediate frequency. Recently Buckmaster and Dering(1965) have shown that the improvement in crystal noise for intermediate frequencies above 100KHz is negligible. Another advantage of the superheterodyne spectrometer is that it can be operated without magnet field modulation. This has advantages when narrow lines are to be observed, and will be discussed further in section 2.4.3.

2.4.2 Display systems

The simplest method of displaying or recording the signal from an E.S.R. spectrometer is to simply plot the rectified detector current as the field is swept through the resonance condition. In order to improve the sensitivity it is usual to use some form of a.c. method.

(a) Video display

In this method of recording the signal the magnetic field is modulated at some relatively low frequency with an amplitude large compared to the linewidth. The output from the detector is amplified in a wide

bandwidth amplifier and displayed on an oscilloscope. The horizontal deflection is derived from the same source as the modulation and fed to the oscilloscope via a phase shifter. The major disadvantages of this method are that most of the noise generated in the detector is passed by the wide band amplifier and the sensitivity is consequently rather poor.

(b) Phase sensitive detection

For weak signals the video display system is not sufficiently sensitive and some method of extracting the electron spin resonance signal from the noise in the detector output must be employed. The method used to do this is to reduce the bandwidth of the system and employ some method of phase sensitive detection. This method employs a field modulation whose amplitude is small compared to the linewidth, and the detector output then contains a signal whose amplitude is proportional to the differential of the electron spin resonance line, as the magnetic field is slowly swept through the resonance condition. This signal is then mixed with one obtained from the same modulation source via a phase shifting network. A mathematical analysis shows that the output from the mixer contains a d.c. component and a low frequency component whose amplitude is proportional to the amplitude of the detected signal multiplied by the cosine of the phase angle between it and the reference signal. It can readily be seen that this output is proportional to the derivative of the electron spin resonance line. An illuminating account of the operation of mixers or phase sensitive detectors, as they are more usually called, has been given by Wright (1962). It is usual to use some form of low pass filter after

the output of the phase sensitive detector to suppress high frequency noise components. The bandwidth of the display system is thus determined only by the bandwidth of the phase sensitive detector and filter, and noise outside this bandwidth will not be passed.

This point can be illustrated by considering a magnetic field $H_0 + h_1 \sin\omega t$ applied to the line shape function g(H) such that

$$g(H) = g(H_0 + h_1 \sin\omega t)$$

If this series is expanded as a Taylor series we obtain

$$g(H) = g(H_0) + g'(H_0)h_1 \cos\omega t + \tfrac{1}{2}g''(H_0)h_1^2 \cos^2\omega t + ... \qquad 2.10$$

provided h_1 is small compared to H_0.

The a.c. component is thus proportional to the derivative of the absorption curve, and can be detected by the method described above. In order to maintain an accurate representation of the resonance line shape equation 2.10 shows that the modulation amplitude must be small compared to H_0. An increase in modulation amplitude produces a broadening of the resonance line as has been discussed by Smith (1964), who shows also that the signal intensity at first increases as the modulation amplitude approaches the linewidth and then decreases as it is further increased.

2.4.3 Choice of modulation frequency

The most important consideration in choosing the optimum modulation frequency is of the noise spectrum of the detecting element. The most common detecting element in microwave spectroscopy is the crystal rectifier.

In such rectifiers the major contribution to the output noise is Flicker noise, i.e. noise due to fluctuations in the effectiveness of the potential barrier. The power spectrum of flicker noise is found to be given by an equation of the form

$$P(f) = K/f$$

where f is the intermediate frequency. From this point of view it is essential to use as high a modulation frequency as possible for maximum sensitivity. As the intermediate frequency is increased above 100KHz the flicker contribution to the crystal noise power will become negligible in comparison to the other noise contributions, such as Shot noise, which are independent of frequency.

It is important also to use a modulation frequency f which is much smaller than the linewidth ΔH expressed in unit of frequency Δf, i.e.

$$f << \Delta f = (g\beta/h)\Delta H$$

For a typical electron spin resonance signal from a free radical having a g factor of 2, the linewidth corresponding to a modulation frequency of 100KHz will be approximately 3×10^{-6} Teslas (30mGauss). For extremely narrow lines (less than 10^{-5} Teslas) it is preferable to use a superheterodyne detection system without field modulation, or to use low frequency modulation.

In many cases the limitation on the modulation frequency is set by experimental considerations rather than theoretical ones. For instance the metallic skin depth given by

$$\delta = (\mu\mu_o\pi\sigma f)^{-\frac{1}{2}} \qquad 2.11$$

where σ is the conductivity of the metal, will obviously prevent the penetration of high frequency fields into the cavity. The problem will be further aggravated at low temperatures where the electrical conductivity increases, reducing δ still further.

In order to detect very broad magnetic resonance lines one requires a much larger amplitude of modulation than for narrow lines. The lines observed for instance from the ferric ion in myoglobin tend to vary in width from 1.5×10^{-2} Teslas (150 gauss) to 8×10^{-2} Teslas (800 gauss) at Q-band and can be expected to increase still further at 4 and 2mm wavelengths. To produce large amplitudes of modulation at 100KHz would require extremely high power amplifiers and the largest amplitude that can realistically be obtained is of the order of 2×10^{-3} Teslas at 100KHz. For this reason it is often more practicable to make use of low frequency modulation, where the loss of signal to noise ratio is offset by the possibility of using large modulation amplitudes.

2.4.4. Sensitivity

The sensitivity of electron spin resonance spectrometers is usually specified as either the minimum detectable r.f. susceptibility, or the minimum detectable number of free spins for a given line width. The case of a spectrometer using a sample cavity and a straight waveguide system will be considered separately.

(a) Spectrometer using resonant cavity

The power absorbed per unit volume when resonance takes place is given by equation 2.8 as

$$\overline{P} = \tfrac{1}{2}\mu_o \omega \chi'' h_1^2$$

Substitution in equation 2.9 gives the decrease in Q factor of the cavity Q_o due to the resonant absorption of power as:

$$\Delta Q = Q_o^2 \eta \chi''$$

where η is the filling factor given by

$$\eta = \frac{\int_{\text{Sample}} h_1^2 \, dV}{\int_{\text{Cavity}} h_1^2 \, dV}$$

This change ΔQ can be represented as a change in the equivalent resistance of the cavity, and Feher (1957) has shown that a resistive change corresponding to this change ΔQ produces a voltage change at a linear detector used with a reflection cavity given by

$$\Delta E = \tfrac{1}{2}\chi'' \eta Q_o E$$

where E is the incident voltage, related to the incident power by

$$P_1 = E^2/4R_o$$

where R_o is the characteristic impedance of the guide. The minimum detectable signal is defined by equating this change ΔE to the R.M.S.

Johnson noise voltage across an impedance at temperature T matched to the waveguide so that:

$$\Delta E = \sqrt{2kTR_o\Delta f} = \tfrac{1}{2}\chi''\eta Q_o E$$

$$\therefore \quad \chi'' = \frac{1}{\eta Q_o}\left(\frac{2kT\Delta f}{P_1}\right)^{\frac{1}{2}} \qquad 2.12$$

This equation is the ideal theoretical case for the minimum detectable susceptibility and assumes an ideal detector. In practice the noise in the output will include noise from the microwave source, flicker noise from the crystal and noise contributed by the first stages of amplification. This can be accommodated in the equation 2.12 by including noise figures F_k for the source, F_a for amplifier and a noise temperature t and insertion loss L for the crystal detector so that:

$$\chi''_{min} = \frac{1}{\eta Q}\left\{F_k - 1 + (t+f_a-1)L\,\frac{2kT\Delta f}{P_1}\right\}^{\frac{1}{2}}$$

For a paramagnetic system obeying the Bloch equations and the Curie Law, it can be shown (Poole 1967) that the minimum detectable number of spins is given by

$$N_{min} = \frac{6V_s kT_s}{Q_o \eta g^2\beta^2 S(S+1)}\left(\frac{\Delta H}{H_o}\right)\left\{(F_k - 1 + (t+F_a-1)L\,\frac{kT\Delta f}{P_1}\right\}^{\frac{1}{2}}$$

where S is the spin quantum number and T_s the sample temperature.

(b) Shorted waveguide sample holder

If the sample is placed in a piece of short circuited waveguide the signal detected will be related directly to the power ΔP absorbed by the sample. This change in power ΔP seen by the detector is related to the R.M.S. voltage change ΔV on the detector by

$$\Delta P = \frac{(\Delta V)V}{R_o}$$

where V is the voltage incident on the detector in the absence of resonance. Defining the minimum detectable signal as that signal equal to the Johnson noise voltage developed across the detector, we obtain for the noise voltage

$$V_{RMS} = \sqrt{2R_o kT\Delta f} = \Delta V$$

Substituting for ΔP from equation 2.8 and integrating over the sample volume we obtain

$$\frac{\frac{1}{2}\chi'' \mu_o \omega R_o}{V} \int h_1^2 dV = \sqrt{2R_o kT\Delta f}$$

$$\therefore \quad \chi'' = \frac{2}{\xi \mu_o \omega} \sqrt{\frac{2kT\Delta f}{P_1}} \qquad 2.13$$

where $\xi = \frac{\int h_1^2 dV}{P_1}$ and is analogous to the filling factor η.

As in section (a) one can now include the effect of the noise contributed by the generator crystal and amplifier and also determine the minimum detectable number of free spins.

In general η will be smaller than ξ and this will partially offset the loss of sensitivity due to the absence of the cavity and explain the figures obtained in practice to be discussed in Chapter VI.

Note on Units

Until recent years it has been the custom of practising physicists to use the c.g.s. system of electrical and magnetic units. Magnetic fields have consequently been measured in "gauss", even though this is strictly the unit of magnetic induction. It is now becoming the custom for physicists to teach physics and to use the M.K.S. system of units, and the use of this system is slowly beginning to spread through the literature. The M.K.S. system will be used throughout this thesis, but to avoid confusion the unit of magnetic field will now be the "Tesla" or "Weber per square meter" which is the direct analogue of the gauss. In general all fields will be given in both units, but a simple conversion can be obtained from the identity:-

$$10^4 \text{ gauss} = 1 \text{ Tesla}$$

REFERENCES

Bloch, F., Phys. Rev. 70 460, 1946.

Buckmaster, H.A. and Dering, J.C., Canadian J. Phys. 43 1088, 1965.

Faulkner, E.A., Laboratory Practice Nov. 1065, 1964.

Feher, G.L., Bell System Tech. Journal, March 1957.

Ingram, D.J.E., 'Spectroscopy at Radio and Microwave Frequencies', Butterworths, 1967.

Montgomery, C.G., 'Technique of Microwave Measurement', McGraw-Hill, 1947.

Pake, G.E., 'Paramagnetic Resonance', Benjamin, 1962.

Poole, C.P., 'Electron Spin Resonance', Interscience, 1967.

Slichter, C.P., 'Principles of Magnetic Resonance', Harper, 1963.

Smith, G.W., J. App. Phys. 35 No. 4 1217, 1964.

Van Vleck, Phys. Rev. 74 1168, 1948.

Vernon, F.L., IRE Trans. AP-14 110, 1952.

Wright, M.J., Electronic Engineering 34 698, 1962.

CHAPTER III

THE PARAMAGNETIC ION IN A CRYSTALLINE SOLID

3.1 Introduction

In the theory outlined in Chapter II it was implicitly assumed that the system to be studied contains some permanent magnetic dipole moments. Many free ions do contain unpaired electrons and a resultant angular momentum, but when they combine to form molecules the electrons tend to pair such that the total angular momentum is zero. For instance, the structure of NaCl is ionic, but the transfer of an electron from each Na atom to each Cl atom assures an inert gas configuration for the electrons of each ion. The requirement of a resultant angular momentum restricts the occurrence of paramagnetism in solids, with a few exceptions, to ions of the transition groups, which have partially filled inner shells.

A detailed theoretical account of the transition metal ion in a crystal lattice would involve a solution of the Schroedinger equation for the whole crystal, which is not yet possible. The problem can be simplified somewhat by considering the electronic orbitals of the molecule, although this necessarily involves certain approximations. A second approach which is somewhat simpler to understand, but which involves even more approximations, is that of the Crystal Field Theory. This theory assumes that the paramagnetic ion resides in a crystalline electric potential produced by point charges (ions) or point dipoles (e.g. H_2O molecules). This interaction with the crystal field is added to

the free ion Hamiltonian to deduce a new set of energy levels for the paramagnetic ion. A more general theory, ligand field theory, considers the central ion to be subjected to a potential, not necessarily electrostatic in origin, from the electrons of the surrounding atoms - the attached ligands. The term 'ligand field theory' has been employed to cover all forms of interaction between a central ion and its neighbours and involves crystal field theory as a special case.

The simpler crystal field theory is adequate to explain many of the results of paramagnetic resonance phenomena and an outline of the basic ideas involved will be given in this chapter. It is therefore useful to commence with a discussion of the Hamiltonian of the free ion.

3.2 General Hamiltonian of the Free Ion

The Hamiltonian for a free ion in the absence of a magnetic field can be represented in a simplified form by

$$\mathcal{H} = \mathcal{H}_c + \sum_{jk} \left(a_{jk} \underline{l}_j \cdot \underline{s}_k + b_{jk} \underline{l}_j \cdot \underline{l}_k + c_{jk} \underline{s}_j \cdot \underline{s}_k \right) + \mathcal{H}_N$$

where $\mathcal{H}_c$, the dominant term in the Hamiltonian is the coulomb interaction between the electrons and the nucleus, and the coulomb repulsion between the various electrons. This term leads to the various Energy levels or Term values of the free ion. The second term, in which a_{jk}, b_{jk} and c_{jk} are constants, represents the magnetic interaction between the electron spins $\underline{s}_k$ and the orbital momentum $\underline{l}_k$ and is the interaction responsible for the splitting of the free ion "Terms" into multiplets. In the more common case of Russell Saunders coupling this term can be reduced to an interaction

of the form $\lambda \underline{L}.\underline{S}$ where $\underline{L}$ and $\underline{S}$ represent the total angular and spin momenta of the ion. The final term H_N represents the interaction of the electrons with the nuclear magnetic and quadrupole moments. The details of the theoretical treatment of the free ion are well understood and further details of its formulation are available in standard texts (e.g. Condon and Shortley 1935). The details of the spin-spin and spin-orbit interactions have been considered by Pryce (1950).

3.3 The Paramagnetic Ion in a Static Crystalline Field

The effect of the ligand atoms surrounding the paramagnetic ion is to set up a static electric field at the central ion, which can be considered as an additional interaction, V_c, on the free ion Hamiltonian. The crystalline electric fields observed in practice can be divided into three groups: (a) strong fields, such that V_c is of the same order as the energy of the coulomb interaction between electrons (i.e. $\sim 10^4 cm^{-1}$), (b) medium fields, where the crystal field interaction is less than the electrostatic interaction but is usually greater than the spin orbit interaction, and (c) weak fields where V_c is less than the spin orbit interaction. The strong field case usually corresponds to a high degree of chemical bonding between the paramagnetic ion and the ligand ions and can give a reasonable account of covalent bonding in some cases. A typical example of such a field occurs in the azide derivative of myoglobin to be discussed later. The medium field case occurs in many of the iron group complexes and is the mechanism responsible for the reduction or "quenching" of orbital momentum. In situations where the crystalline field can be

termed "weak" the magnetic electrons usually lie deep within the ion and are well screened from the crystal field; a situation typified by ionic compounds of the actinide and rare earth transition groups.

If the surrounding charges do not overlap the central ion the potential V_c will obey Laplace's equation, so that

$$\nabla^2 V_c = 0$$

The solutions of Laplace's equation can be expanded as a set of generalised Legendre Polynomials, and so following Bleaney and Stevens (1953)

$$V_c = \sum_n \sum_{m=n}^{-n} \sum_k A_n^m r^n Y_n^m (\theta_k \phi_k) \qquad 3.1$$

and

$$Y_m^n(\theta\phi) = (-1)^n \left[\frac{1}{4\pi} \frac{(2n+1)(n-|m|)!}{(n+|m|!)}\right]^{\frac{1}{2}} P_n^m \mathrm{Cos}\theta e^{im\phi}$$

where the summation k is over all electrons. The symmetry of the site invariably reduces the number of terms in the expansion of equation 3.1. For instance the solution for a six fold cubic co-ordination can be expressed as

$$V_c = D_4 \left[\tfrac{7}{2} Y_4^0 + \tfrac{1}{4}(70)^{\frac{1}{2}}(Y_4^4 + Y_4^{-4})\right] + D_6 \left[\tfrac{3}{4} Y_6^0 - \tfrac{3}{8}(14)^{\frac{1}{2}}(Y_6^4 + Y_6^{-4})\right] \qquad 3.2$$

The potential can also be expressed in cartesian co-ordinates, so that equation 3.2 becomes

$$V_c = C_4(x^4 + y^4 + z^4 - \tfrac{3}{5}r^4) + D_6\left[(x^6 + y^6 + z^6) + 15\tfrac{1}{4}(x^4y^2 + x^2y^4 + x^2z^4 + x^4z^2 + y^2z^4 + y^4z^2) - 15\tfrac{1}{14}r^6\right]$$

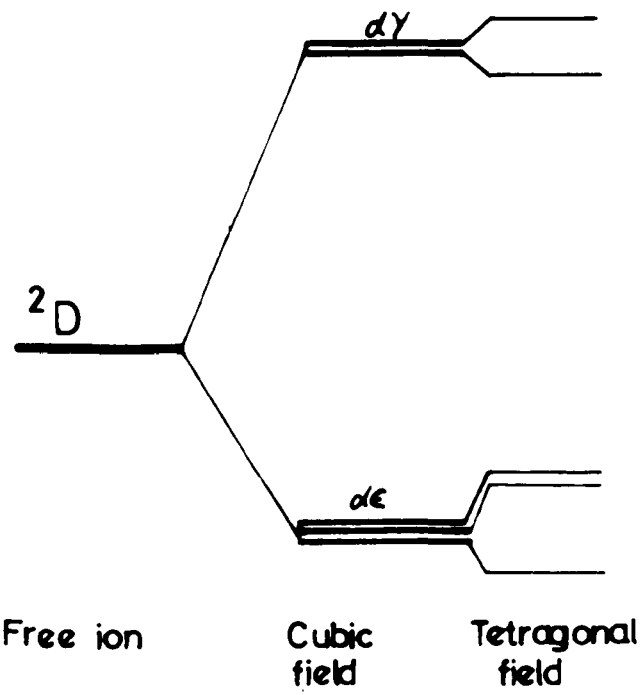

Fig 3·1 Splitting of the ^{2}D term by a tetragonally distorted cubic field

The majority of the potentials commonly found in paramagnetic crystals have been tabulated by Low (1960), who also gives a detailed account of the treatment outlined here.

The method employed to calculate the energy levels of the paramagnetic ion is to apply the potential V_c as a perturbation on the free ion Hamiltonian. It would be applied before or after the spin-orbit coupling and electrostatic interaction terms depending on the magnitude of the crystal field. The calculation of the matrix elements required for the perturbation calculation is considerably simplified by the use of the operator-equivalent method of Stevens (1952). This method makes use of the fact that the matrix elements formed with operators such as x, y and z are proportional to the matrix elements of the angular momentum operators J_x, J_y and J_z for a particular J manifold. The operator equivalents for the various crystal field potentials have been tabulated by Stevens (1952) and Low (1960).

An illustrative example is shown in Figure 3.1 where the splittings of the ^2D Term of a $3d^1$ configuration by medium crystal fields of cubic, and tetragonally distorted cubic, symmetry are shown. The orbitals appropriate to an ion in a cubic field are selected from a linear combination of the free ion d orbitals, such that the new orbitals reflect the lower symmetry of the ion within the crystal lattice. The application of a cubic potential as a perturbation on the free ion energy states now splits the ^2D term into a two fold ($d\gamma$ or e_g) and a three fold ($d\varepsilon$ or t_{2g}) orbitally degenerate level. The application of a

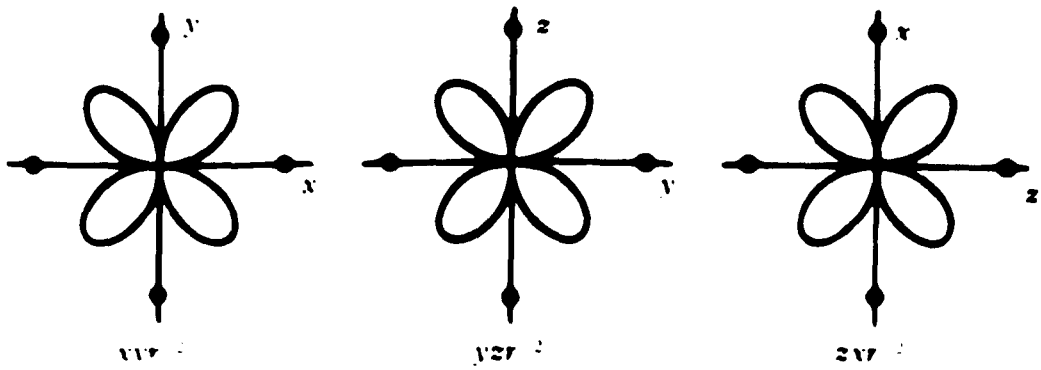

$d\epsilon$

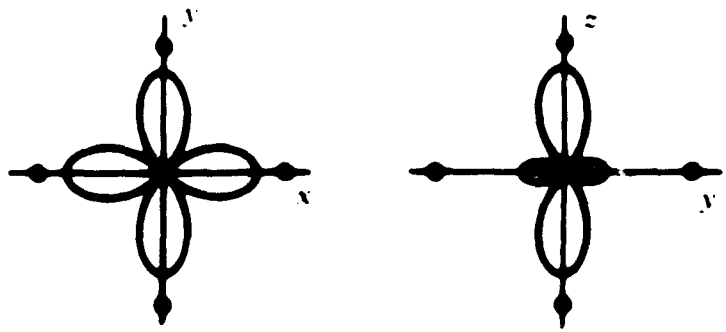

$d\gamma$

Fig 3·2 d electron orbitals (after Pake)

tetragonal distortion to this field can be shown to lift the degeneracy of these levels further. The effect of spin-orbit coupling can now be applied as a further perturbation $\lambda \underline{L}.\underline{S}$ on these levels since this is a medium field case.

A more powerful tool for deducing the energy level scheme of the ion in the crystal lattice is to apply group theoretical methods, and it is from the ideas of group theory that the notation $d\gamma$, $d\varepsilon$, t_{2g} and e_g have been derived.

The physical principles involved in the splitting of the d orbitals are more clearly illustrated in Figure 3.2. The d orbitals appropriate to cubic symmetry are shown in the conventional manner, and the positions of the ligand atoms are shown along the co-ordinate axes. It is evident from the diagram that the $d\varepsilon$ orbitals (xy yz zx) will all have the same interaction energy with the ligand ions, and that this interaction will be less than the interaction by the $d\gamma\left[(x^2-y^2),(3z^2-r^2)\right]$ orbitals. It can also be seen that a distortion along the z axis will reduce the degeneracy still further.

Orbital Quenching

An important result of the theory outlined above is that in the strong and medium octahedral fields the expectation value of the orbital angular momentum operator L_z is never greater than one. The implication of this is that the d electron in an octahedral electric field never exhibits its full orbital angular momentum, which is to say that the orbital momentum is quenched.

Once again it is useful to turn to a classical picture to visualise the physical processes involved in "quenching". In many instances the crystal field is sufficiently large to break down the coupling between the $\underline{L}$ and $\underline{S}$ vectors. The $\underline{L}$ vector then has a large interaction with the electric field and precesses about it with the usual (2L+1) allowed orientations. In general the separation in energy between these orientations will be larger than kT at room temperature and so only the lowest level will be populated. The spin vector $\underline{S}$ does not interact with the electric field directly so each level corresponding to an orientation of $\underline{L}$ will be (2S+1)-fold degenerate.

In practice the spin-orbit coupling is not completely broken so the $\underline{S}$ vector can sometimes interact with the crystal field via the spin-orbit coupling. In this way the degeneracy of the spin system may be partially removed. When the number of unpaired electrons is odd, it has been shown by Kramer that the electric field cannot reduce the degeneracy of a level below two.

3.4 Kramer's Theorem

Kramer's theorem states that there will always be a two-fold degenerate level in the presence of electric fields having any kind of symmetry, provided that there are an odd number of electrons present. In the absence of an external magnetic field the Hamiltonian is invariant under time reversal since it contains only quadratic terms of momentum. Application of the time reversal operator to the eigenstates of an n electron system gives degenerate states when n is odd.

If an external magnetic field is applied the Hamiltonian is not invariant under time reversal since it contains linear terms of the form $\underline{H}.\underline{S}$. This means that the Kramer's degeneracy is lifted by the application of a magnetic field.

In a system containing an odd number of electrons (i.e. F^{3+}, Mn^{2+}, Mn^{4+}, Ti^{3+}) it will thus always be possible to induce a magnetic resonance transition between one pair of Kramer's doublets.

3.5 The Spin Hamiltonian

The energy levels of the paramagnetic ion in a crystal lattice can be derived using the free ion Hamiltonian plus the additional interaction V_c due to the crystal field. The interaction with an external magnetic field can be considered by including in the Hamiltonian a term $\beta(\underline{L}+g_e\underline{S})$ where $g_e = 2.0023$ (the anomalous g factor of the electron) and neglecting terms giving rise to diamagnetism. The ground state can be derived by using the coulomb and crystal field interactions and then treating the spin-orbit, spin-spin and magnetic interactions as a perturbation on these levels. These perturbations can be shown using operator equivalents (Low 1960) to reduce to a Hamiltonian:-

$$\mathcal{H} = (\lambda-\tfrac{1}{2}\rho)(\underline{L}.\underline{S}) - \rho(\underline{L}.\underline{S})^2 + \beta\underline{H}.(\underline{L}+2\underline{S})$$

It has been shown (Abragam and Price 1951) that a Hamiltonian of this form can be expressed in terms of spin operators only and the energy levels are eigenstates of this operator. The Hamiltonian operator so derived is called the "Spin Hamiltonian".

The general form of the Spin Hamiltonian for a paramagnetic ion in an axial crystal field with a Rhombic distortion is

$$\mathcal{H} = \beta(g_z H_z S_z + g_x H_x S_x + g_y H_y S_y) + D\{S_z^2 - \tfrac{1}{3}(S+1)S\}$$
$$+ E(S_x^2 - S_y^2) + \text{Terms involving nuclear spin operators.}$$

The first term represents the splitting of the energy levels in an external magnetic field where the effective g factor may be anisotropic. The term $D\{S_z^2 - \frac{1}{3}S(S+1)\}$ represents the splitting of the ground state in the absence of an external field by the axial component of the crystal field. The term $E(S_x^2 - S_y^2)$ represents any splitting by crystal field components of lower symmetry. These two terms describe what are called the "Zero Field Splittings".

The Spin Hamiltonian enables the ground states of a paramagnetic ion, between which magnetic resonance transitions occur, to be described in terms of a relatively small number of parameters. The General Hamiltonian would describe the levels in terms of complex wave functions containing mixtures of various orbital and spin wave functions of the free ion. The spin Hamiltonian treats only the lowest lying levels and describes them in terms of a fictitious spin S', for which the magnetic dipole has $2S' + 1$ orientations in a magnetic field. The effective magnetic moment is now given by $g_{eff}\beta S_z'$ where g_{eff} will in general be different from the Landé g factor of the free ion.

If the external field H has direction cosines l, m, n with respect to a set of axes x, y, z the g value is given by

$$g^2 = l^2g_x^2 + m^2g_y^2 + n^2g_z^2 \qquad 3.3$$

The ferric ion in certain derivatives of myoglobin gives a useful illustration of the use of the fictitious spin S'. The $^6S_{5/2}$ ground term of the ferric ion is split into three Kramer's doublets by the crystal field and the separation between doublets is so large that at ordinary microwave frequencies only transitions between the lowest doublet are observable. The observed spectrum can be described in terms of a fictitious spin of $\frac{1}{2}$ with an effective g value ranging from 2 to 6. Alternatively it is possible to describe the spectrum by a spin $S = \frac{5}{2}$ with a g value of approximately 2. The case of myoglobin will be referred to again in more detail in Chapter IV.

3.6 S State Ions

For a half filled shell the ground state of the free ion is an orbital singlet (i.e. Mn^{2+} and Fe^{3+} has a ground term $^6S_{5/2}$), and in a medium or weak crystal field the ground state will remain an orbital singlet. The ground state will thus have a (2S + 1) fold spin degeneracy which is not lifted by a first order interaction with the crystal field. It is found in practice that there is a splitting of the ground state both by a cubic field and fields of lower symmetry. The observed paramagnetic resonance spectrum can usually be fitted to a spin Hamiltonian of the form:-

$$\mathcal{H} = g\beta\underline{H}.\underline{S}. + D(S_z^2 - \tfrac{1}{3}S(S+1)) + E(S_x^2 - S_y^2)$$
$$+ \tfrac{1}{6}a(S_x^4 + S_y^4 + S_z^4) + c\,S_z^4 \qquad 3.4$$

Several attempts have been made to explain the observed splitting of S state ions by a crystal field but as yet no conclusive explanation is available. It is found that the only way in which a splitting can be obtained is to include a coupling between spins and orbits and regard the problem as one in which the ground state is degenerate. Van Vleck and Penney (1934) showed that for a $^6S_{5/2}$ ground state it is necessary to go to a high order of perturbation theory before any splitting is obtained. Most experimentally observed splittings are too large to be described by the above process and Pryce (1950) has suggested that the splittings are due to a spin-spin interaction, which also couples spins with orbits. He attributed the quadratic part of the Hamiltonian (DS_z^2) to a process which involves the first powers of the spin-spin interaction and the axially symmetric crystalline potential via an intermediate state $3d^4 4s\,^6D$, and calculated the co-efficient D. To account for the term $^a/6(S_x^4 + S_y^4 + S_z^4)$ he used a fifth order interaction, quartic in the spin-orbit interaction and linear in the cubic crystalline field, through intermediate states formed from $3d^5$. The problem has been considered in detail by Watanabe (1957) and more recently by Orbach, Das and Sharma (1964).

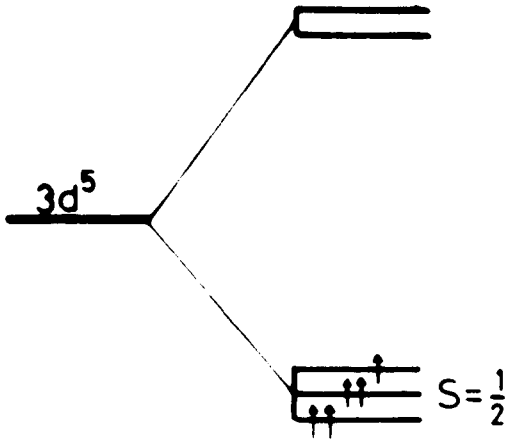

Fig 3·3a Splitting of the $3d^5$ configuration by a strong crystal field

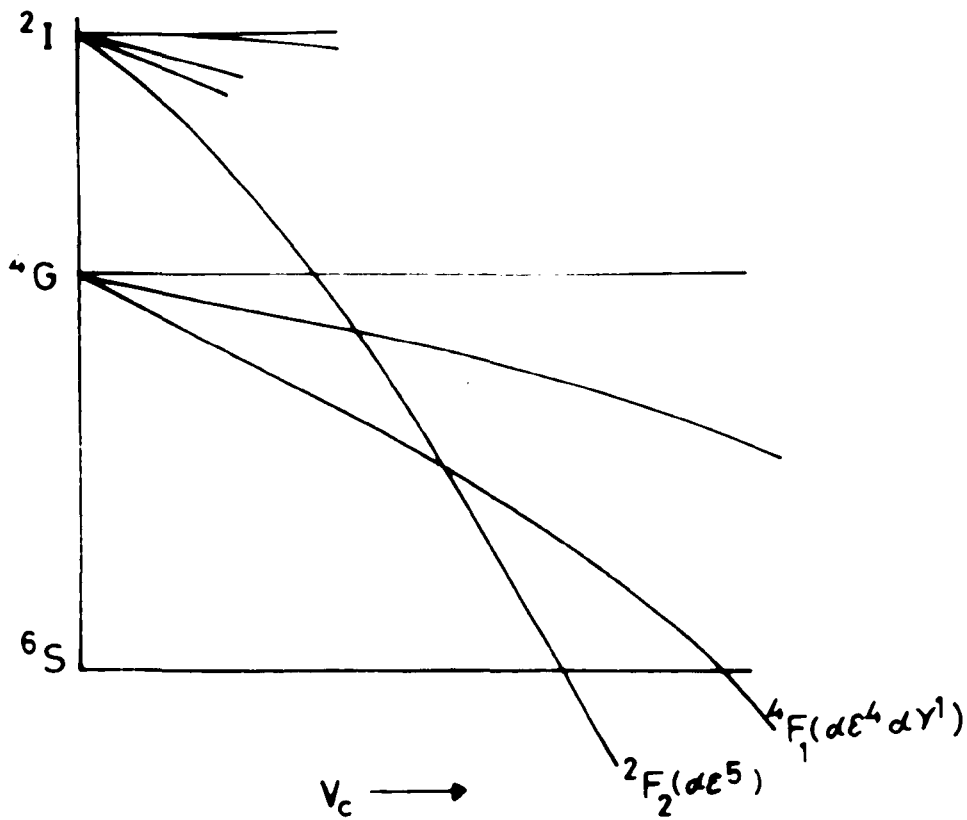

Fig 3·3b Energy level diagram for the $3d^5$ configuration as a function of crystalline potential

The Ferric Ion in a Strong and Medium Crystal Field

The ion Fe^{3+} has 5 d electrons and the lowest lying terms of the free ion are $^6S_{5/2}$, ^4G and ^2I and in a medium crystal field the ground state will be $^6S_{5/2}$ since the medium field will not split the S state other than under the circumstances referred to above.

If a strong field is applied the lowest lying term will be $^2\Gamma_2$, which is two fold degenerate, having a spin $S = \frac{1}{2}$. Physically this corresponds to the 5d orbitals of the free ion configuration being split by the crystal field into 3 fold and 2 fold orbitally degenerate states. This splitting arises because the crystal field is greater than the mutual repulsion between electrons. Only the lowest levels will be occupied leaving a spin value of $S = \frac{1}{2}$. The situation is illustrated in Figure 3.3a. In Figure 3.3b the effect of an increasing crystal field on the free ion terms is illustrated and it can be seen that in strong fields the $^2\Gamma$ term lies lowest.

In the medium field (or high spin) case the paramagnetic resonance data can be fitted to a Spin Hamiltonian of the form given in equation 3.4 with $S = 5/2$. For a purely axial crystal field this Hamiltonian reduces to

$$\mathcal{H} = D(S_z^2 - \tfrac{1}{4}) + g\ \beta H.S_z + g\ (\beta H_x S_x + H_y S_y)$$

In a strong axial crystal field (i.e. such that $D >> g\beta H$) there will be a large splitting between the three Kramer's doublets and only transitions between the lowest Kramer's doublet will be observed in a

paramagnetic resonance experiment. This line will be highly anisotropic having a g-value ranging from 2 to 6. In the simple case if we consider the lowest doublet as being completely isolated from the higher levels, the spectrum can be explained by calculating the matrix elements of S_x and S_z between the pair of states $|\pm\frac{1}{2}>$. The matrix for S_z is diagonal with elements $\pm\frac{1}{2}$, so that the resonance with H parallel to z can be explained with an effective g value, $g = 2$. The matrix for S_x has only off diagonal elements of $\pm 3/2$ so that in a magnetic field the eigenvalues are $\pm 3/2 g_e \beta H$, where g_e is the free electron g value. The observed spectrum can thus be explained by an effective g value, $g = 6$ and a fictitious spin $S' = \frac{1}{2}$.

In practice the excited states are rarely completely removed from the ground states, and the states are mixed by the magnetic field. With the magnetic field parallel to the z axis M_z is a good quantum number and the eigenstates are the zero field eigenstates represented by $|\pm\frac{1}{2}>$, $|\pm 3/2>$, $|\pm 5/2>$. When the magnetic field is perpendicular to the z axis the states become mixed by the magnetic field, and the zero field eigenstates no longer form a diagonal representation of the eigenstates in a magnetic field. The levels of the lowest lying doublet will each contain a mixture of the states $|\pm\frac{1}{2}>$ and $|\pm 3/2>$. If the Hamiltonian contains quadratic or quartic terms in S_x or S_y then admixture with higher states will occur even in zero field.

To calculate the eigenvalues with a particular Hamiltonian requires a solution of the secular determinant in the usual manner.

In the case of Fe^{3+} this involves the diagonalisation of a six by six matrix, which can only be done numerically on a computer or by perturbation methods. If the term DS_z^2 is very much larger than the interaction with the magnetic field, $g\beta H$, then the usual method is to treat the magnetic field interaction as a perturbation on the zero field Hamiltonian. If one carries out this calculation for the above Hamiltonian one derives, using third order perturbation theory, an effective $g_\perp$ value for the lowest doublets of:

$$g_{eff} = 3g_\perp \left[1 - \frac{2(g_\perp \beta H)^2}{(2D)^2} \right] \qquad 3.5$$

Thus for large D and $g_\perp = 2.0$ we have $g_{eff} = 6$, but as the D value is steadily reduced the effective g-value will deviate from six. If other terms such as a Rhombic term, or a term in S_x^4 etc., occurs in the Hamiltonian they may be treated by the same method providing they are small.

The situation described above occurs in acid metmyoglobin and will be described in more detail later.

References

Abragam, A. and Price, M.L., Proc. Roy. Soc. A205 135, 1951.

Bleaney, B. and Stevens, K.W.H., Rep. Prog. Phys. 16 108, 1953.

Condon, E.U. and Shortley, G.H.,"Theory of Atomic Spectra" Cambridge, 1955.

Low, W., Advances in Solid State Phys. Supp. 2 13, 1960.

Orbach,R., Das, T.P. and Sharma, R.R., Proceedings of the International Conference on Magnetism, 330, 1964.

Price, M.L., Phys. Rev. 80 1107, 1950.

Stevens, K.W.H., Proc. Phys. Soc. A65 209, 1952.

Watanabe, H., Prog. in Theor. Phys. 18 No. 4 405, 1957.

CHAPTER IV

THE PROPERTIES OF MYOGLOBIN

4.1 The Haem-Proteins

The haem-proteins are so named because they consist of a globular protein together with one or more haem prosthetic groups. The structure of this group varies only slightly from one haem-protein to another and consists basically of a porphorin ring surrounding an iron atom. The protein molecules however vary considerably both in physical size and in the sequence of amino acid units from which their polypeptide chains are constituted.

Myoglobin is of particular interest because it is one of the smallest of the haem-proteins and it is closely related to the blood pigment, haemoglobin. Because of its comparatively low molecular weight and its ability to form single crystals it was chosen by Kendrew for the first detailed X-ray study of a protein. Myoglobin is contained within the tissue cells and its physiological function is to act as a temporary storehouse for the oxygen carried to it by the haemoglobin in the blood. The part of the molecule responsible for the reversible combination with oxygen is the haem group, and it is the electronic properties of the central ion of this group which are the subject of this thesis. The myoglobin used for the X-ray study and for this work is that of the Sperm Whale. A whole range of myoglobin from a variety

of species of aquatic mammals has been studied by Kendrew and his associates, who have shown that apart from minor differences in amino acid composition, the myoglobin obtained from most species is very similar (Kendrew and Parrish 1954).

The molecular weight of myoglobin is 17000 whilst that of haemoglobin is 65000, and this one to four relationship is repeated in the number of haem groups contained in each protein. These facts, together with the similar physiological properties, suggest that the haemoglobin molecule could be made up of four sub-units, each one similar to a molecule of myoglobin. X-ray measurements have shown that the haemoglobin molecule is made up of four sets of polypeptide chains whilst the myoglobin molecule has only one, but the arrangement of the amino and units within each polypeptide chain is not the same in haemoglobin and myoglobin.

The X-ray analysis of myoglobin has now been completed to 1.4Å and the co-ordinates of the various atoms are known. The position of the haem group relative to the rest of the molecule is known and the structural information available from electron spin resonance studies can be compared with the X-ray data.

4.2 Crystal Structure

Myoglobin can be crystallised in several forms depending on the species and the method used to prepare the crystals. The various crystal forms, labelled types A to J, have been listed by Kendrew and Parrish (1954). Single crystals can be prepared by precipitating the

TABLE 4.1

atom	x	y	z	
Haem section				
iron (I)	24.05	43.76	6.93	
nitrogen	23.59	41.64	8.85	
"	23.69	41.45	4.95	
"	25.30	45.58	5.21	
"	25.19	45.77	9.12	
Histidine				
nitrogen	18.38	46.09	6.96	
carbon (1)	20.33	45.60	7.80	
nitrogen	21.12	44.72	6.45	to iron
carbon (2)	19.61	44.67	4.75	
carbon	17.87	45.53	5.04	
Water Molecule				
oxygen	27.00	41.75	7.00	(accuracy doubtful)

x is in 96^{ths} of unit cell edge a

y is in 48^{ths} of unit cell edge b

z is in 48^{ths} of unit cell edge c

Unit cell dimensions

a = 64.5A, b = 30.86A, c = 34.7A, $\beta = 106^{\circ}$.

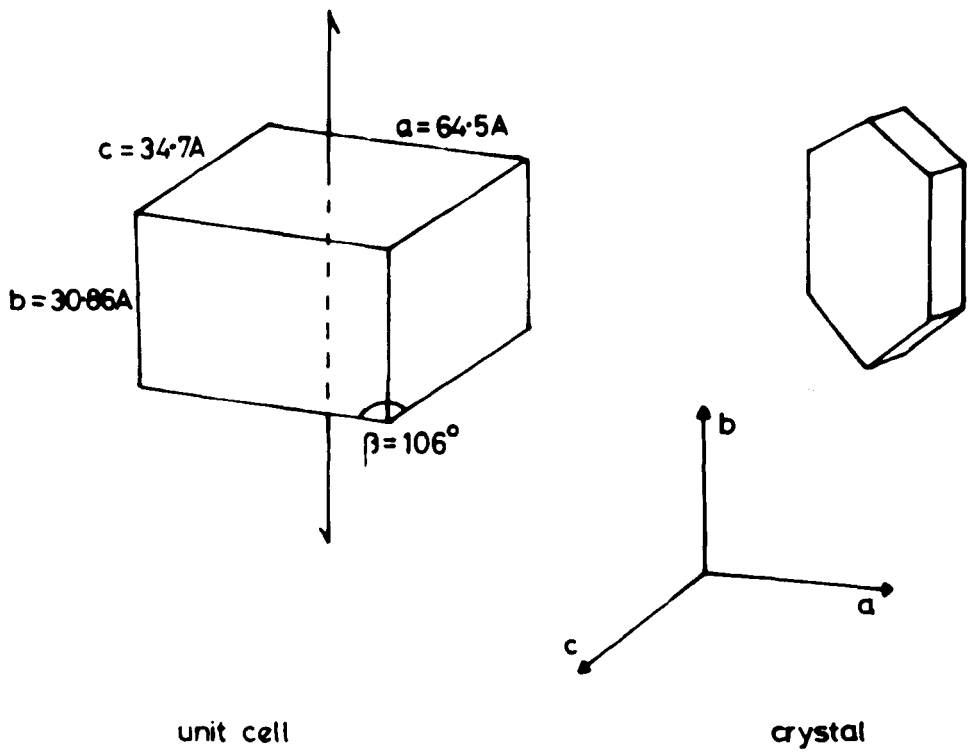

Fig 4·1 TYPE A SPERM WHALE MYOGLOBIN

protein from an aqueous solution using either ammonium sulphate or phosphate buffer. The method used to prepare the crystals for this study is that of Kendrew and Parrish (1956). The myoglobin in a salted paste is dissolved in distilled water and dialised against distilled water until salt free. The protein is then precipitated from the solution using either ammonium sulphate or phosphate buffer ($NaH_2PO_4.2H_2O$: K_2HPO_4), during which time the pH of the solution is kept constant with buffer solution. A detailed account of the preparation of the crystals used in this investigation will be given in Chapter VII.

The crystals of Sperm Whale myoglobin prepared from ammonium sulphate are a monoclinic form known as type A, whilst those grown from phosphate buffer solution are an orthorhombic form known as type B. The crystals used in this investigation were all of type A grown from ammonium sulphate. These crystals form flattened four sided prisms, whose axis is b. If they are grown at pHs below 7 they are flattened in the {001} plane but at higher pH they are flattened in the {100} plane. A diagram of a typical type A crystal is shown in Figure 4.1. The type A crystal has two molecules per unit cell and the space group is $P2_1$.

The X-ray analysis of the structure of the myoglobin molecule has now been completed to a resolution of 1.4Å and the co-ordinates of most of the atoms in the unit cell are known. A list of the co-ordinates of the various atoms in and around the haem group is given in Table 4.1. These figures were supplied by Dr. H.C. Watson of the Medical Research Council unit of Molecular Biology at Cambridge.

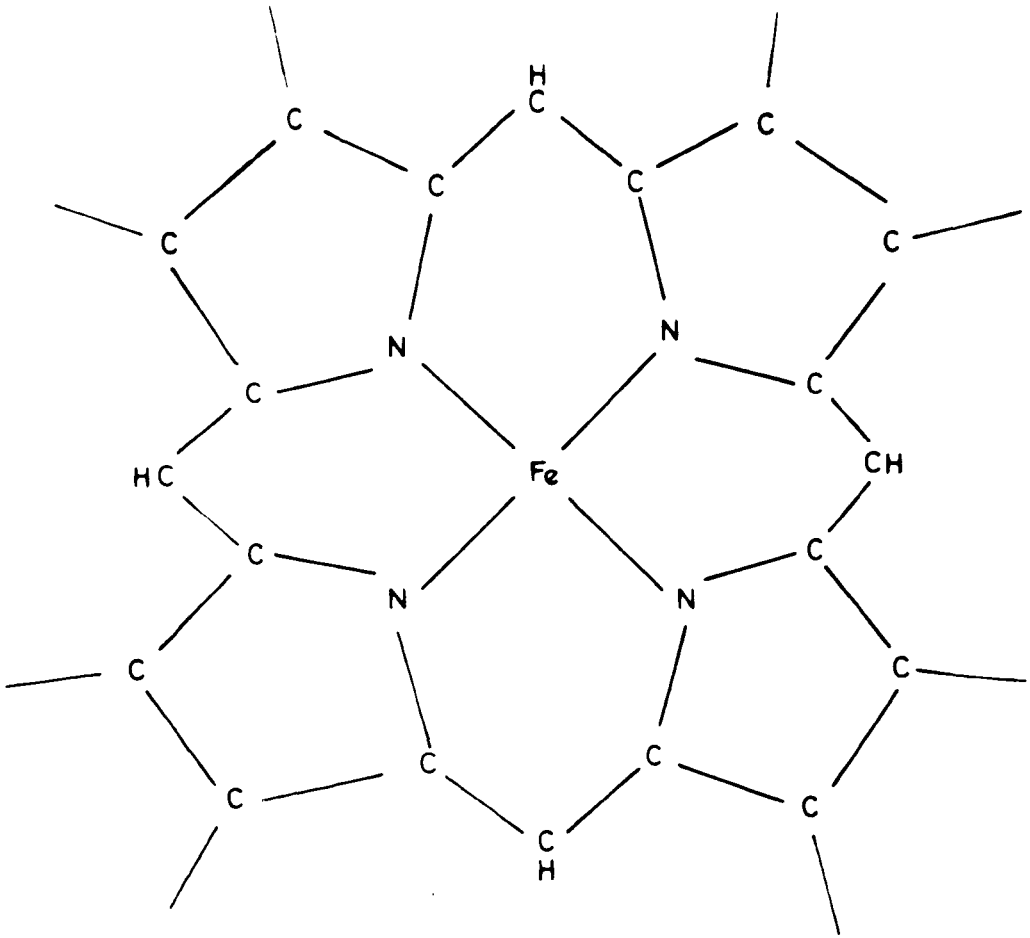

Fig 4·2 CHEMICAL FORMULA OF HAEM GROUP

The myoglobin molecule consists of a single polypeptide chain which is folded in a complex and unsymmetrical manner to form a roughly triangular prism with dimensions roughly 45 x 35 x 25Å. The molecule is extremely compact and there is virtually no water inside it. The haem group is situated with its plane almost normal to the surface, with one edge at the surface and the rest buried deep within the molecule. The haem group is attached to the rest of the molecule via the nitrogen atom of a histidine ring, called the linked histidine, and the sixth co-ordination point of the iron atom is available for radical formation. The protein chain, in enfolding the haem group, brings into close proximity another histidine ring, called the distal histidine ring, which in some cases is thought to form bonds with the sixth ligand.

Although there is no water inside the coiled protein chain, a whole single crystal of myoglobin has a very open structure and contains a considerable amount of water. This water presents a problem in that it damps out the high Q of an electron spin resonance cavity, but the open structure is useful in that it allows the radical attached to the iron atom to be changed after the crystal has been grown.

4.3 The Iron Atom

The location of the iron atom has already been described, and a diagram showing the chemical structure of the haem group is shown in Figure 4.2.

When in its natural environment the iron atom is in the ferrous state, but on isolation and crystallisation the iron is oxydised to the ferric form, known as ferri- or metmyoglobin. In the met form the sixth co-ordination point is occupied by a water molecule (acid met-myoglobin) if the pH is below 7, and a hydroxyl group at higher pH values. It is relatively easy to change the radical occupying the sixth co-ordination point either by changing the pH, or by adding a suitable solvent. In the acid met case the ferric ion is in the high spin state with $S = 5/2$, but if an azide or cyanide group is attached the ion takes on the low spin form with $S = \frac{1}{2}$. These two situations have been described in Chapter III.

The number of unpaired electrons in a paramagnetic ion can be determined by measurements of the paramagnetic susceptibility, and extensive measurements of the magnetic susceptibility of haem proteins have been made. The measurements up to 1946 have been reviewed by Hartree (1946). In general these measurements agree with the division into high and low spin complexes, but in several cases deviations from the expected values have been obtained. For instance, five unpaired d electrons would be expected to have a magnetic moment of 5.92 Bohr magnetons if all the orbital angular momentum was quenched. In fact, acid methaemoglobin has a magnetic moment of 5.80 Bohr magnetons, and this was originally attributed to haem-haem interaction by Pauling (1936). Later measurements on solutions of acid metmyoglobin, where there is only one haem group per molecule and consequently no haem-haem interaction,

gave a similar value to that obtained for acid methaemoglobin. This indicated that the deviation from the value expected was brought about by some orbital momentum contributing to the total angular momentum.

Susceptibility measurements can give considerably more information if taken over a large temperature range and on single crystals as will be shown in section 4.5.

4.4 Electron Spin Resonance Studies

Several electron spin resonance studies have now been made of both the high and low spin derivatives of myoglobin but only those particularly relevant to this investigation will be reviewed here. The initial measurements by Bennett, Gibson and Ingram (1957) showed that in single crystals a very large g-value anisotropy exists. With the magnetic field parallel to the haem normal a g-value ($g_{\parallel}$) of 2.00 occurs, whilst with the magnetic field perpendicular to the haem normal a g-value ($g_{\perp}$) of approximately 6.0 is detected. These initial measurements were used to determine the orientation of the haem planes relative to the crystal axes in type A Sperm Whale myoglobin. The measurements were subsequently extended to several other crystal types (B, C, D and F) (Bennett et al. 1961).

The low spin azide derivative has a g-value spread around the free spin value of 2.0 and a lowering of the axial symmetry found in the high spin derivatives. The g-values and the direction cosines of the principle axes were reported by Gibson and Ingram (1957) and have

subsequently been compared with the detailed X-ray information now available (Helcké, Ingram and Slade 1968). The directions of the principal axes have been used to interpret some of the results obtained at 4mm wavelengths and so they will be quoted here along with the principal g-values:-

		α	β	γ
g_x	= 1.71	$95^\circ 27'$	$104^\circ 18'$	$15^\circ 20'$
g_y	= 2.19	$57^\circ 40'$	$146^\circ 25'$	$98^\circ 6'$
g_z	= 2.82	$33^\circ 13'$	$59^\circ 42'$	$77^\circ 40'$

where α, β and γ are the angles made with the a, b and c* axes respectively. g_x and g_y lie in the haem plane and g_z makes an angle of 9° with the haem normal.

(a) g-value studies in acid metmyoglobin

A more accurate measurement of the g-value in the haem plane of acid metmyoglobin has revealed that it is slightly less than 6.0. This situation has been described in Chapter III and was first considered by Griffith (1956). For large D values in the Hamiltonian given in equation 3.4 and situations where the microwave quantum is small compared to D the value of $g_\perp^{eff}$ is given by equation 3.5. Griffith originally estimated that the zero field splitting between the lowest pair of Kramer's doublets was of the order of $10cm^{-1}$. More recently Eisenberger and Pershan (1966) have measured the value of $g_\perp^{eff}$ in single crystals at 13GHz and 35GHz and deduced, using equation 3.5, that the zero field splitting is $8.75cm^{-1}$. However there is evidence that there is a departure

from axial symmetry even in the high spin derivative (Helcké et al. 1968) and Eisenberger and Pershan have taken no account of this, nor have they been specific about the particular crystal plane in which the measurements were made. At Q-band frequencies the g-value in the haem plane varies between 5.98 and 5.86 and the change in g-value in going from 13GHz to 35GHz observed by Eisenberger and Pershan is considerably less than this variation.

(b) Electron spin resonance linewidths in metmyoglobin

The electron spin resonance signals from both the acid met and azide derivatives of myoglobin show an interesting variation with orientation. The linewidths vary from .08 Tesla (800 gauss) to less than .01 Tesla (100 gauss), and a detailed account of the variation has been given by Helcké, Ingram and Slade (1968) and Helcké (1963). The general features of the variation in acid metmyoglobin are that the linewidth is a minimum in the haem plane and then increases out of the plane towards the normal. In the azide derivative the variation is somewhat more complex.

The unusually large linewidths make it possible to discard many of the more common line broadening mechanisms on the basis of simple order of magnitude calculations. The contribution of spin lattice relaxation to the linewidths must at low temperatures be very small since no change is observed on cooling from 77°K to 20°K. There will be a contribution due to the dipolar interaction between the magnet moments of neighbouring iron atoms. The magnitude of this interaction can be

calculated since the distances to nearest neighbours are known from X-ray data. An upper limit to the broadening from this source can be calculated to be .0014 Tesla (14 gauss).

The mechanism which has been proposed for the broad lines found in single crystals of myoglobin is a result of the peculiar crystalline structure of these proteins. Essentially it supposes that the g-values of all the haem groups contributing to the resonance are not strictly parallel to each other, but are scattered about a mean orientation. For axial symmetry the g-value at any angle θ is given by

$$g_\theta^2 = g_{\parallel}^2 \, Cos^2\theta + g_{\perp}^2 Sin^2\theta$$

The linewidth, ΔH, is proportional to the rate of change of g with θ, so that

$$\Delta H \propto \frac{dg}{d\theta} = \frac{(g_{\perp}^2 - g_{\parallel}^2)Cos\theta Sin\theta}{g_\theta}$$

For haem groups whose normals make angles between $\theta + \Delta\theta$ and $\theta - \Delta\theta$ with the magnetic field direction, the spread in g-values is given by

$$\Delta g = \frac{(g_{\perp}^2 - g_{\parallel}^2)}{2g_\theta} Sin2\theta Sin2\Delta\theta$$

Using equation 2.6 we see that the linewidth is given by

$$\Delta H = \frac{h\nu}{\beta} \frac{(g_{\perp}^2 - g_{\parallel}^2)}{2g_\theta^3} Sin2\theta Sin2\Delta\theta + const \qquad 4.1$$

where the constant is included to account for other residual broadening mechanisms. This expression gives a reasonable account of the linewidth variation in acid metmyoglobin. To account for the variation in cases where there is no axial symmetry a more complex equation can be derived involving the azimuthal variation in g-value. The curves obtained from equation 4.1 were fitted to the experimental curves by suitable choice of $2\Delta\theta$. This corresponds to twice the standard deviation in haem plane orientation and good agreement was found with $2\Delta\theta$ equal to 3.3°.
A useful check on the validity of this expression is available from the linewidth variation at 4mm wavelengths where one would expect the linewidth to increase in proportion to the frequency. This point will be discussed further in Chapter VII.

4.5 Magnetic Susceptibility

It is possible to obtain an estimate of the zero field splittings of the ferric ion in acid metmyoglobin from a study of the temperature variation of the paramagnetic susceptibility. This was first carried out by McKim (1961) and considered theoretically by Kotani (1961). Kotani's treatment will be briefly outlined here.

The paramagnetic susceptibility is usually expressed in terms of the Curie Law:

$$\chi = \frac{np^2\beta^2}{3kT\mu_o}$$

where p is called the effective Bohr magneton number and n the number of magnetic ions per unit volume. For an assembly of free ions we have

$$p^2 = g^2J(J+1)$$

but in paramagnetic solids where orbital quenching occurs we must often use the spin only value for p, viz:

$$p^2 = g^2S(S+1)$$

In the case of acid metmyoglobin, if we consider the lowest lying levels to be represented by the Hamiltonian of equation 3.4 for an axial field we have

$$= DS_z^2 + 2\beta \underline{S}.\underline{H}$$

if we neglect the constant terms which serve only to shift the overall energy zero.

Using the treatment outlined in Chapter III, the eigenvalues of this Hamiltonian are:

for H parallel to z

$$E = \begin{matrix} (5/2)^2D \pm 5H \\ (3/2)^2D \pm 3H \\ (1/2)^2D \pm H \end{matrix}$$

and for H perpendicular to z

$$E = \begin{matrix} (5/2)^2D + 5/4\ \frac{\beta^2H^2}{D} \\ (3/2)^2D + 11/4\ \frac{\beta^2H^2}{D} \\ (1/2)^2D \pm 3H - \frac{4\beta^2H^2}{D} \end{matrix}$$

The magnetic moment for each of these levels is given by $-\frac{\partial E}{\partial H}$ and using the Boltzmann distribution to determine the population of each level it is possible to determine the susceptibility parallel and perpendicular to the haem normal, so that

$$\chi_{\parallel} = \frac{Ng^2\beta^2}{kT\mu_o} \frac{\{\frac{1}{4} + 9/4 \exp(\frac{-2D}{kT}) + 25/4 \exp(-\frac{6D}{kT})}{(1 + \exp(\frac{-2D}{kT}) + \exp(\frac{6D}{kT})}$$

and a similar expression for $\chi_{\perp}$.

By measuring the magnetic susceptibility as a function of temperature and fitting the curve so obtained to these equations McKim was able to estimate the zero field splitting to lie between 5 and 10cm^{-1}. The accuracy of this measurement is little better than the estimate of Griffiths from the g-value measurements, but by pursuing the susceptibility measurements to liquid hydrogen temperatures it ought to be possible to improve on this.

4.6 Summary

The evidence from electron spin resonance studies of the lowest lying doublet and from susceptibility measurements indicates that the zero field splitting in acid metmyoglobin lies between 7 and 10cm^{-1}. The initial object of this investigation was to measure the zero field splitting directly, using high microwave frequencies and magnetic fields. If this proved impracticable it was expected that the use of high frequencies would give a more accurate estimate from the deviation of $g_{\perp}$ from 6.0. In addition the use of high frequencies would be expected to reveal more clearly any deviation from axial symmetry, indicated by the Q-band studies. It was with these aims in mind that the apparatus described in the next two chapters was constructed.

References

Bennett, J.E., Gibson, J.F. and Ingram, D.J.E., Proc. Roy. Soc. A240 67, 1957.

Bennett, J.E., Gibson, J.F., Ingram, D.J.E., Haughton, T.M., Kerkut, G.A. and Munday, K.A., Proc. Roy. Soc. A262 395, 1961.

Eisenberger, P. and Pershan, P.S., J. Chem. Phys. 45 2832, 1966.

Gibson, J.F. and Ingram, D.J.E., Nature, Lond. 180 29, 1957.

Griffith, J.S., Proc. Roy.Soc. A235 23, 1956.

Hartree, E.F., Ann. Rep. Chem. Soc. 43 287 (1946).

Helcké, G.A., Ph.D. Thesis, Univ. of Keele, 1963.

Helcké, G.A., Ingram, D.J.E. and Slade, E.F., Proc. Roy. Soc. B169 275, 1968.

Kendrew, J.C. and Parrish, R.G., Nature 174 946, 1954.

Kendrew, J.C. and Parrish, R.G., Proc. Roy. Soc. A238 305, 1956.

M^{c}Kim, F.R., Proc. Roy. Soc. A262 287, 1961.

Pauling, L. and Coryell, C.D., Proc. Nat. Acad. Sci. 22 210, 1936.

CHAPTER V

MILLIMETER TECHNIQUES

Introduction

The techniques used to generate, propagate and detect millimeter radiation are many and varied. The problem has been approached from the microwave region by scaling down conventional components, and from the infra-red region of the spectrum by using a range of quasi optical techniques, with equal success. This chapter will review the situation paying particular attention to any techniques which are new to the field of microwave spectroscopy and pointing out the problems involved. Where the available technique simply involves a scaling down of a generally understood microwave technique without any new problems, it will not be considered in any detail. The points considered in detail are those which are directly concerned with the design and construction of millimeter wave electron spin resonance spectrometers.

5.1 Generation of Millimeter Radiation

(a) Harmonic generation

The generation of millimeter radiation by using the harmonics of some lower frequency radiation has probably been the most common source of millimeter power until recent years. The basic requirement of an harmonic generator is some non-linear reactive or resistive element and a method of filtering out the unwanted harmonics which may be present.

The simplest method is to use the non-linear properties of a microwave detector or mixer crystal. The characteristic of a microwave diode can be represented by a power series of the form

$$i = ae + be^2 + ce^3 \ldots\ldots \qquad 5.1$$

where e is the applied oscillating electric field and it is easily shown that the crystal generates all harmonics. The practical methods of using the properties of this type of crystal have been described by many authors (Johnson et al. 1954, Gordy 1948, Smith et al. 1949, Gordy 1964). The simplest method is to place the crystal across the guide and then taper the guide to a suitable size for the harmonic required. Matching is then carried out by means of stub tuners in each waveguide region. The most popular alternative is to use the crossed waveguide method, in which two lengths of waveguide are arranged at right angles to one another with the converting element, in this case a crystal, located across the junction. The waveguide dimensions in one direction are such as to propagate the dominant mode of the fundamental frequency, and in the other direction such as to propagate the dominant mode of the desired harmonic. The harmonic guide can be designed to filter out all frequencies below the harmonic required. Tuning plungers are located in both guides behind the crystal. This type of harmonic generator can be designed either to use a commercially available microwave diode (Johnson et al. 1954) or to enable the rectifying junction to be formed in the generator using replaceable crystals and whiskers (Gordy 1948).

The power generated by an ideal resistive element in this type of detector can be shown to be proportional to n^{-2}, where n is the harmonic number, and to be related to the fundamental power by a relation $P_n \propto {}^{a}/_{n^2}\, P_1^{\,s}$, where $s \geq 1$ and P_1 is the fundamental power. In practice the lowest conversion loss for generating the first harmonic in the 2 or 4mm region are of the order of 20dbs, but figures up to 30dbs are more usual. This is largely due to instabilities in the microwave structure and a departure from the non-linear characteristic of the crystal as the frequency is increased. The conversion ratio for higher harmonics is usually even further from the ideal case because of the narrow bandwidth of the supporting structure.

In contrast to the relatively low theoretical power available from the non-linear resistive element of a crystal diode, a purely reactive element should be capable of producing 100% conversion of fundamental power into harmonic power. In recent years this has become a practicable possibility with the advent of varactor diodes capable of operating in the millimeter wavelength region. Here there is little loss of energy in the resistive part of the diode and the non-linear reactance enables practical values for the conversion ratio as high as 12dbs to be obtained.

A variety of harmonic generators have been recently produced which use the non-linear properties of a plasma-metal junction as an harmonic generator (Froome 1962,63). Unfortunately such generators are intrinsically noisy and are not really suitable as sources for solid state spectroscopy.

(b) Thermionic oscillators

A fruitful approach to the problem of millimeter wave generation has been made by the scaling down of conventional klystrons and magnetrons to produce increasingly higher frequencies. Such tubes require increasingly small and accurate dimensions and reduced tolerances in the electron beam focus. The problem is further aggravated by the difficulty of producing cavities with high Q factors for use at these wavelengths. This arises from a combination of the small dimensions involved and a reduction in the conductivity of copper. The surface resistance of pure copper is inversely proportional to the square root of the wavelength in this wavelength region, and thus sets a very considerable limit to the Q factors obtainable.

The magnetron can now be made to produce considerable power at wavelengths as low as 2mm, but the radiation is comparatively noisy and generally unsuitable for E.S.R. work. Several klystrons are now available which will produce up to 100m.w. at 4 and 2mm wavelengths. Unfortunately they are extremely expensive and have relatively short lives.

Millimeter wave power can now be generated very effectively using extended interaction oscillators, such as Backward Wave Oscillators. The operation of this type of oscillator depends on the interaction of an electron beam with a slow wave structure such as a helix.

They have the advantage that their frequency depends only on the accelerator voltage and consequently can be made very stable. They also have a much wider bandwidth than any other type of vacuum tube

generator since they do not contain any tuned elements. The principle disadvantage is that they require very large, stable power supplies, and the high frequency ones have a rather short cathode life, due to the high beam current density required.

(c) Other sources

An alternative approach to the problem of generating millimeter radiation is to approach the problem from the infra-red end of the spectrum. In this region, black body sources are the most common, and unfortunately the power radiated by a black body source falls off very rapidly towards the millimeter region of the spectrum. Some interesting spectroscopic measurements have been reported in the millimeter region using radiation from a black body source, the most applicable of which is that of Feher and Richards, who reported the direct measurement of the zero field splitting between the ground state levels of the Ferric ion in haem chloride (Feher 1967).

The most fruitful coherent source of radiation in the millimeter band other than vacuum tube oscillators will probably be from quantum generators. Several masers have now been constructed to operate in the low millimeter region, the most powerful of which seems to be the water vapour laser of Mathias et al. (1964).

Other possible millimeter sources include Cherenkov radiation, tunnel diode oscillators and the Josephson superconducting junction. Although, in theory, the Cherenkov interaction is weak, high current densities should enable appreciable amounts of power to be generated,

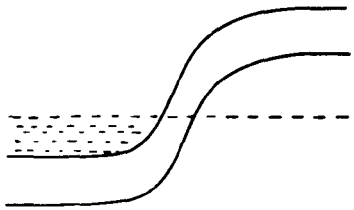

Zero bias (a)

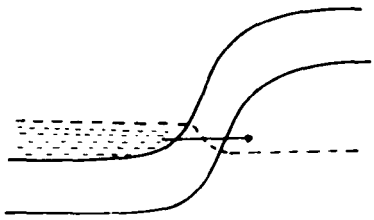

Small forward bias (b)

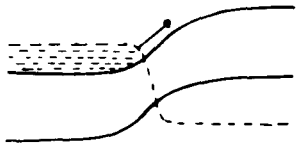

Large forward bias (c)

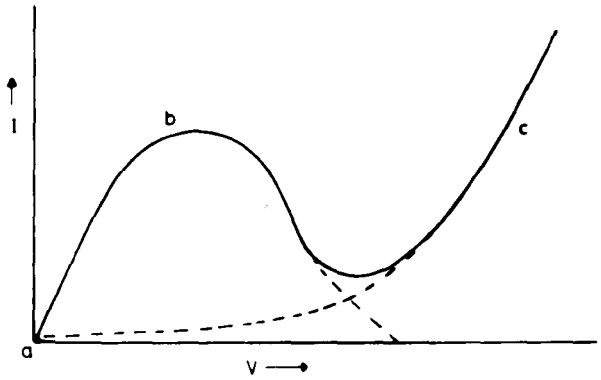

Fig 5·1 ENERGY LEVELS & CHARACTERISTIC OF A TUNNEL DIODE

and in 1960 the first experimental results in a 35GHz Cherenkov radiator driven by a 0.042 ampère beam gave output powers approaching 1 watt. In practice, megavolt power supplies are required and the need for filters poses a considerable problem (Coleman et al. 1960).

Tunnel diodes are highly doped p.n. junction diodes, wherein quantum tunnelling in the abrupt junction gives rise to a negative resistance region for small forward bias voltages. Since tunnelling is a majority carrier effect with no limitation of minority carrier drift time, the tunnel diode should be expected to operate at very high frequencies. Since the bias voltage is of the order of a few hundred m.v., the diodes cannot be expected to produce high powers (Sommers 1959). The tunnel diode is a very low impedance device, and consequently the circuitry and design of the diode pose a considerable problem. So far the maximum operating frequency seems to be about 103GHz and the maximum power 0.3μW. The operation of a tunnel diode is illustrated in Figure 5.1.

The Josephson junction, a junction between two films of superconductor separated by a very thin insulating layer, has been shown to generate very small amounts of microwave power ($\sim 10^{-11}$W). The power is generated by the oscillating Josephson current flowing between the two superconductors, and the frequency is determined only by the applied e.m.f. An upper limit to the frequency is set by the energy gap between the superconducting and the normal states and this usually corresponds to wavelengths of the order of 1mm. A lucid account of the operation of the Josephson Junction and the problems associated with the application of

such junctions as millimeter wave generators has been given by Langenberg et al. (1966).

Although there is every likelihood of many new devices being developed to generate millimeter radiation in the near future, at present the vacuum tube oscillators and harmonic generators are still the most practicable sources for spectroscopic purposes. Of these, the klystron and backward wave oscillator are obviously the best, but both are exceedingly expensive and short-lived and spectroscopists are forced to fall back on harmonic generation. At the present time, since millimeter varactor diodes are not readily available, the crystal diode is still the most convenient, despite the disadvantage of its having a poor conversion ratio.

5.2 Propagation of Millimeter Radiation

The problem of propagating millimeter radiation can also be approached from both the optical and the microwave sides. The first approach follows the principles of geometrical optics and requires components, such as lenses, whose dimensions are many orders of magnitude larger than the wavelengths concerned. The second approach simply involves the scaling down of standard microwave components, with many associated technological difficulties. Because of the difficulties involved in these two approaches several alternative methods have been developed which employ combinations of the two.

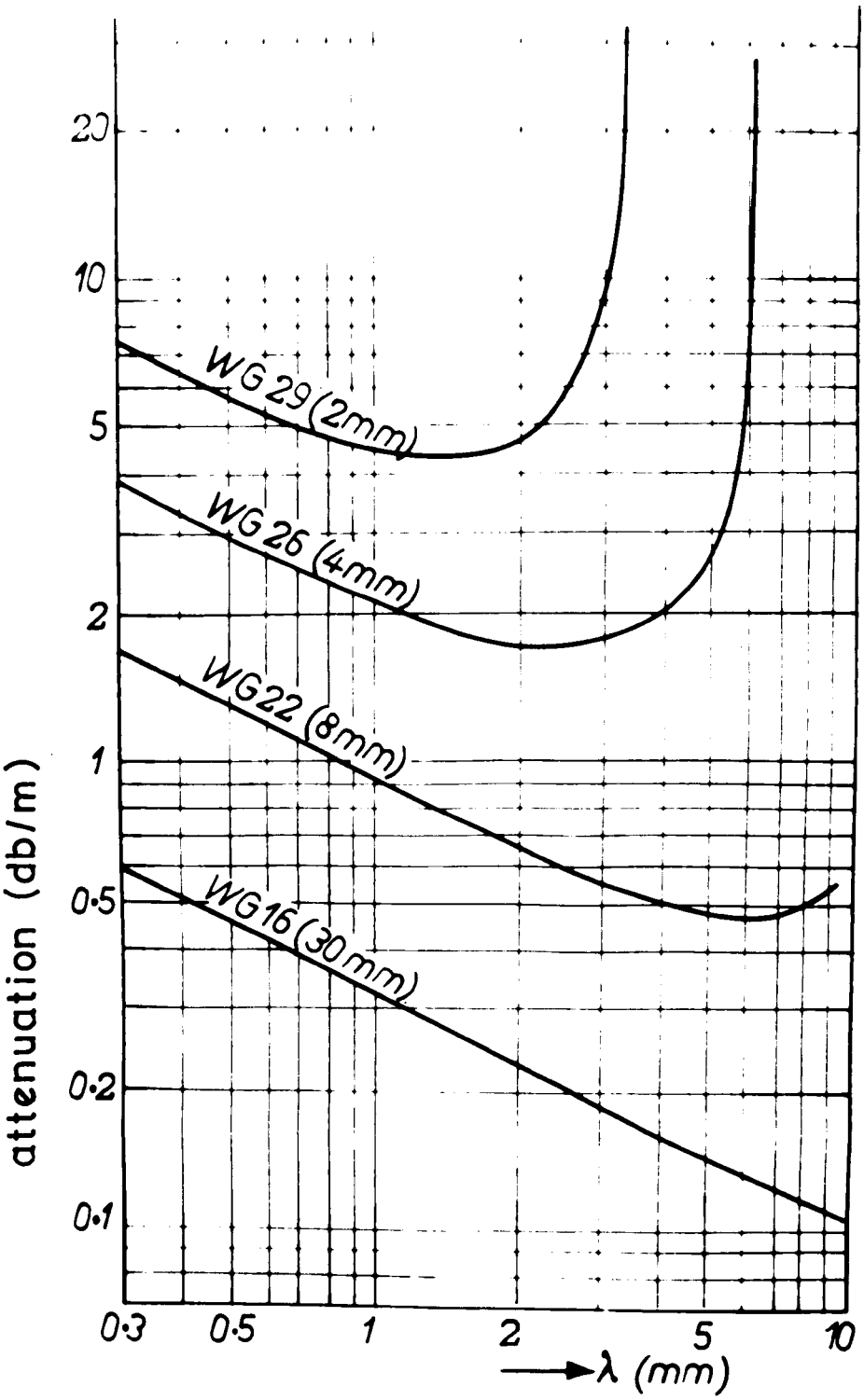

Fig 5·2 WAVEGUIDE ATTENUATION

(a) Standard waveguide techniques

An important limitation to the use of standard waveguides is set by the transmission losses, especially the dissipation in the metallic walls. The attenuation constant, for H_{01} modes, defined in the usual way for a conventional transmission line is given by:-

$$\alpha_{H_{01}} = \frac{R_s}{b} \frac{E E_o}{\mu \mu_o} (1 + {}^{2b}/_{a}({}^{\lambda}/_{2a}))(1 - ({}^{\lambda}/_{2a})^2)^{-\frac{1}{2}} \qquad 5.2$$

Where R_s is the surface resistance of the guides material, a the large dimension and b the short dimension of the guide cross-section. It can be seen that the attenuation constant increases with decreasing wavelength, especially since R_s increases at a rate proportional to ${}^{1}/\sqrt{\lambda}$. A plot of equation 5.2 is shown in Figure 5.2, from which it is seen that at 4mm wavelengths, the attenuation is 2db/metre and at 2mm it has risen to 5db/metre.

In order to ensure single mode propagation in the dominant mode, the dimensions of the guide must be of the same order as the wavelength and this introduces very considerable manufacturing difficulties which further increase the attenuation. In practical waveguides the attenuation is usually at least twice the values given in Figure 5.3.

In a microwave spectrometer a fairly long run of waveguide is usually required to carry the microwaves down to the sample and magnetic field and a large attenuation in this area of the microwave bridge would considerably reduce the sensitivity of the spectrometer. The problem is further aggravated by the need to use a guide constructed of some material

having a low heat conductivity for use in a low temperature system, consistent with as good an electrical conductivity as possible. A practicable material would necessarily have a greater surface resistance and a correspondingly higher attenuation constant. One would expect a one metre length of german silver 4mm waveguide to have an attenuation of at least 10db.

(b) Oversized waveguides

One of the possible techniques for millimeter wave propagation entailing lower losses and easier construction is the oversized waveguide. At a given wavelength, an oversized guide is one which is large enough to propagate many higher order modes in addition to the dominant one.

Such rectangular oversized guide is normally at least ten times larger than the conventional guide in each cross-sectional dimension; the ratio a/b usually remains close to 2. In any waveguide the guide wavelength λ_g is given by

$$1/\lambda_g^2 = 1/\lambda_o^2 - 1/\lambda_c^2$$

and thus becomes very close to the free space wavelength λ_o for oversized waveguides.

If the oversized guide is fed by careful tapering from standard guide, the same mode as is propagated in the feeding guide is transferred to the oversized system. The field distribution in the cross-sectional plane, though on a larger scale, is the same as in the standard guide. It is possible to propagate many degenerate modes in a guide which is only

slightly oversized, which would constitute lost power when the radiation is again coupled to standard waveguide. It is therefore essential to launch the wave with considerable care, using very accurately constructed tapers.

The expression given in equation 5.2 is also valid for oversize guides. It can easily be seen from this expression and from Figure 5.2 that for constant frequency, enlarging the dimensions gives a reduction of the attenuation, provided the dominant mode is maintained. For example, a 3cm rectangular guide (X-band) used for 2mm wave propagation has a theoretical attenuation of 0.23db/m, while the theoretical attenuation in the standard 2mm waveguide is 4.6db/m.

Oversizing can also be applied to a single dimension of a rectangular guide, resulting in the so-called "tall guide". If the oversized guide is turned through 90° so that the electric field is parallel to the large dimension of the guide, and the ratio of dimensions $a'/b' = 0.5$, the attenuation is further reduced by a factor of 2 as can be seen from equation 5.2. Of course this cannot be applied to standard guide or no radiation would propagate.

(c) Other guiding structures

The decrease in attenuation for smaller ratios of a/b might suggest extending the guide width"b"to infinity whilst keeping "a" constant. In such a structure, called Parallel Plate Guide, the modes may be regarded as limiting forms of the modes in a rectangular waveguide.

Guiding structure		Theoretical attenuation in dB/m at λ_o = 4mm	2mm	1mm	0.5mm	Effective guide cross section	Modes	Advantages	Disadvantages	Components
Standard guide		2	4.6	17	48	$\sim 0.28\ \lambda_o^2$	Single mode	Design flexible and well known	High attenuation; small size	Standard components
10 times oversized waveguide		0.11	0.24	0.88	2.5	$\sim 28\ \lambda_o^2$	Many modes possible	Low attenuation, adequate size	Pure mode feeding required; accurate construction of guide and components	Simply but precisely made components
same guide as tall guide		0.057	0.12	0.46	1.3					
15 times oversized waveguide		0.057	0.2	0.6	1.7	$\sim 63\ \lambda_o^2$				
same guide as tall guide		0.04	0.1	0.3	0.85					
H-guide		0.75	1.7	5.5	15.5	$\sim 15\ \lambda_o^2$	Single mode	Improved attenuation, flexible design	Small size in one direction	Not many components known
oversized H-guide		0.15	0.3	0.6	1.0	$\sim 75\ \lambda_o^2$	Several modes possible	Low attenuation	Pure mode feeding required	Constructions may be complicated
Dielectric rod	$2a/\lambda_o$=0.3	0.34	0.68	1.36	2.72	$\sim 100\ \lambda_o^2$	Single mode	Very low attenuation	May radiate; supports and components may cause difficulty	
$\tan\delta = 4\times10^{-4}$										
$\varepsilon = 2.5$	$2a/\lambda_o$=0.5	3.4	6.8	13.6	27	$\sim 15\ \lambda_o^2$				
Image line	$2a/\lambda_o$=0.3	0.9	2.3	5.7	15	$\sim 50\ \lambda_o^2$	Single mode	Supports and components easily applicable	Higher attenuation than diel. rod	Simple constructions
$\varepsilon = 2.5 \tan\delta = 4\times10^{-4}$										
$\sigma = 5.8\times10^7$ S/m	$2a/\lambda_o$=0.5	5.3	12.1	28.5	69	$\sim 8\ \lambda_o^2$				
Beam waveguide	$R/\lambda_o = 5$	3.7	7.5	14.5	29	$\sim 75\ \lambda_o^2$	Many beam modes possible	Open structure easily accessible; for large lenses improved attenuation	For moderate size lenses, high attenuation; large structure	Simple constructions based upon optical techniques
	$R/\lambda_o = 50$	0.04	0.07	0.15	0.3	$\sim 7500\lambda_o^2$				

Table 5.1. COMPARISON OF MILLIMETER WAVE PROPAGATION TECHNIQUES

In general for magnetic resonance applications it is of little practical use since very large plates are required before the losses due to radiation from the sides are reduced to acceptable values.

Several other guiding structures have been developed in the last few years including Groove Guide (Tischer 1963), a modification of Parallel Plate Guide, and H guide (Tischer 1959) where a dielectric slab is placed between the parallel plates to confine the wave between them.

It can be shown (Cullen et al. 1959) that the propagation of short wavelength radiation can be obtained in a dielectric rod if the major part of the radiation travels outside the rod. Low loss dielectric rods, and a fascinating modification of them, Image Lines, (King et al. 1962) have been used successfully to propagate millimeter radiation.

In most instances dielectric guiding structures are not convenient for use in millimeter wave magnetic resonance spectrometers because of the difficulty in producing the sophisticated components which are required.

A summary of the available methods of propagation and their advantages and disadvantages is shown in Table 5.1.

5.3 Millimeter Wave Components

A large number of components have been constructed for use with standard waveguide at millimeter wavelengths and are commercially available (Van Es et al. 1960, Meredith 1963). In general they are simply scaled down versions of the corresponding X or Q band component, using new mechanical devices to overcome manufacturing difficulties. The components

usually use very short waveguide runs and consequently the attenuation does not become a serious problem until the wavelength region below 2mm is reached.

(a) Components for oversize waveguide

The basic requirement for an oversize waveguide component is that it should interact with the wave in a similar fashion over the entire cross-section of the wave in order to avoid the generation of high order modes. Consequently normal waveguide techniques can no longer be employed. In general the methods employed involve a combination of optical and waveguide techniques. For instance, a bend in oversized waveguide is designed by treating the wave as if it were purely optical and reflecting it through a suitable angle using a metallic reflector. Useful bends in oversized waveguide have been described by Bled et al. (1964).

The most frequently required component for oversized waveguide is some device for launching the wave into the guiding structure. In general most millimeter wave generators have conventional rectangular waveguide outputs, and these must be adapted to the oversize guide with a taper. The major problem in designing a taper is to avoid introducing any appreciable phase lag across the wavefront. This is never completely avoidable, since the path length in the centre of the waveguide is shorter than at the boundaries. It is usual to make a compromise and design the taper to be as gentle as possible, consistent with the available space. Attempts have been made to overcome this difficulty using dielectric rods

and lenses in the taper (Taub et al. 1963), but for most applications conventional tapers with slopes of less than 10° are acceptable. The methods used to construct tapers will be described in Chapter VI.

Many of the components normally required can be constructed in oversize waveguide, including directional couplers, phase shifters, attenuators and detector mounts, and a detailed description of them can be found in the papers by Bled et al.(1964), Taub et al. (1963) and Griesonsmann et al. (1959).

(b) Resonators

Almost all microwave spectrometers require some form of resonant structure, for use as a wavemeter, reference cavity or sample cavity, and in the millimeter region of the spectrum it often becomes difficult to scale down the corresponding centimeter wave resonator. The reasons for this are primarily the difficulties involved in manufacturing small components to any high degree of accuracy and the decrease in electrical conductivity with increasing frequency and the consequent increase in skin depth. The former difficulty can partially be overcome by using higher order modes, but care must then be taken to suppress any unwanted modes and as far as sample cavities are concerned, the filling factor is reduced as one increases the mode order. Providing considerable care is taken in their manufacture, conventional cavities are still useful as wavemeters and sample cavities at wavelengths as short as 4mm, but at 2mm wavelengths they are becoming a little impracticable.

One alternative to this problem is to again turn to optical techniques and consider some of the Fabry-Perot type of optical resonators which have been extended to the millimeter and infra-red region of the spectrum for use in masers. The type of resonator most applicable to the millimeter wave region is the confocal Fabry-Perot resonator as described by Boyd and Gordon (1961) and Zimmerer (1962).

This resonator consists of two similar spherical mirrors separated by approximately twice their radius of curvature. The mirrors can be fabricated in brass using ordinary machining techniques, and power is coupled in via a small hole in the centre of one mirror. This type of resonator has the property of exceedingly high Q factors and is a manageable size. It can easily be machined in brass for use at millimeter wavelengths. A wavemeter using this cavity has been described by Zimmerer (1962).

The modes generated in this resonator are of a very high order and have been discussed in detail by Boyd and Gordon. Because of its large physical size one would expect it to have a very small filling factor when used as an E.S.R. sample cavity, although it would obviously prove ideal for gaseous spectroscopy.

A second type of resonator which has been suggested for use in the millimeter region is the dielectric tube resonator (Becker 1959). The resonator consists of a tube of dielectric material with metallic end plates, and power is coupled in through one end plate. Its main advantage lies in the fact that only cylindrically symmetric modes (i.e. H_{omn}) can

be generated and so fairly high order modes can be used without the problem of generating many unwanted modes. Such cavities have been successfully used as E.S.R. sample cavities at X and Q bands (Rosenbaum 1964), but at higher frequencies they become rather difficult to manufacture.

Conventional microwave cavities still appear to be the most suitable for use as sample cavities at frequencies up to 75GHz and their method of manufacture will be described in Chapter VI. The problem of a sample cavity for use in the 2mm band has yet to be solved.

5.4 Detection of Millimeter Radiation

Introduction

In recent years several advances have been made in this field and at the present time the experimentalist has a large number of available devices from which to choose. Most of the available microwave detectors, such as conventional crystals and bolometers, and the infra-red detectors such as the golay cell and several types of photoconductive devices, have been successfully used in the millimeter region. They all have their advantages and disadvantages, depending on the application for which they are required and the degree of sensitivity needed for the particular experiment. From the point of view of the use of any detector in a microwave spectrometer one must obviously compromise between the maximum available sensitivity and the convenience of operation. Before discussing particular detection systems it is necessary to consider the fundamental limits of performance of an ideal detector.

(a) Ideal detectors

The performance of a radiation detector can best be described in terms of three parameters which are defined as follows:

(i) The Responsivity $R = \frac{\Delta V}{\Delta W}$

where ΔV is the change in output voltage for a charge ΔW in input power.

(ii) Noise Equivalent Power (N.E.P.): defined as the signal power required to give an output equal to the noise output from the whole detection system.

(iii) The response time τ.

The noise sources contributing to the noise equivalent power can be conveniently divided into three components, such that the total mean square noise output from the detector, $\overline{\Delta V^2}$ is given by

$$\overline{\Delta V^2} = \overline{\Delta V_D^2} + \overline{\Delta V_S^2} + \overline{\Delta V_A^2}$$

where $\overline{\Delta V_D^2}$ is the Johnson noise component from the detector itself, $\overline{\Delta V_S^2}$ is the noise from random fluctuations in the source, including any spurious room temperature radiation, and $\overline{\Delta V_A^2}$ is noise introduced by the amplifying system. $\overline{\Delta V_A^2}$ can be represented by an equivalent noise resistance, r, for the amplifier such that

$$\overline{\Delta V_A^2} = 4kTBr$$

where B is the bandwidth of the amplifier.

An ideal detector is one in which

$$\overline{\Delta V_S^2} \gg \overline{\Delta V_D^2} + \overline{\Delta V_A^2}$$

In the optical region where the energy of one photon ($h\nu$) is always greater than kT, the single photon represents the ideal limit of sensitivity. However, as the wavelength is increased to the millimeter region, kT is of the same order as $h\nu$ even as the temperature tends to zero. For instance, $kT = h\nu$ for a wavelength of 1cm at approximately $1^{\circ}K$. Thus it can be seen that the noise in the system sets the limit of detection in the millimeter region even if the detector is cooled to helium temperatures.

The simplest ideal detector is the thermal detector, where the incident radiation produces a rise in temperature and a corresponding rise in resistance. In the ideal case, such a detector is capable of detecting a minimum of about 10^{-11} watts of black body radiation at $300^{\circ}K$ in a system with 1Hz bandwidth. If the detector is cooled and attempts are made to prevent unwanted room temperature radiation from reaching the detector using cooled filters, this figure can be improved by up to two orders of magnitude.

(b) Point contact crystal detectors

Crystal rectifiers have been the principal detector and multiplier in the microwave region for many years, and they are available for use in the sub-millimeter region. However, as the wavelength is reduced their performance deteriorates considerably due to the shunting effect of the contact capacitance.

The performance of a crystal detector is usually expressed in terms of a noise figure and the conversion loss (Torrey and Whitmer 1948), although in recent years manufacturers have tended to specify the sensitivity of millimeter detectors in terms of the rectified current per milliwatt of incident power. This latter method is rather unsatisfactory in that it gives no indication of the minimum detectable signal.

At X and Q band frequencies typical noise figures are 7db and 15db respectively and modern techniques have produced a figure as low as 15db for selected 4mm crystals. However, at wavelengths shorter than 4mm the performance deteriorates markedly and a typical figure for a 2mm detector would be nearer 40db. The response time of the crystal rectifier is faster than any other detector available in this region of the spectrum, typical values being usually in excess of 10^7Hz.

Crystal rectifiers for use at centimeter wavelengths are usually formed within a sealed cartridge, but at millimeter wavelengths this practice has been generally abandoned, and the method of forming the point contact in the actual waveguide, as first suggested by Gordy (1948), is commonly used. This removes the problem of reflections in the guide from a detector window or sensing electrode, and enables many whiskers to be used with one crystal. The performance of these detectors is very sensitive to whisker pressure and to moisture present in the system. They are also rather unstable. Despite the disadvantages involved in their operation they remain the most widely used detector in the millimeter region, especially in experiments where the only requisite is to

detect relatively large amounts of 2mm power. Typical noise equivalent powers for these detectors are in the region of 2×10^{-11} watts at about 1mm wavelength, when used as a video detector. This is at least an order of magnitude worse than the average centimeter wave crystal rectifier.

The principal sources of noise in a crystal rectifier are the Johnson noise of the resistive element and the Shot and Flicker noise from the rectifying contact, of which the latter is by far the greatest at low frequencies. The frequency spectrum of the Flicker noise is inversely proportional to the intermediate frequency. The behaviour of various crystal detectors in E.S.R. spectrometers has been analysed by various authors and recently Buckmaster and Dering (1966) have shown that there is little improvement to be gained in working at intermediate frequencies above 100KHz. However, the use of narrow band detection at higher intermediate frequencies does improve the performance of the detectors and the figures quoted above could probably be improved by an order of magnitude using a 100KHz I.F. or in a superheterodyne system.

(c) Thermal detectors

Thermal detectors or bolometers make use of materials which show a marked change of electrical conductivity with temperature. It is arranged that the absorption of radiation causes the detector temperature to rise, thus producing a change in resistance which can be detected. It can be shown (Jones 1953) that the responsivity and time constant are given by

$$R = \alpha V/(G - \alpha Q)$$

$$\tau = C/(G - \alpha Q) \quad \text{providing } \omega\tau < 1$$

where V is the voltage applied to the bolometer and Q the electrical power dissipated in it. C is the thermal capacity of the element, G the thermal conductance between the element and constant temperature bath and α is the temperature coefficient of resistance. It can be readily seen that the major requirements of a bolometer are a large value of α, a small thermal capacity and good thermal contact with the constant temperature bath.

Thermal fluctuations within the detector may be considerably reduced by lowering the temperature and consequently increasing the noise equivalent power. A reduction in temperature will also reduce the thermal capacity of the device and consequently decrease the response time.

The two most common bolometers in use in the millimeter region of the spectrum are the carbon and germanium bolometers. Certain types of commercial carbon resistors have very large temperature coefficients of resistance and small heat capacity, making them very suitable for use as a bolometer. A typical value for the noise equivalent power of a carbon bolometer at $4^{\circ}K$ is about 10^{-11} watts, and the response time is usually of the order of 10ms (Boyle 1959).

The germanium bolometer shows considerable improvement on the carbon variety, with a noise equivalent power of around 10^{-13} watts at $4^{\circ}K$ and a response time of around 400μsecs. Since pure germanium is transparent to longer wavelength radiation, whose energy is insufficient

to excite electrons from the valence band to the conduction band, very heavily doped germanium must be used, where the donor levels merge with the conduction band. There are thus many conduction electrons present at $4^{o}K$ and it appears that the free carriers are responsible for absorbing the incident radiation. The electrons are still tightly coupled to the lattice and the absorbed energy thus raises the lattice temperature.

A second type of bolometer makes use of the marked temperature coefficient of resistance of a superconducting metal near its transition temperature. The transition can take place in a very pure metal over as little as $.001^{o}K$ but small variations in the material used and method of preparation may increase this range slightly. This type of bolometer has a long time constant and generally does not have a greater sensitivity than the germanium detector. In addition it requires fairly sophisticated temperature control to keep the element within a fraction of one degree Kelvin of its transition temperature.

(d) Indium Antimonide detectors

The normal photoconductive detectors rely on the excitation of carriers from the valence band or from impurity levels to the conduction band in a semiconductor. They can thus be constructed to operate over the whole of the infra-red band with a long wave cut off corresponding to the energy required to excite electrons across the energy gap.

In Indium Antimonide (InSb) the effective mass for electrons is very small ($.013m_e$) and the dielectric constant is comparatively large. The impurity levels are consequently very shallow and the Bohr radius for hydrogenic impurity centres is very large. This causes the orbits for each impurity centre to overlap unless the material is exceedingly pure ($<10^{13}$ impurity centres per cc) and the impurity levels thus merge with the conduction band. The material is thus metallic in behaviour, even at very low temperatures.

In a high mobility semiconductor such as InSb the conduction electrons are very weakly coupled to the lattice at low temperatures, and under the action of weak electric fields the mean energy of the carriers is raised above the thermal energy of the lattice. Since the carrier mobility depends on the mean energy of the carriers this increase in energy causes a change in mobility, and a corresponding change in conductivity. The carriers can also absorb energy from a high frequency field, and the associated change in conductivity can be used to detect the presence of the high frequency field. At long wavelengths this "hot electron" effect is independent of wavelength, but as wavelength is reduced to about 1mm the absorption of radiation begins to fall and the sensitivity of the detector is reduced (Putley 1965).

If a medium magnetic field (up to 0.6 Teslas) is applied to a semiconductor the conduction band is split into a series of sub bands of "Landau levels", and with each such level is an associated impurity level. These impurity levels correspond to the quantised orbits of

impurity electrons spiralling about the applied magnetic field. At helium temperatures only the lowest Landau levels are populated and the mobility is now even more dependent on the mean energy of the carriers above the thermal energy of the lattice. The sensitivity of the detector is increased, because of the reduction in the mobility, and the increased dependence of mobility on mean carrier energy.

If large magnetic fields are applied at low temperatures only the lowest Landau level is populated (Magnetic Freeze Out) and the sensitivity of the detector falls to zero (Putley 1960). However, in the presence of a large field it is possible for radiation at the cyclotron resonance frequency to excite electrons from one Landau level to the next, making possible a tuneable detector.

Indium antimonide detectors are usually operated at liquid helium temperatures where the mean energy of the lattice is much lower than that of the hot electrons. They have an exceptionally fast response time, usually less than 1 micro-second, and since they show a very non-linear current voltage relationship they can be used successfully as mixers as well as detectors (Arams et al. 1966). Typical values for the N.E.P. are of the order of 10^{-13} watts with a magnetic field and 10^{-11} watts in the absence of a magnetic field.

(e) Golay detector

This detector is a room temperature bolometer relying on the expansion of a gas as it absorbs the incident radiation. The gas is contained in an enclosure having one flexible wall and the expansion is detected by reflecting a light beam from the outer side of this membrane

PERFORMANCE OF SUB-MM DETECTORS

Detector	Sensitive Area mm^2	Operating Temperature ^oK	NEP for 1 cps Bandwidth w	Responsivity vpw	Response time sec	Operating Wavelength and other conditions
Ideal Superheterodyne		300	4×10^{-21}			$\lambda >$
		300	2×10^{-18}			λ = 1mm "1000 photon condition"
		300	2×10^{-17}			λ = 0.1mm
Ideal thermal receiver	100	300	5.5×10^{-11}			Background at operating temperature
	100	1.5	9.8×10^{-17}			
	100	1.5	3.6×10^{-13}			300^oK background for $\lambda > 100\mu$
	100	1.5	1.8×10^{-14}			300^oK background for 10% band at 500μ
Golay pneumatic detector	1.5	300	3×10^{-10}	$\sim 10^5$	0.015	λ < 5mm
Carbon bolometer	20	2.1	1×10^{-11}	2.1×10^4	0.010	Operates over whole of sub-mm band at least
Germanium bolometer	15	2.15	5×10^{-13}	4.5×10^3	4×10^{-4}	As for carbon bolometer
	15	2.15	3×10^{-12}		1×10^{-4}	
Superconducting tin bolometer	6	3.7	3×10^{-12}		1.25	As for carbon bolometer
Ideal photoconductive detector	100	1.5	6.5×10^{-13}			$\lambda = 100\mu$. 300^oK background for $\lambda > 100$
	100	1.5	6.5×10^{-14}			$\lambda = 1000\mu$. 300^oK background for 10% band at 500μ.
	100	1.5	1.8×10^{-14}			
InSb wide-band detector using magnetic field	5	1.5	2×10^{-11}	200	2×10^{-7}	$\lambda = 200\mu$
			1×10^{-11}	500		$\lambda = 500\mu$
			5×10^{-12}	1000		$\lambda = 1000\mu$
InSb detector without magnetic field	15	4	10^{-12}		3×10^{-7}	λ 0.5 to 8mm. This sensitivity was achieved with a narrow-band amplifier not permitting full exploitation of fast response.
Ge cyclotron resonance detector	2	4	2×10^{-12}	$\sim 10^6$	5×10^{-9}	λ = 8mm
Tuned InSb detector	25	4	5×10^{-11}		10^{-6}	Responds over a bandwidth of about 12% within range 150μ - 60μ.
Meredith and Warner superheterodyne		300	7×10^{-15}		10^{-9}	λ = 2mm

Table 5.2. MILLIMETER WAVE DETECTORS

on to a photocell (Golay 1947). The detector is independent of frequency, the long wavelength limit only being set by the size of the aperture admitting the incident radiation. It has a sensitivity comparable with most other thermal detectors, but its main disadvantage is its long time constant (~ 15msecs) and its sensitivity to mechanical vibration. It does not, however, require any low temperature apparatus.

A comparison between the various types of detector is shown in Table 5.2.

5.5 Conclusion

The various techniques for the generation, detection and propagation of millimeter radiation have been discussed with particular emphasis on those techniques which differ from conventional microwave techniques. The obvious source of millimeter power is the backward wave oscillator, but the short lifetime and high cost of tube and power supply make this an impracticable choice. The next best source is a high-power reflex klystron from which several harmonics can be generated, and this was the method chosen for the studies reported in this thesis.

Several detectors have been compared experimentally and the results obtained with them will be compared in Chapter VI.

References

Arams, F., Allan, C., Peyton, B. and Sand, E., Proc. IEEE 54 612, 1966.

Becker, R.C. and Coleman, P.D., Proc. Symp. on mm. waves, New York p.191, 1959.

Bled, J., Bresson, A., Papoular, R., and Wegrove, J.G., Orde Elect. XIIV 26, 1964.

Boyd, G.D. and Gordon, J.P., Bell Syst. Tech. Journal 60 489, 1961.

Buckmaster, H.C. and Dering, J.C., Canadian Journal of Physics 43 1088, 1965.

Burros, C.A. and Tarambula, R., Proc. R.E. 49 1075, 1961.

Cullen, A.L. and Gillespie, E.F.F., Proc. Symp. on mm waves, New York p.109, 1959.

Feher, G. and Richards, P.L., Proc. Int. Conf. of Magnetic Resonance in Biol. Systems, Stockholm, 1967.

Froome, K.D., Proc. IEEE 1933 1169, 1962.

Froome, K.D., Proc. 3rd Int. Conf. on Quantum Electronics 2 1527, 1963.

Golay, M.J.E., R.S.I.I 18 357, 1947.

Gordy, W., Rev. Mod. Phys. 20 668, 1948.

Gordy, W. and Jones, G., Phys. Rev. 135A 295, 1964.

Griensmann, J.W.E. and Birenbaum, L., Proc. Symp. on mm. waves, New York, 1959.

Johnson, C.M., Slager, D.M. and King, D.D., R.S.I. 25 213, 1954.

Jones, R.C., J. Opt. Am. 43 1, 1953.

King, D.D. and Schelsinger, S.P. IRE Trans. on MTT MTT5 31, 1957.

Langenberg, N. Scalapino, D.J. and Taylor, B.N., Scientific American, 214 5 30, 1966.

Mathias, L.E.S. and Crocker, A. Physics Letters 13 35, 1964.

Meredith, R. and Preece, J.H., IEEE Trans. M.T.T. MTT11 322, 1963.

Putley, E.H. "Hall Effect and Related Phenomena" Ch. 4 p.180, 1960.

Putley, E.H., Applied Optics 4 649, 1965.

Rosenbaum, F.J., R.S.I. 35 1550, 1964.

Smith, A.G., Gordy, W., Sommers, J.A. and Smith, W.V., Phys. Rev. 75 266, 1949.

Sommers, G., Proc. I.R.E. 47 1201, 1959.

Taub, J.J., Hinair, H.J., Hinkelmann, O.F. and Wright, M.L., IEE Trans M.T.T. MTT11 338, 1963.

Tischer, F.J., IEEE Trans. M.T.T. MTT11 291, 1963.

Torrey, H.C. and Whitman, C.A., "Crystal Rectifier Radiation Lab. Series", McGraw Hill, 1948.

Van Es, C.W., Phil. Tech. Rev. pp.122-181, 1960.

Vernon, F.L., Homodyne Spect. I.R.E. Trans. A.P. 14 110, 1952.

Zimmerer, R.W., R.S.I. 33 858, 1962.

CHAPTER VI

CONSTRUCTION AND USE OF APPARATUS

In order to make measurements on magnetically dilute systems containing paramagnetic ions with large zero field splittings a spectrometer, having as large a sensitivity as possible and operating at the highest practicable microwave frequency, is needed, as has been discussed in Chapter II. The limits to microwave frequency were set by the availability of a suitable source at a reasonable cost.
The spectrometer was also designed for use in a more conventional form for such investigations as g-value variations and line width studies at high magnetic fields, and consequently another limit to the microwave frequency was the availability of suitable magnetic fields. At the time when the spectrometer was initially designed the maximum available field at reasonable cost and suitable homogeneity was 5.0 Teslas (50 Kilogauss) from a superconducting magnet. The maximum useful frequency is thus of the order of 140GHz, and the greatest versatility was available by generating the 140GHz power as a harmonic from a 70GHz klystron, thus enabling the fundamental to be used as a source for a 70GHz spectrometer in addition.

6.1 Design of Spectrometer

The design of any millimeter spectrometer is severely limited by the availability of millimeter components. Modern sophisticated designs using homodyning and balanced mixing are not readily applicable at

millimeter wavelengths since such components as circulators and balanced mixers have not yet been developed. For reasons outlined previously a 4mm klystron was chosen as the fundamental source of power, and conventional waveguide techniques were employed to propagate the power, except where long waveguide runs were needed. In such cases oversized waveguide runs were used. The final factor determining the choice of spectrometer system concerns the resonator. Any resonator for use at 4mm or shorter wavelengths will have dimensions of the same order of magnitude as the wavelength and thus a single waveguide coupling scheme would appear to be most practicable. For these reasons a straightforward reflection spectrometer using magnetic field modulation was chosen. The major advantages and disadvantages of the various techniques available have been discussed and the reasons for the choice of components outlined in Chapter V.

The particular components of the four and two millimeter spectrometer will now be discussed in more detail.

6.2 The 4mm Klystron

The klystron used in the spectrometer is a Phillips YK1010 Reflex klystron operating in the frequency range of 68GHz to 72.3GHz. It has a maximum power output of 110mW, although this figure varies considerably from valve to valve, and steadily decreases as the klystron ages. The klystron is operated with the cathode at -2.5KV, the reflector at -400V relative to the cathode, and the grid between 0 and -150V relative to the cathode. The current drawn from the power supply is of the order of 18mA, but this value falls rapidly as the valves age.

Klystrons of this type are still rather thermally unstable and tend to exhibit a very marked hysteresis effect. The problem of thermal instability was partially overcome by fitting water cooling jackets to the valve. These jackets fit in good thermal contact to the external surfaces of the resonator and the coupling and matching waveguides pass through them. The hysteresis problem makes tuning of the klystron to any particular frequency rather difficult, and the klystron must be tuned mechanically and electronically simultaneously. The tuning of the klystron is normally carried out by modulating the reflector supply at 50Hz and displaying the klystron mode on an oscilloscope. The absorption due to a wavemeter or sample cavity can thus be easily observed. As the amplitude of the modulation is reduced the klystron frequency shifts considerably and mechanical tuning of the resonator is necessary to keep the frequency constant. The problem of tuning is also aggravated by the fact that the oscillating frequency is slightly dependent on the direction in which the reflector voltage approaches the required value (hysteresis).

Even with the aid of the water cooling it was necessary to automatically lock the klystron frequency to some reference frequency and the method used to do this will be described later.

The klystron is supplied with a suitable power supply by the manufacturers, but this proved to be most unsatisfactory in operation, since it delivered voltages having several millivolts of 50Hz hum and several volts of higher frequency, irregular pulses superimposed on the d.c. value. This effect introduced a very serious source of noise on the microwave power. The klystron was therefore studied as carefully as

TABLE 6.1

Electrode	Sensitivity
Heater	1 GHz/Amp (at 1.75 amps)
Grid	~ 10 MHz/volt (over 20 volt range)
Reflector	2 MHz/volt (at mode centre)
Cathode	7 MHz/volt (at 2500 volts)

TABLE 6.2

Supply	Stability	Ripple
Cathode		
300v - 3000v 0 - 60mA	2 parts in 10^6	2mV p-p
Reflector and Grid		
20v - 600v	1 in 10^4	200μV p-p
Heater		
0 - 7v	1.5 in 10^4 (voltage)	10mV p-p
0 - 3.5A	1.2 in 10^4 (current)	

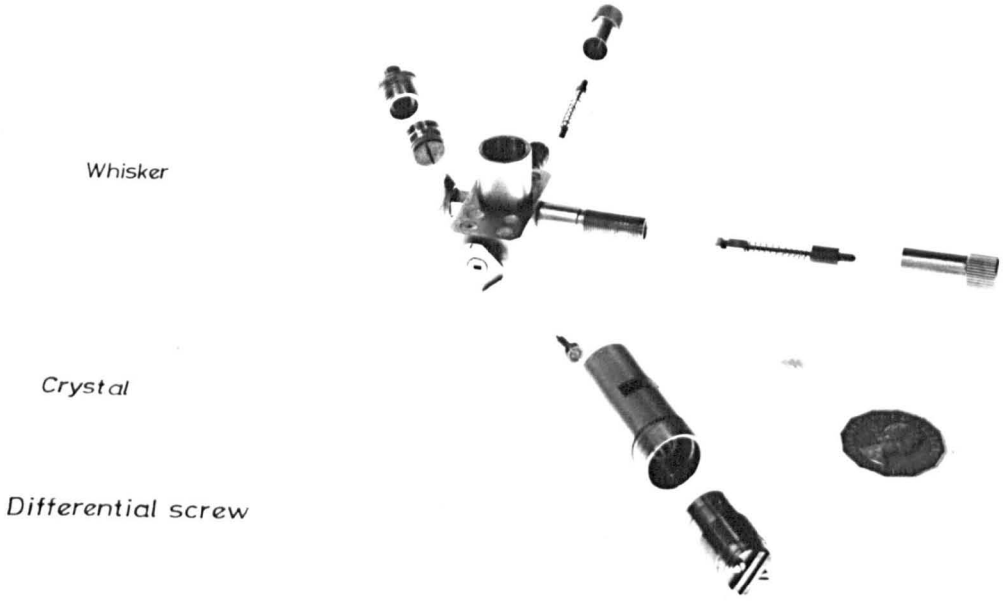

Fig 6·1 2mm HARMONIC GENERATOR

possible using battery driven power supplies where possible to determine the frequency dependence of the output as a function of each supply voltage independently. The accuracy of such an investigation was limited to the accuracy of the wavemeter, and the required stability is set by the width of the spectral lines which are being studied. In this case, the limit to the minimum detectable linewidth is set by the magnet, so this can also be used to determine the minimum frequency stability required. The frequency dependence of the klystron as a function of the various electrode voltages is given in Table 6.1a. These figures were used to determine a minimum specification for the klystron power supply, and a supply having an even better specification than that required was manufactured by the Phillips Research Laboratories in Eindhoven and exchanged for the original. The specifications are given in Table 6.1b and the experimentally determined values were found to be at least as good as these.

The klystron frequency was also found to be very sensitive to stray magnetic fields, and so it was screened with mu-metal to cut down this effect. In view of the large attenuation involved in waveguide runs it was not practicable to move the klystron away from the magnet.

6.3 2mm Harmonic Generator

The 2 millimeter wavelength radiation is generated in an harmonic generator using the YK1010 4mm klystron as the fundamental source. The generator is of the crossed waveguide type as has been described in Chapter V. Its construction is illustrated in Figure 6.1.

The separate silicon crystal is mounted on a short brass pillar which can be moved into the 2mm waveguide by a differential screw mechanism which moves the crystal 0.4mm per revolution. The whisker and its mount are held in a spring loaded clamp and pass through the 4 millimeter guide into the 2 millimeter guide to make a rectifying contact in the 2 millimeter waveguide. The contact is made as follows. The crystal is withdrawn from waveguide with the differential screw and the whisker is pushed slowly into the guide with a simple tool provided by the manufacturer. The whisker is observed with a magnifier as it enters the 2mm guide, and it is pushed most of the way across the guide, leaving a small gap between it and the guide wall. The generator is then placed in a waveguide run, the four millimeter power applied to it. A microvoltmeter is then connected across the contacts to crystal and whisker. The crystal is then slowly screwed into the waveguide until contact is made with the whisker. The point of contact is indicated by a deflection on the microvoltmeter. The pressure on the contact is increased slightly to ensure stability. At this point two millimeter power can be detected in the 2mm waveguide run.

If it is required to amplitude modulate the 2 millimeter power this can be done by applying the modulating signal across the terminals of the harmonic generator. A signal of 2 volts R.M.S. is sufficient to switch the harmonic power off once per cycle.

D.C. bias can also be applied to the generator via these same contacts, but this does not improve the performance of the harmonic generator.

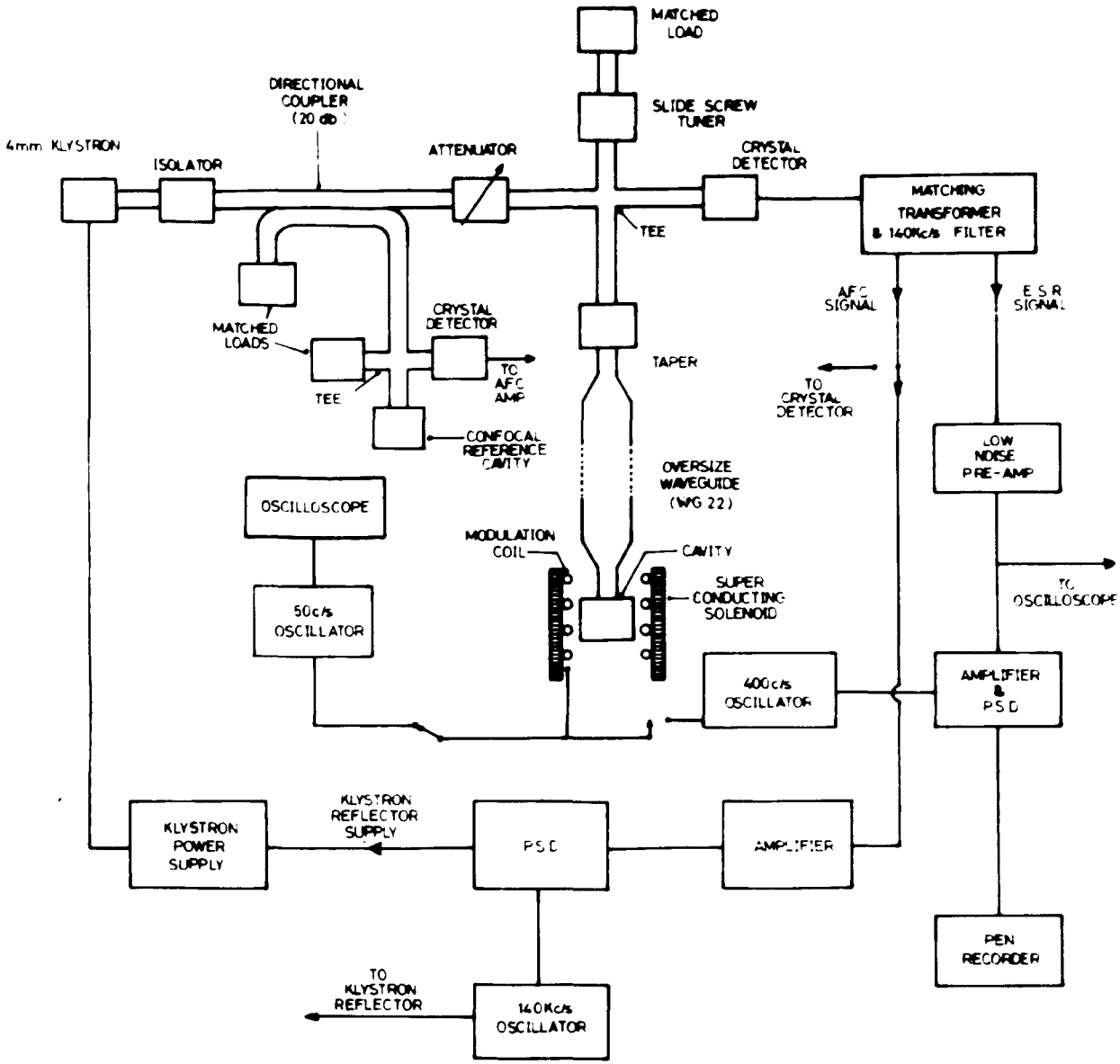

Fig 6·2 4mm. SPECTROMETER.

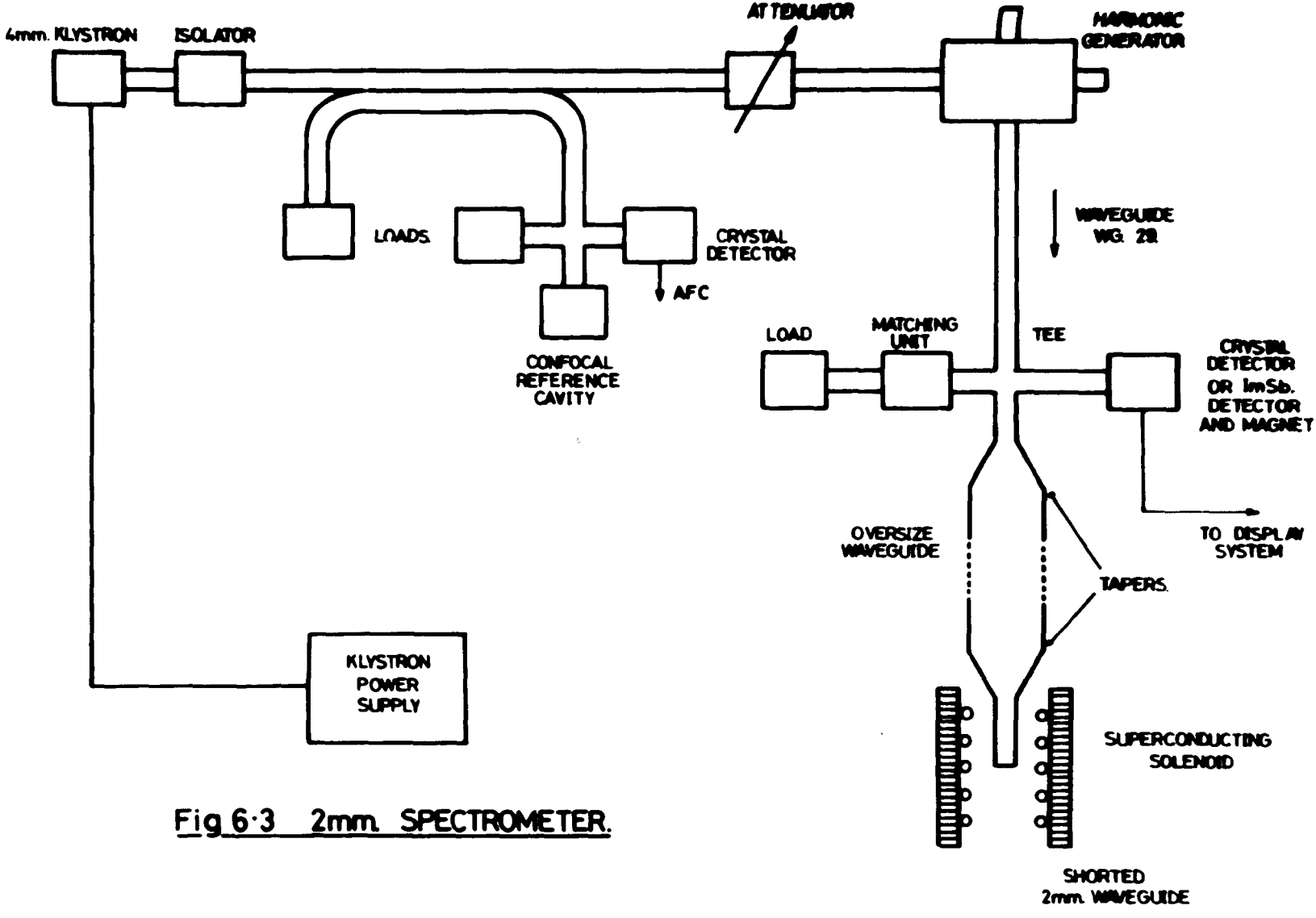

Fig 6·3 2mm. SPECTROMETER.

6.4 2 and 4mm Waveguide Systems

The waveguide systems for the four and two millimeter wave spectrometers are shown in Figures 6.2 and 6.3. In both cases 4mm power is fed along standard 4mm waveguide through an isolator, 20db directional coupler and an attenuator, to either a magic tee or harmonic generator. It was also necessary to screen the isolator magnetically since its properties were found to be very dependent on stray magnetic fields. The directional coupler is used to couple out fundamental power in order to operate one of the forms of automatic frequency control.

To operate the 4mm spectrometer the power is fed from the attenuator to a millimeter wave bridge consisting of a magic tee used in the conventional manner. Power is fed from one arm of the tee to the sample, using tapers to W.G.22 (Q-Band) and a suitable length of oversized waveguide. A slide screw tuner is placed in series with this line to match out reflections from the tapers and to match the standard waveguide to the tapers and oversize waveguide. The sample is contained in either a piece of short circuited waveguide or a sample cavity. The power is transferred back to standard waveguide in order to facilitate coupling to 4mm cavities. If the spectrometer is being used with a shorted waveguide sample holder, it is generally more practicable to use shorted oversize waveguide, and to overcome the loss in sensitivity by using a larger sample. The sensitivity of the spectrometer using a cavity and a length of shorted waveguide will be discussed later in this chapter.

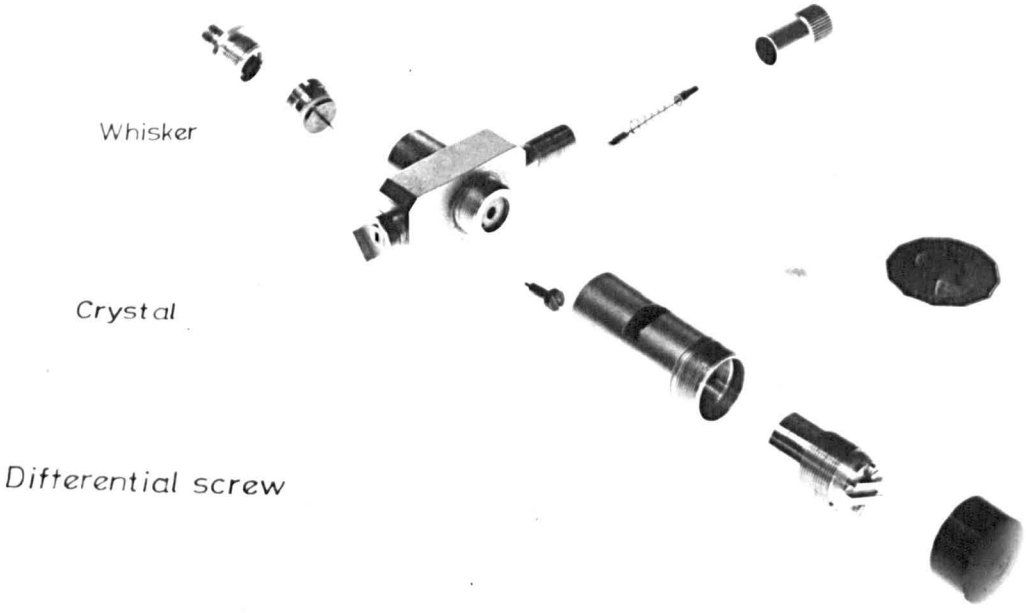

Fig 6·4 2mm CRYSTAL DETECTOR

The balance arm of the magic tee contains a slide screw tuner and a matched load. From this arm a small amount of power of variable amplitude and phase can be reflected back to provide the necessary microwave bias to the detector, should this be required. Careful use of this reflected power also makes possible the detection of the dispersive component of the electron spin resonance signal, by changing the phase by 90° using the slide screw tuner. Observation of the dispersive component can only be observed when the klystron is locked to the reference cavity since otherwise the klystron frequency follows the frequency change of the cavity corresponding to the dispersive signal.

6.5 Millimeter Wave Detection System

6.5.1 Crystal detectors

The IN53 crystal is the most convenient detector in the 4mm region, although it is not quite so sensitive as other detectors which are available. The crystal is mounted in a commercially manufactured holder of conventional design, but having the additional refinement that the crystal can be moved across the waveguide to obtain the most sensitive position. This type of detector is very convenient to use but its performance is very frequency dependent and it requires fairly careful matching to the waveguide run, using a slide screw tuner.

The crystal detector used at 2mm is of the type described in Chapter V where the metal-semiconductor junction is formed in the waveguide by the experimentalist. A diagram of the particular detector used in this spectrometer is shown in Figure 6.4. The junction is formed in exactly the

same way as for the harmonic generator except that the diode is placed in an audio-frequency circuit to detect when a rectifying junction has been formed, since only small amounts of two millimeter power are available. The detector, like the harmonic generator, is very susceptible to mechanical vibration and atmospheric humidity and the junction usually has to be reformed every time it is used. At two millimeters this detector proved to be extremely noisy, rather insensitive and very troublesome to use successfully.

6.5.2 Golay detector

The performance of a Golay cell as a detector of both two and four millimeter radiation was compared with the corresponding crystal detectors. The output from the photocell of the Golay head is fed via an internal impedance matching device to a phase sensitive detector or oscilloscope. At two millimeters the Golay output at 15Hz was of the order of three times larger than that from a crystal detector but no detailed comparisons were possible since the Golay detector was only available for a short period.

At four millimeters a comparison was made by observing an electron spin resonance line from a sample of iron doped rutile using a crystal detector and the Golay. The Golay was very much inferior to the crystal detector, giving a signal to noise ratio of the order of 2:1 compared with at least 20:1 for the crystal detector. No attempt was made to match the waveguide to the Golay window and no doubt a large amount of power was reflected at the sharp transition from waveguide to Golay window.

The detector was also found to be very microphonic. The experiment simply proved that the Golay cell can be used as a detector in a millimeter wave electron spin resonance experiment and it may even prove to be a more practicable detector at 2mm wavelengths provided that careful precautions are taken to provide a rigid mount, and a suitable waveguide transition is designed.

6.5.3 Indium antimonide detector

The third type of detector assessed in the construction of the spectrometer was an indium antimonide photoconductive detector, the semiconducting element of which was supplied by the physics division of the Royal Radar Establishment. The principle of operation of this detector has been described in Chapter V.

To test the performance of the detector a 70KMHz electron spin resonance signal was observed at room temperature using the 8" electromagnet, from Fe^{3+} in rutile. The detecting element was placed at the end of a length of oversized waveguide in the superconducting magnet. The element was cooled to $4.2^{o}K$ along with the superconducting magnet and the whole experiment was carried out with the detector at $4.2^{o}K$, no attempt being made to reduce the temperature further. The performance was once again compared with a crystal detector, but it must be noted that a long length of waveguide and a transition were needed in order to transport the power to the InSb detector which were not included in the run to the crystal detector. The electron spin resonance line was observed using the crystal and the InSb detector, the latter being biased from a small battery with currents up to 100μA. The output from the detector was taken via a

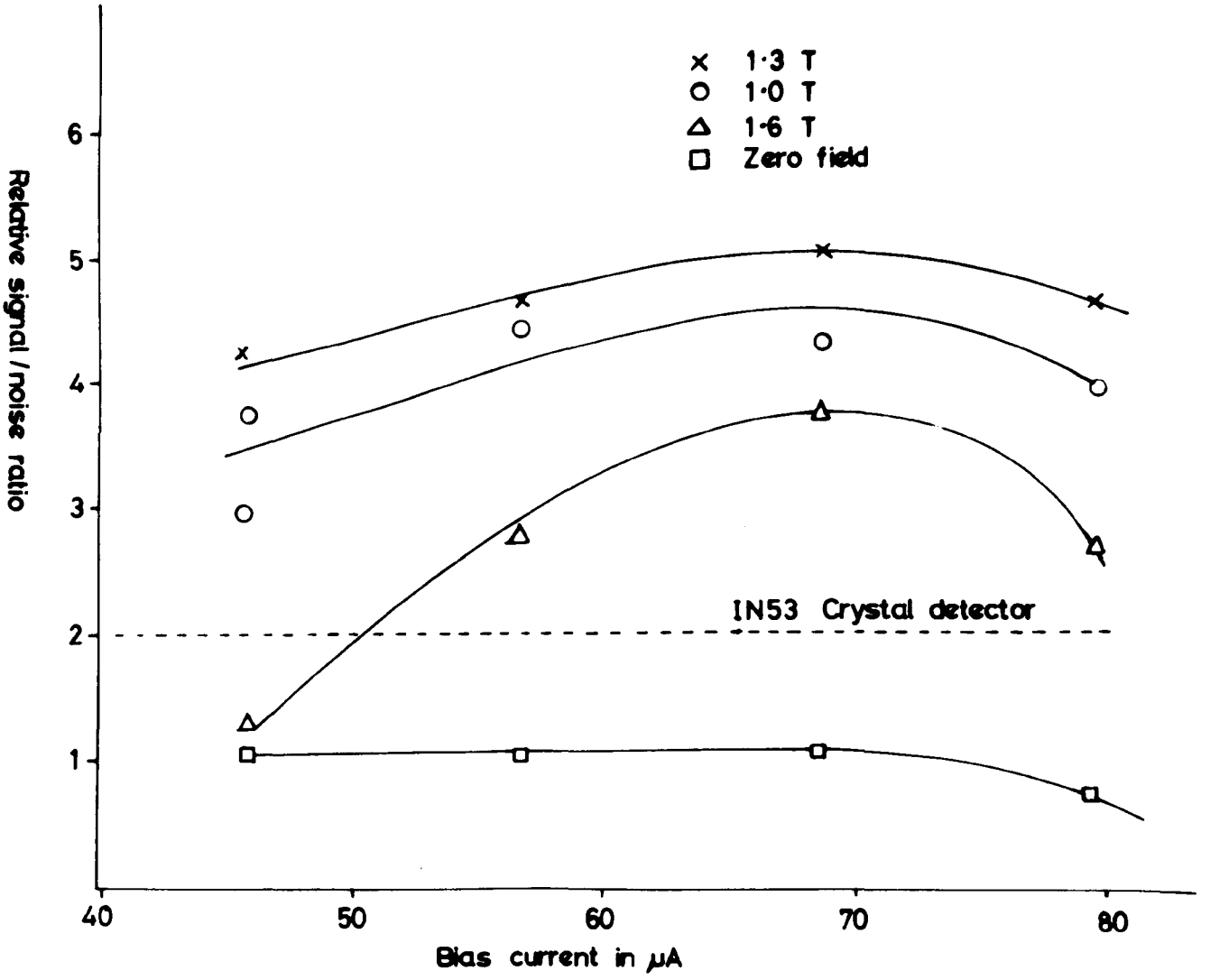

Fig 6·5 PERFORMANCE OF INSB DETECTOR

capacitor, to isolate the d.c. bias supply, to a room temperature transformer which matched its low impedance to that of the low noise pre-amplifier. The performance of the detector is shown in Figure 6.5 as a function of bias current and magnetic field. The signal to noise ratio of the e.s.r. signal is compared to that from the crystal detector. It is noticeable that under optimum conditions an improvement by a factor of 2.5 was obtained despite the long attenuating waveguide run. This could doubtless be improved several times by careful design of the cryogenic system so as to avoid waveguide bends and long runs of oversized waveguide. In this case, once again, no attempt was made to ensure accurate matching and the performance could further be improved by using a carefully shaped element.

The optimum operating conditions for the particular element used are a bias current of 70μA and a field of 1.3 Teslas (13 Kilogauss). Since this detector requires liquid helium, and nearly as high sensitivities are available with a crystal detector as will be shown later, the use of this detector will rarely be justified in a 4mm spectrometer. However, at 2mm where crystal detectors are very unsatisfactory it may prove an ideal alternative. Unfortunately no comparable test to the above could be made at 2mm, since, due to the low powers available and the low fields available from the electromagnet, no e.s.r. signal could be observed in this way.

6.6 Electronic Detection System

The basic techniques used to observe electron spin resonance signals have been described in Chapter II and so only a brief description of the method employed in this spectrometer will be given here.

6.6.1 Crystal video detection

The absorption curve can be displayed on an oscilloscope in the conventional manner using a video detection scheme. The magnetic field is modulated at 50Hz, and the amplified output displayed on an oscilloscope, whose time base is derived from the same source as the field modulation. The amplitude of the field modulation is made several times larger than the electron spin resonance linewidth where possible. In general this is possible by direct modulation of the electromagnet, except for very large linewidths, but with the superconducting magnet one is limited to a field modulation amplitude less than 3×10^{-4} Teslas (3 gauss) peak to peak because of limitations imposed by the power supply which will be described later. The amplified output from the detector is displayed on an oscilloscope, whose X-deflection plates are swept from the same source as the magnetic field modulation. A phase shift network and blanking circuit are included in the oscilloscope sweep circuit to facilitate the display.

The pre-amplifier is a model CR-4 low noise amplifier manufactured by the Princetown Applied Research Corporation. It is a four stage amplifier having an overall voltage gain of 10^4, high and low impedance input stages and a filter capable of reducing the bandwidth

in a series of fixed steps. The crystal impedance is matched to the amplifier using a transformer whose secondary impedance is a maximum at the modulation frequency, 405Hz. Under the conditions at which the spectrometer is operated the pre-amplifier has a noise figure of 6db. The maximum bandwidth of the amplifier is 300KHz, but this can be reduced with a series of switched high and low frequency roll off filters having attenuations of 12db per octave. The gain of the amplifier can thus be peaked at a series of fixed frequencies. Since the filters are placed after the amplifier it is often possible to saturate the amplifier with noise pulses which are outside the filter bandwidth. The amplifier is used in the wide band condition for the crystal video mode of operation and the bandwidth is adjusted so that the 6db points occur at 300Hz and 1KHz for operation with the phase sensitive detector.

The presence of the matching transformer detracts from the performance of the spectrometer when used in the crystal video mode of operation since it is matched at one frequency only. However, since the spectrometer is generally only used to observe large signals with this method this is not a serious consideration. The transformer also serves to provide a low impedance d.c. path for the rectified current of the detector; a method generally employed to reduce the overall noise power output from the crystal (Robinson 1962).

In the case of the 2mm crystal detector the transformer is usually committed since this detector is, of necessity, operated at very low bias powers, where its impedance is comparatively large, and the matching is so poor as to reduce the performance of the detector.

6.6.2 Phase sensitive detection

For the detection of low intensity E.S.R. signals a phase sensitive detection system is employed. The phase sensitive detector used in this spectrometer is a Princetown Applied Research Corporation, model J.B.4. This instrument can be operated at any frequency between 15Hz and 15KHz. It consists of a tuned amplifier feeding a full wave coherent detector. The reference signal can either be derived from an internal oscillator or from some other generator. It is usually employed with its own oscillator which also delivers a variable output. This output is used to drive a power amplifier which feeds the field modulation coils. The output from the phase sensitive detector contains the usual R-C integrating network, with time constants ranging from .001secs to 10secs, with the facility for changing the cut off rate of the integrating network from 6db per octave to 12db per octave. The derivative of the electron spin resonance absorption curve derived from this method of detection is displayed on a Varian G-10 potentiometric recorder.

A block diagram of the electronic detection system is shown in Figure 6.2.

6.7 Klystron Frequency Stabilisation

Despite the success of the water cooling jackets in overcoming the thermal instability of the klystron it was still found necessary to automatically lock the klystron frequency to some reference cavity or to a sample cavity, in order to use sample cavities having high Q factors.

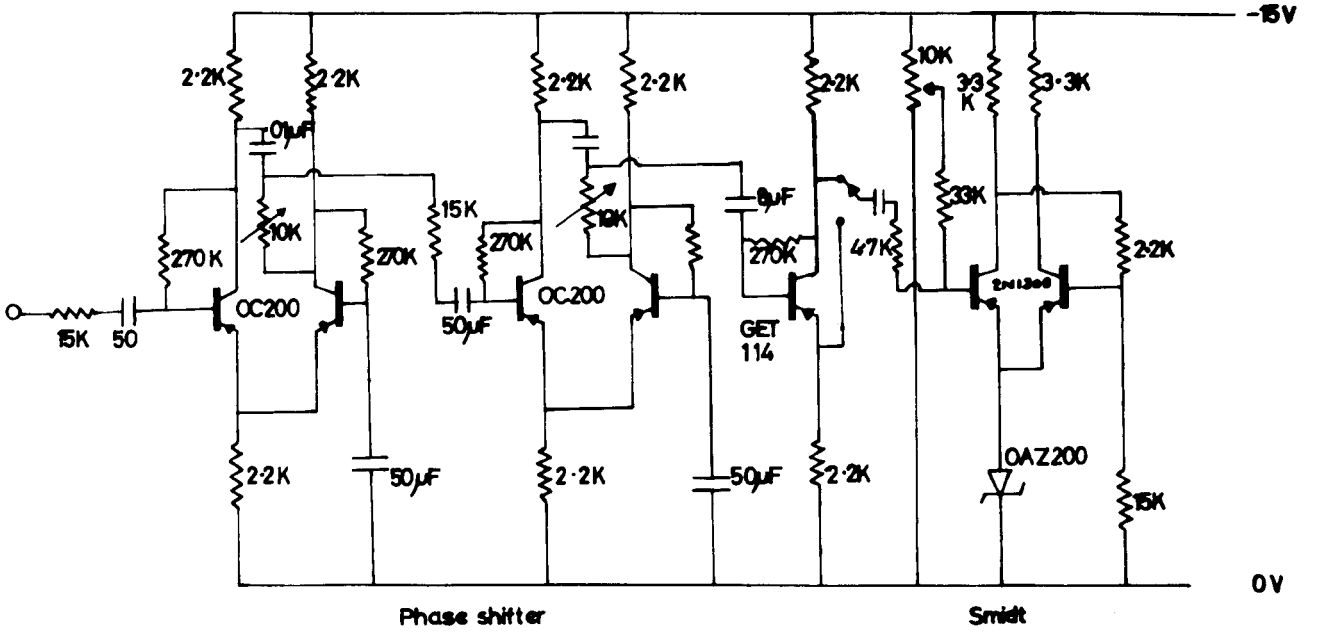

Fig 6-6 PHASE SHIFTER AND SQUARE WAVE GENERATOR

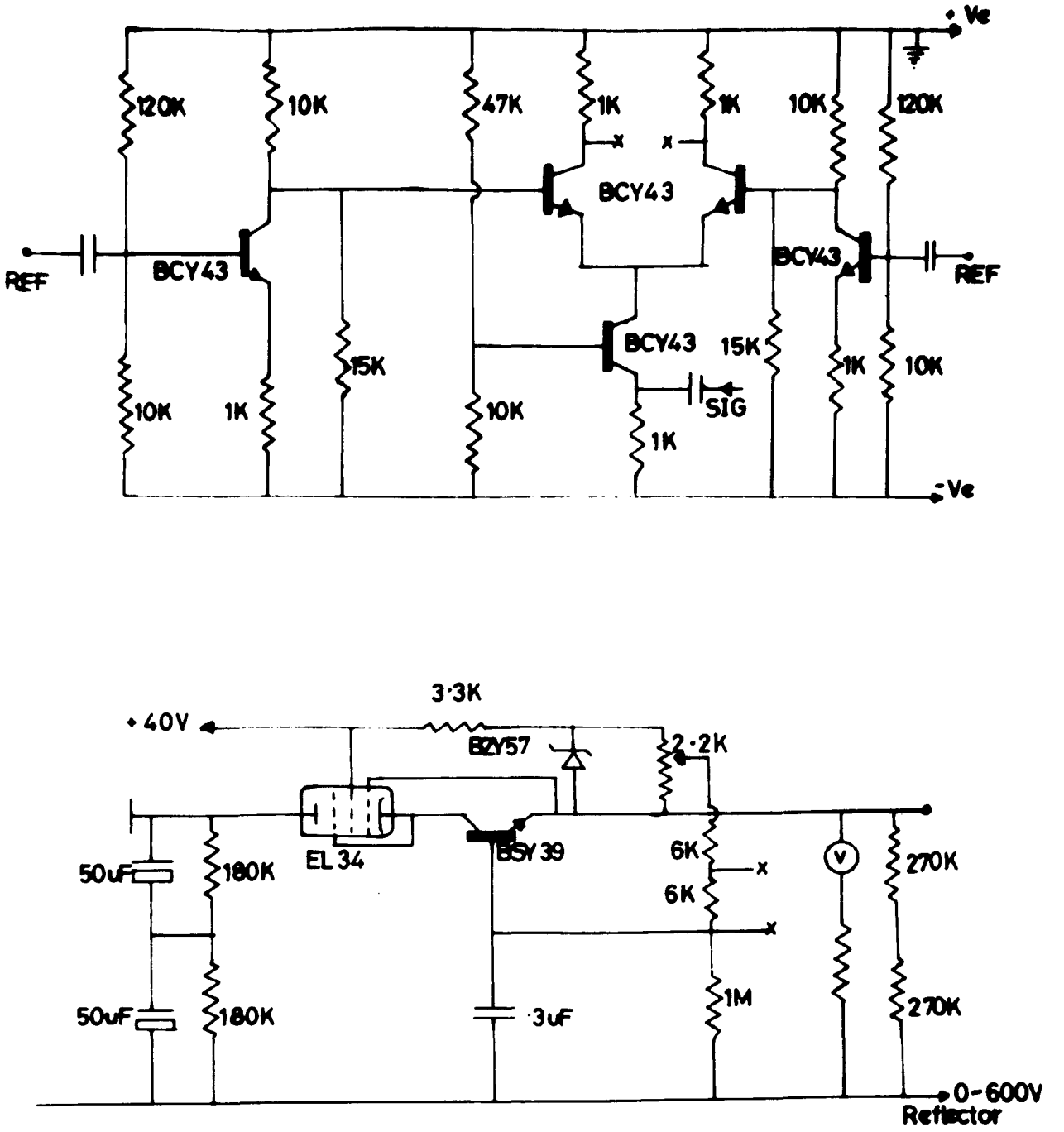

Fig 6·7 P. S. D. AND REFLECTOR SUPPLY

The method used to do this was basically that described by Poole (1958), although in these studies transistorised circuits have been used throughout.

To lock the klystron to the sample cavity the klystron reflector is modulated at 60KHz, producing a 60KHz frequency modulation on the microwave power. An error signal is taken from the detector crystal using an R-C filter to eliminate any field modulation frequency components. This error signal will only contain harmonics of the 60KHz modulation frequency when the klystron is tuned to the resonant frequency of the cavity, but will contain a 60KHz component of increasing amplitude as the klystron is detuned. The phase of this error signal will depend on whether the klystron frequency has increased or decreased from the cavity resonant frequency since the impedance of the cavity changes from being capacitive to inductive on tuning through the resonance. The error signal is amplified in a high gain amplifier and fed to a phase sensitive detector, of the type described by Faulkner (1966). The reference signal for the phase sensitive detector is derived from the same oscillator as is used to modulate the klystron reflector. The reference signal is first fed through a two stage transistor phase shifter and then to a Smidt Trigger in order to produce a square wave. The circuit diagrams of the phase shifter and the Smidt Trigger are shown in Figure 6.6, and the phase sensitive detector in Figure 6.7.

In the presence of an error signal the phase sensitive detector produces a d.c. voltage of amplitude and phase proportional to the deviation of the klystron frequency from that of the resonant cavity.

This voltage is applied to the klystron reflector power supply in series with its own stabilising control voltage as shown in the circuit diagram of Figure 6.7. This avoids the usual need for d.c. amplification after the phase sensitive detector since such amplification is likely to introduce instability, and add noise to the reflector supply. To avoid introducing further modulation components at or near the modulation frequency from the phase sensitive detector a time constant of the order of 100μs is introduced after the phase sensitive detector.

Since the output of the phase sensitive detector must float at -2.5 to -3KV the whole of the phase sensitive detector, phase shifter and Smidt Trigger are insulated and floated at the reflector potential, the a.c. reference and error signals being fed to them via isolating transformers, potted in Araldite.

The frequency stability of the klystron when locked to the sample cavity was estimated using a wavemeter and a second phase sensitive detector. The wavemeter was connected in place of the reference cavity and the klystron locked to the sample cavity. Since the wavemeter has a quality factor several times larger than the sample cavity it could thus be used as a discriminator to detect variations in the klystron frequency. The output from the second crystal detector, measuring the 60KHz component in the klystron output, was fed to a second phase sensitive detector using the same reference source as the stabilising system. A d.c. signal was thus obtained giving a measure of the deviation of the klystron frequency from that to which the wavemeter was tuned. The accuracy of this method is obviously limited but it was

possible to obtain an estimate of the klystron frequency stability. The stability was estimated to be at least 1 part in 10^5 over several hours by this method when the klystron was locked to the sample cavity.

The confocal reference cavity has a quality factor which is several times larger than the wavemeter (in fact ~15000) so this was not a practicable method of measuring stability in this case since the lower Q cavity does not detect any frequency fluctuations. However, since the klystron remains locked to the reference cavity for long periods one can assume that it is at least as stable, if not more so, than when locked to a sample cavity.

This type of A.F.C. system does not produce such a monochromatic source of power as the more sophisticated systems described by Pound and others (Pound 1946, 1947, Zimmerer 1959 etc.). However, it is considerably more simple to construct and to operate, and since the presence of the 60KHZ sidebands are well within the average electron spin resonance linewidth, the loss of a purely monochromatic source is not a serious consideration. In addition to this it is found that 4mm microwave components are exceedingly sensitive to small changes in frequency, a property which would make the setting up of a pound system even more tedious. The ultimate answer to the problem of a stable microwave source at 4mm would seem to be to use an X-band source, phase-locked to a crystal, and to phase-lock the 4mm klystron to the X-band source. Such a stabilisation system has been described by Meier (1964).

6.8 Resonant Cavities

Sample cavities operating in the H_{012} cylindrical mode have been successfully manufactured for use at 4mm wavelengths, but not at 2mm. Two types of cavity are required; one for each type of magnet. The choice of the H_{012} cylindrical mode is determined by the need to make the cavity as physically large as possible to simplify manufacture, consistent with not generating any unwanted oscillatory modes. The H_{012} cylindrical mode has a smaller filling factor than the H_{011} or H_{111} modes, which are also commonly used in E.S.R. sample cavities, but in the case of a 4mm cavity this is more than offset by the increased Q factor.

Cavities have been manufactured in copper by electroforming on stainless steel and aluminium mandrels and in silver by the same technique. They have also been manufactured by machining in copper, aluminium and brass, and invariably the cavities machined in brass have proved to have higher Q factors, despite the increased conductivity of copper, silver and aluminium. In an electroformed cavity the only dimension which can be guaranteed as accurate and to have a good surface finish is the bore of the cylinder, and it would appear that poor finish on the ends of the cylinder account for the poor Q factor. With a machined cavity by far the better finish is obtained with brass and this would seem to be the reason for the higher Q factor obtained with brass cavities. This idea is born out by the fact that there is very little increase in Q factor on cooling the cavity to liquid helium temperatures,

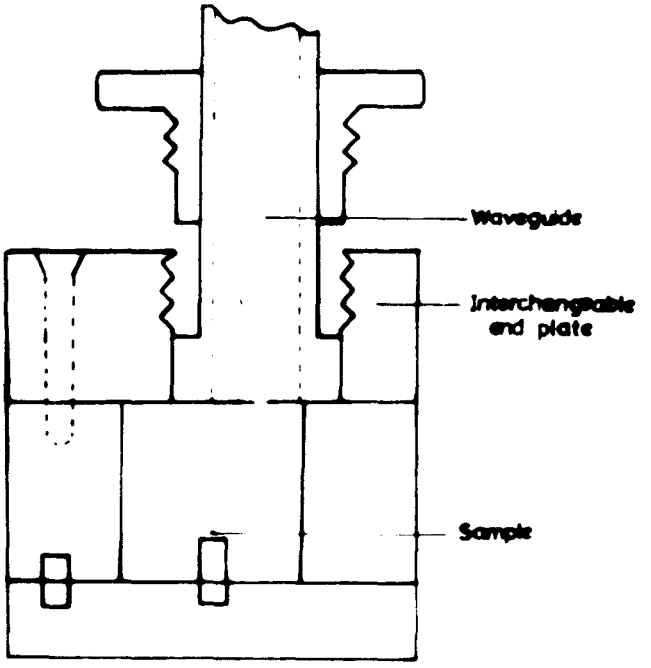

Fig 6·8 H_{012} Cylindrical cavity for use with electro-magnet

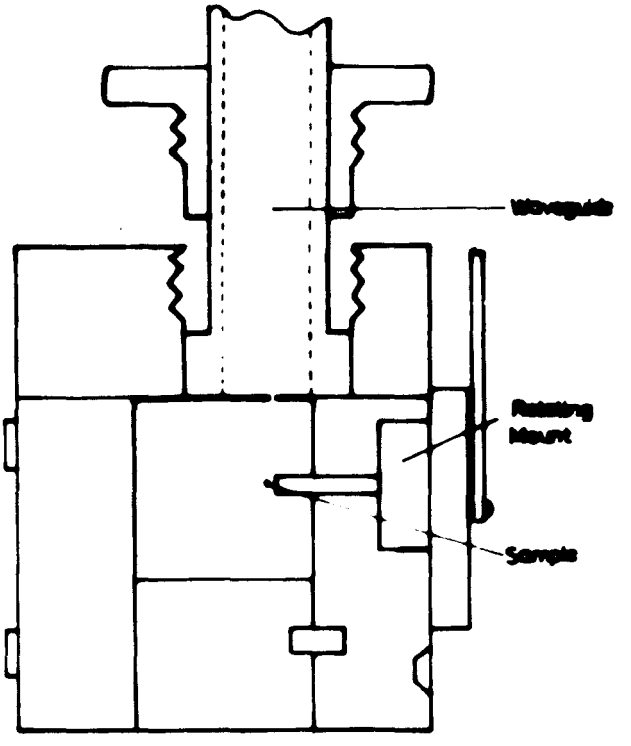

Fig 6·9 H_{012} Cylindrical cavity for use with superconducting magnet

despite a considerable increase in electrical conductivity. This would indicate that it is a mechanical property of the cavity which is setting the limit on the Q factor. The following method has therefore been adopted in the construction of 4mm wavelength cavities.

The piece of brass is first faced on a lathe, bored slightly undersize and parted off slightly oversize. The end faces are then ground on a surface grinding machine to within .001" of the required length. The bore and end faces are then hand lapped with varying grades of diamond lapping paste until the finish is better than 2 micro inches C.L.A. The end plates are also hand lapped to the same finish.

6.8.1 Cavities for use in electromagnet

The cavity used in the electromagnet is shown in Figure 6.8. It consists of a cylindrical hole bored eccentrically in a brass bar and finished as described above. The coupling hole is integral with the end plate of the cavity and is placed so as to be situated one quarter of the distance across a diameter of the cylinder. The end plate is held in position by two 10 B.A. screws. The waveguide is attached to the end plate by a screw and collar as shown in the figure. The base plate contains a small hole located so as to lie along the cylinder axis, and two locating pins are contained in this end plate, in order to ensure accurate location of this hole. The hole is used to locate a short length of quartz rod on which the sample is placed. The locating pins are a pressed fit so that they may be removed in order to re-polish the end plate.

The coupling to the cavity can be changed by using different upper end plates with different sized coupling holes, and also by rotating the coupling waveguide so that its long dimension is not parallel to a radius of the cavity. The amount of power coupled to the cavity for a fixed size coupling hole will then be approximately proportional to the cosine of the angle between the radius of the cylinder and the large dimension of the waveguide.

6.8.2 Cavities for use in superconducting magnet

The cylindrical cavity for use with the superconducting magnet has its axis of symmetry horizontal in order to keep the d.c. and r.f. fields mutually perpendicular, and power is coupled in via a hole on one side of the cylinder. The optimum size of this hole was determined by trial and error, and can only be changed by changing the whole cylinder. The coupling can also be varied by rotating the long dimension of the waveguide relative to the horizontal axis of the cavity. Rotating the waveguide in this manner could be expected to launch the E_{012} cylindrical mode, which is degenerate with the H_{012} mode, in the cavity. Fortunately, this does not appear to be the case, possibly because the E_{012} mode is suppressed by the relatively high impedance to radio frequency wall currents at the junction between the cylinder and its end plates.

It is frequently necessary to change the orientation of a crystalline sample relative to the external magnetic field. Normally this is done by rotating the magnet, but such a method is not possible with a superconducting magnet whose field is produced along the axis of

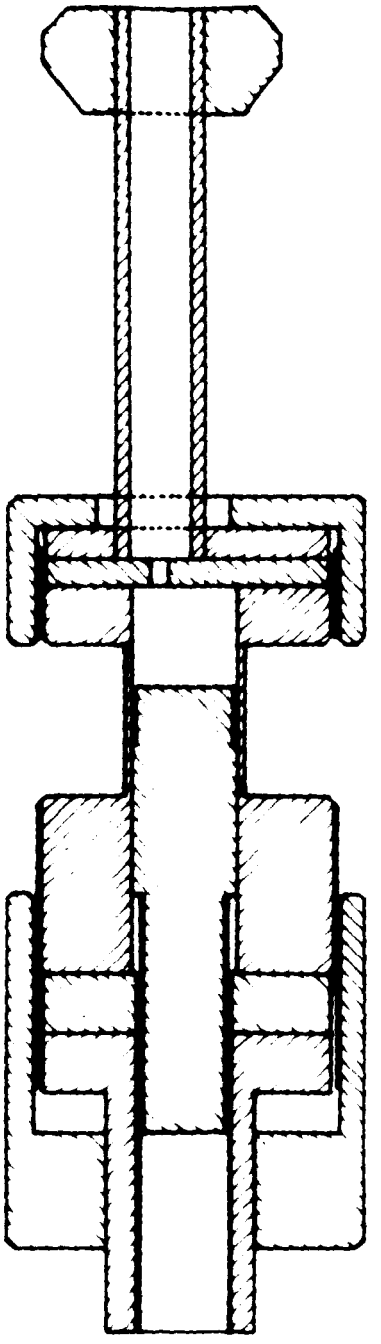

Fig 6·10 TUNEABLE CAVITY

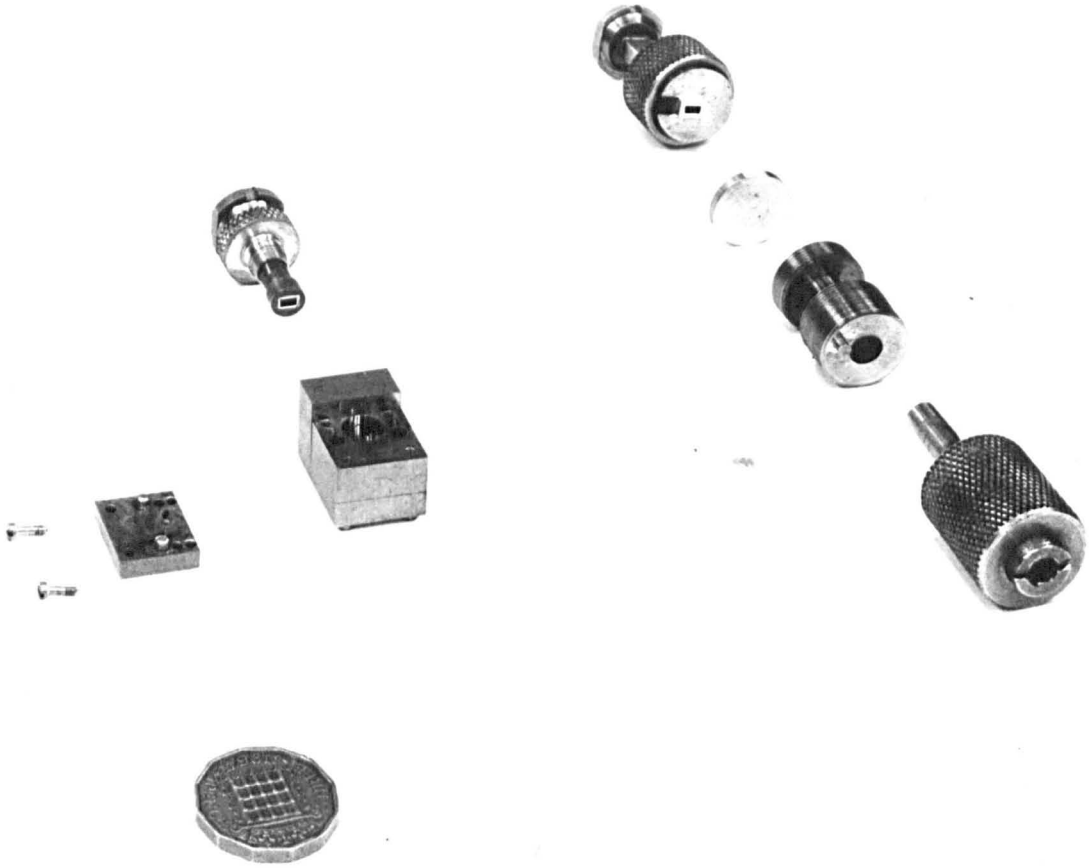

Fig. 6.IO(a) 4mm SAMPLE CAVITIES.

a solenoid. Consequently the cavity was designed so that the crystal could be rotated from outside the cryostat. This was done by drilling a hole through one end plate and attaching the quartz sample support to a separate circular plate. The plate is held in position by a countersunk hole in the end plate and by a small bracket. The rotation is brought about by pulling or pushing the plate at right angles to a radius via a long thin metal rod passing along the outside of the waveguide. The orientation is adjusted in known intervals using a fine thread and nut outside the cryostat. A diagram of the cavity is shown in Figure 6.9.

Cavities having a variable resonant frequency have also been manufactured in a similar manner. Here the frequency is varied by forming the lower end plate as a plunger attached to a screw adjustment, as shown in Figure 6.10. The adjustable cavity has a Q factor of about 2,000, whereas the fixed frequency cavities have Q factors lying between 7,000 and 11,000.

Attempts to manufacture dielectric tube resonators for use at 4mm wavelengths were invariably fruitless. The material used for such resonators must have as low a dielectric constant as possible in order to keep the physical size of the resonator as large as possible, have a low dielectric loss and be machinable. The most suitable material found was "Stycast Lo K" resin; a commercially available microwave dielectric having a dielectric constant of 1.6 at 10^{10}Hz and a loss tangent of 10^{-3} at 10^{10}Hz. Tube resonators manufactured in this material had such a low Q factor as to be useless as microwave resonant cavities. The reason for this was presumably the poor surface finish on the tube.

Attempts were made to use a confocal resonator as a sample cavity, but these attempts invariably failed. This was assumed to result from the very low filling factor which more than offset the increase in Q factor, and a considerable distortion of the resonant mode when large samples were used. This type of resonator, however, proved to be an excellent reference cavity for the automatic frequency control system.

6.9 Fabrication of Millimeter Wave Components

In addition to cavities several other millimeter components need to be fabricated either because they are not commercially available or to exercise economies. The most useful components include waveguide tapers, bends in oversize waveguide, detector whiskers and crystals.

Tapers to launch 4 and 2mm power into oversized waveguide were fabricated by electroforming on a stainless steel mandrel. The mandrels were ground from S80 stainless steel to the internal shape of the taper and the surfaces polished. Copper was then electrodeposited on the mandrels from an acid copper bath, consisting of 200 grams copper sulphate, 12g potash alum, 56 grams sulphuric acid dissolved in distilled water. The mandrel was rotated slowly during the whole electroforming process and the current reversed for 10 seconds every 30 seconds to ensure an even deposition. The first layer of copper was deposited slowly with a current of a few milliampères and the current gradually increased to several ampères per square foot of mandrel surface. The mandrels were extracted from the finished article after the outer surface had been machined and the flanges fitted, by heating the taper and mandrel in hot

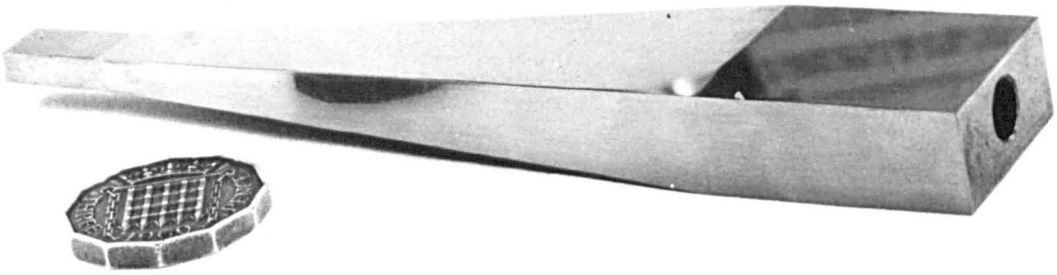

Fig 6.11 STAINLESS STEEL TAPER MANDREL

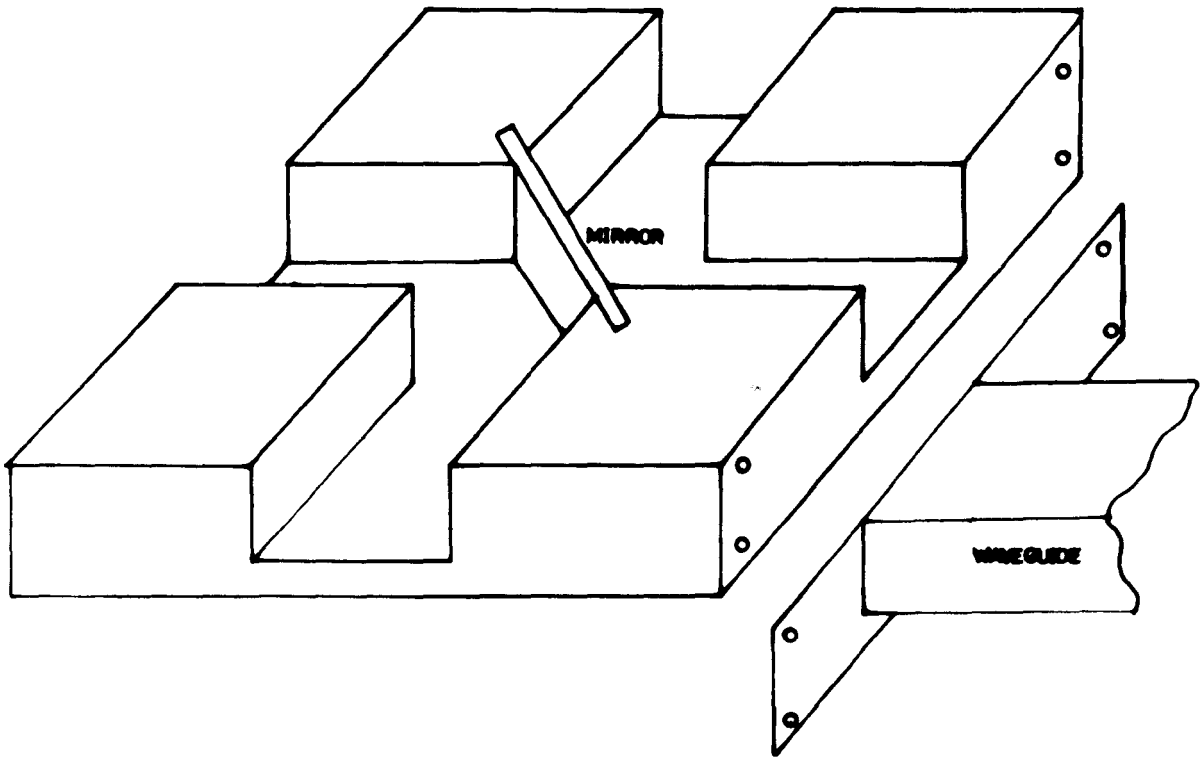

Fig 6 12 BEND IN OVERSIZED WAVEGUIDE
(Top plate omitted)

oil. Tapers manufactured in this way were found to have a very low insertion loss indeed and only minute amounts of power were reflected from them. A photograph of a typical mandrel is shown in Figure 6.11.

A bend in oversize waveguide was constructed using a polished brass plate as a reflector. Two rectangular grooves at right angles to one another were machined in a solid brass block with dimensions equal to the internal dimensions of the oversized guide and a mirror was placed across the junction. A brass plate was placed over the grooves and flanges attached to the ends. A diagram showing a bend in a band guide for use at 2mm wavelengths is shown in Figure 6.12. A directional coupler can be manufactured by replacing the mirror with a piece of dielectric.

Whiskers for use in the harmonic generator and 2mm detector are made by spot welding a piece of .001mm diameter tungsten wire onto the old whisker mount and etching the point in caustic soda as described by Torrey and Whitmer (1948). Replacement silicon crystals were obtained by using chippings from X and K band crystals and resoldering them onto the old crystal mount. One side of the chip was first coated with nickel in an evaporating chamber and the chip was then soft soldered to the mount. The rectifying surface was finally etched in hydro-fluoric acid. Replacement crystals and whiskers made in this manner proved to be just as satisfactory as those purchased from the manufacturer of the detector and harmonic generator.

6.10 Magnet Systems

The spectrometer can be used with either of two magnets, depending on the experiments being carried out. For low field work at temperatures down to 20°K, a Newport 8" electromagnet was used. This magnet has a face diameter of 3cms and a gap of 7.8cms. It is driven by a Newport motor generator power supply and the maximum field available is approximately 2 Teslas (20KGauss). The coned pole pieces are shimmed to improve the field homogeneity and adjustment screws are fitted in the yoke of the magnet to facilitate accurate alignment of the pole faces. Since this magnet was more frequently used with a Q-band spectrometer the shims and pole alignment were adjusted to give optimum homogeneity at 1.2 Teslas (12KGauss). The homogeneity at this field was in the region of 1 part in 10^5 over a cubic centimeter. At higher or lower fields the homogeneity deteriorated. The stability of the field as determined by the power supply was nominally 1 part in 10^5 over periods of up to one hour.

For work at high fields and liquid helium temperatures a superconducting magnet was used. This superconducting magnet was designed and manufactured by the Oxford Instrument Company to specifications required for the project. Ideally one requires a magnet homogeneity at least an order of magnitude better than the narrowest spectral line likely to be studied. If one assumes that at 2mm wavelengths electron spin resonance lines are still to be found as narrow as 10^{-5} Teslas (100mG), then one would require a field homogeneity of the order of 1 part in 10^6

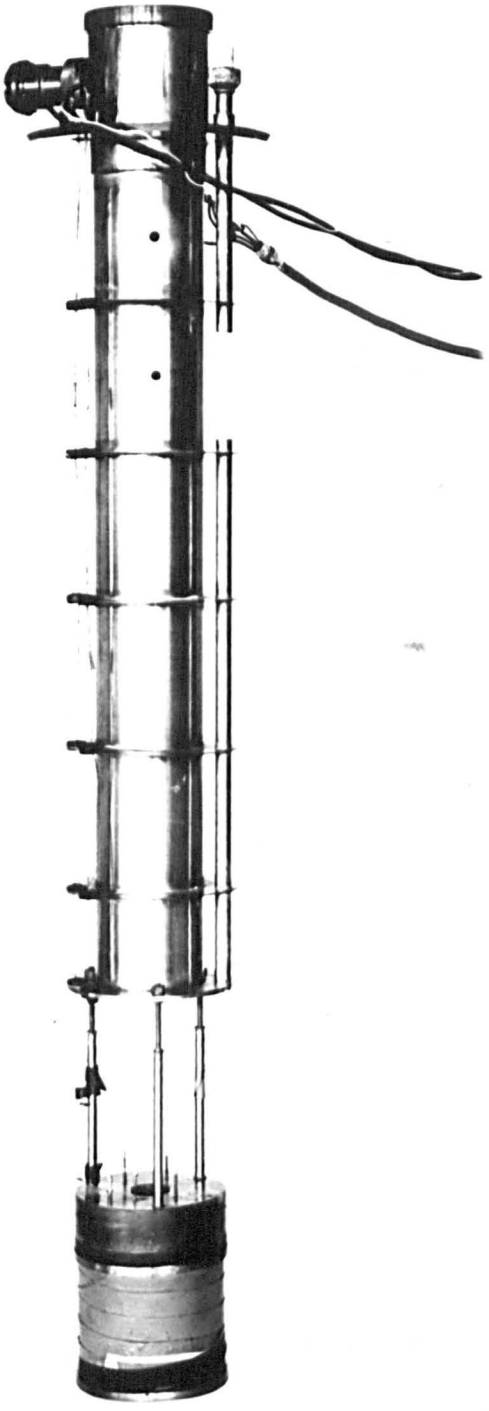

Fig 6.13 SUPERCONDUCTING MAGNET AND SUPPORT.

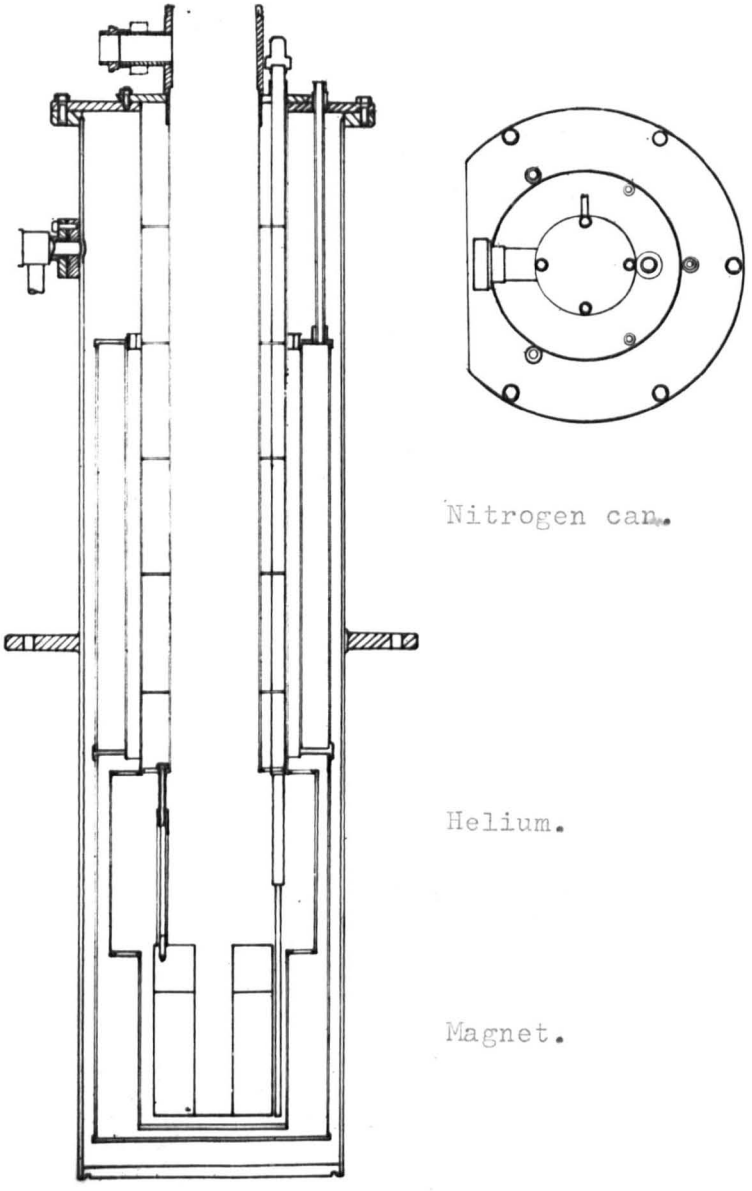

Fig. 6.I4 SUPERCONDUCTING MAGNET AND CRYOSTAT.

over the sample volume. Such a magnet would have been beyond the scope of the manufacturers at the time when the magnet was ordered, and too expensive to be considered. In addition such homogeneity could only be obtained with a superconducting solenoid by using many compensating coils which would have to be adjusted for each field value. In general it is more convenient in electron spin resonance experiments to sweep the magnetic field rather than the microwave frequency, and so the use of compensating coils was a little impracticable. A compromise was obtained by specifying a homogeneity of at least 1 part in 10^4 over a cylinder of length 5mm and diameter 4mm. The homogeneity would obviously be better than this over the smaller sample volumes likely to be used. In addition it should be noted that very narrow lines only occur in rare circumstances such as F-centre resonances in ionic solids and the line widths found in myoglobin are of the order of several tenths of Teslas at Q-band and increase with frequency, thus reducing the homogeneity still further. The magnet is capable of a maximum field in excess of 5 Teslas with a specified homogeneity over a 5mm cylinder of 3 parts in 10^5. A photograph of the magnet and its support system is shown in Figure 6.13 and a diagram of the magnet and its cryostat in Figure 6.14.

The magnetic field modulation is applied by a single layer coil of superconducting wire wound beneath the field windings on the magnet solenoid. This coil is capable of producing a field modulation of 5×10^{-4} Teslas peak to peak when carrying a current of 4 amps R.M.S. at 400Hz.

A thermally operated superconducting switch is placed across the magnet coil to enable the magnet to be run in the persistent mode if the need arises. This switch is operated by a 35mA current supplied by the magnet power supply.

The magnet is powered by a current stabilized power supply of nominal stability of 1 part in 10^4. The power supply also contains a device for switching off the current in the event of the magnet being driven normal. This is done by measuring the voltage across the output terminals and arranging to switch off the supply if this uses above 0.1 volts. It is this trip mechanism which prevents the magnetic field being either modulated at a large amplitude or at very high frequencies. The modulating field induces an e.m.f. in the circuit containing the magnet coil and the induced e.m.f. is detected by the trip mechanism.

The field can be swept either by a motor and variable speed gearbox attached to the controlling potentiometer or by an electronic ramp wave fed into the supply in series with the regulating reference voltage. This ramp is derived from the same sweep unit as is used to drive the sweep on the electromagnet power supply. The superconducting field must be increased at a slow rate or less than 1 amp/min. in order to avoid driving the magnet normal, and so the electronic sweep can only be used to increase the field or the flyback will trip the magnet into its normal state.

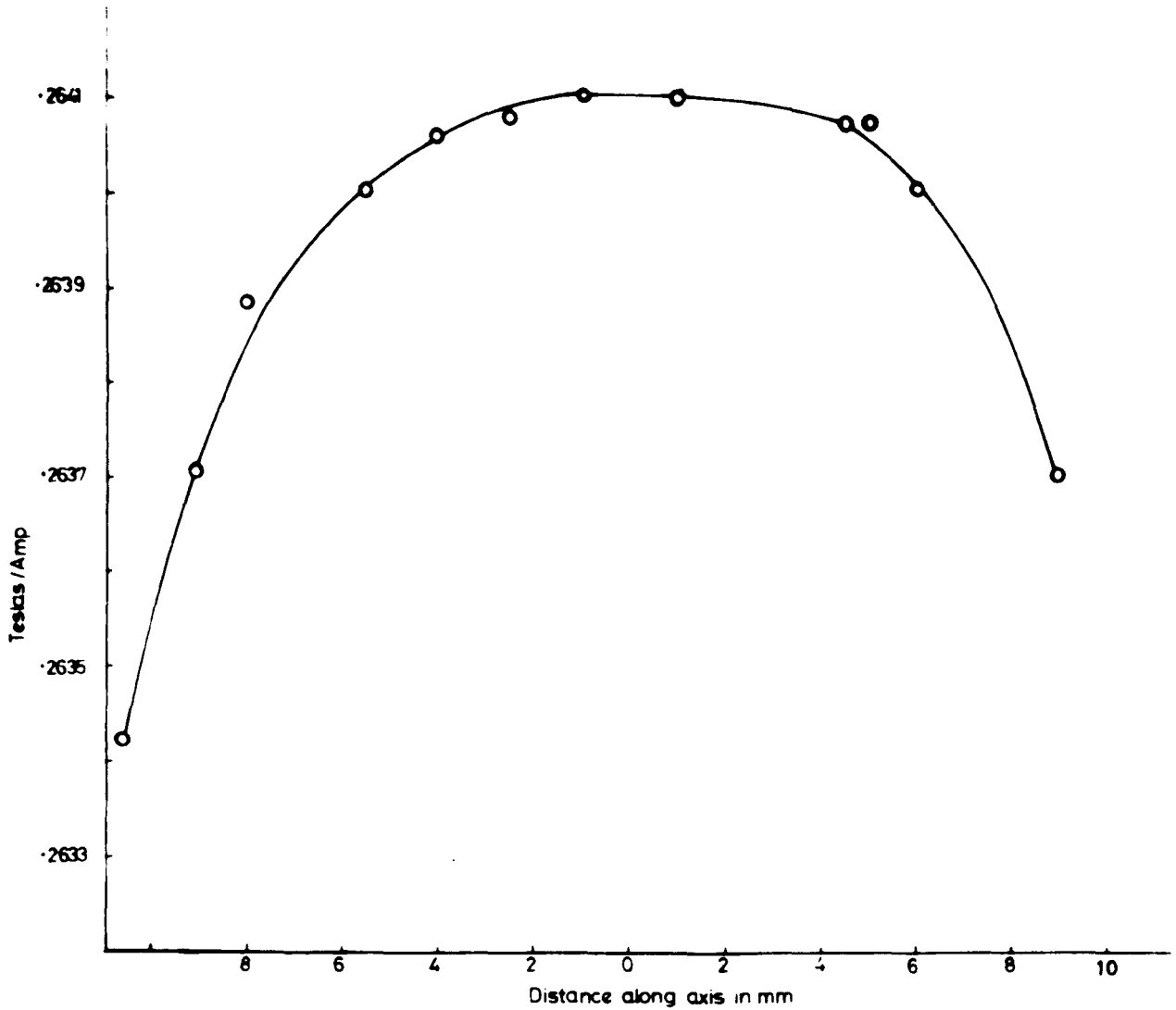

Fig 6·15 SUPERCONDUCTING MAGNET CALIBRATION

The calibration of the magnet and its homogeneity were checked using a Q-band spectrometer and a sample of phosphorous doped silicon, giving an e.s.r. signal with an accurately known g-value. A special H_{011} mode cylindrical cavity operating at 35GHz was constructed for use in the superconducting magnet using a design similar to that described for use at 4mm. Electron spin resonance signals were observed simultaneously from a sample at 4.2°K in the superconducting magnet and a sample at room temperature in the electromagnet. Two microwave bridges were used, each being fed from the same klystron using a 3db directional coupler. The klystron frequency was locked to the resonant frequency of the cavity in the helium since this would obviously be the most stable. Using the two samples it was possible to adjust the field in both magnets to the same value and measure the field in the electromagnet using a proton resonance unit (see Section 6.10). A check had previously been made to ensure that the g-value of the signal from phosphorous doped silicon did not change with temperature. Since the field is a linear function of current and exhibits no detectable hysteresis effects, a measurement of the current at one known field is sufficient to check the calibration. The homogeneity was checked in the same experiment by moving the sample vertically along the axis of the solenoid, using a piece of flexible waveguide and a sliding seal at the top of the cryostat. A plot of the magnet calibration as a function of distance along the solenoid is shown in Figure 6.15.

In the centre of the solenoid the calibration is 0.2641 ± .0001 Teslas per ampère and the homogeneity is well within specification. The calibration computed by the manufacturer is 0.2958 Teslas per ampère; a rather significant difference. The only explanationswhich can be suggested are that the computed value is in error, or that some turns on the coil were ommitted or have subsequently become short circuited. The latter explanation may be a feasible one especially when one notes that the variation in field along the axis, as shown in Figure 6.15, is not symmetrical about the centre position.

6.11 Magnetic Field Measurement

The field in the superconducting magnet is measured by making an accurate measurement of the current and assuming the linearity of the field. This is done by passing the magnet current supply through a standard resistance of 0.01 ohms. This resistor is immersed in an oil bath to maintain a constant temperature, and the temperature checked regularly during any experiment. The voltage across this standard resistance is measured with a thermocouple potentiometer. Whilst the field is being swept the recorder tracing can be marked at a fixed point as the potentiometer comes to its balance condition. The potentiometer can then be reset at another fixed point and another marker put on the recorder tracing. In this way a series of field markers can be put on the trace at intervals determined by the rate of field sweep and the skill of the operator. A further increase in accuracy is obtained by plotting a separate calibration chart for each sweep.

The field in the electromagnet is measured by observing the frequency of nuclear resonance of the protons in water. The radio frequency power for this measurement is provided by a limited transistor oscillator followed by an I.F. amplifier designed by Robinson (1965). The original circuit has been modified to include a variable capacity diode in the tank circuit, so that the frequency of oscillation can be varied remotely by varying the d.c. bias on this varactor diode. The proton resonance can be observed on an oscilloscope screen when the field is modulated at the magnetic resonance modulation frequency of 400Hz. The frequency of the proton resonance unit can thus be increased in short steps as the field is swept and marker pips put on the recording. The frequency of the proton resonance unit is measured at each step with a Hewlett Packard frequency counter.

6.12 Low Temperature Equipment

The superconducting magnet is used in conjunction with a liquid helium cryostat, also manufactured by the Oxford Instrument Company. This cryostat has a reserve helium capacity of about 3 litres and requires approximately 6 litres of liquid nitrogen to cool and fill the nitrogen jacket. The vacuum jacket of the cryostat is pumped before each experiment with an air cooled diffusion pump to a pressure of 10^{-5} torr. A $\frac{3}{8}$" internal diameter tube is attached to the magnet mount to serve as a guide for the helium transfer syphon. This tube is thin walled and is made in two separate sections to avoid heat leakage into the helium. The magnet

support is fitted with a series of copper baffles to create a long gas path from the liquid to the top of the cryostat. To further reduce the boil off of helium a good thermal contact is constructed between the inner surface of the dewar and the nitrogen jacket at a point six inches from the top of the cryostat.

The level of liquid helium in the dewar is monitored by three carbon resistors placed above the magnet. The resistance of the resistors changes from about 500 ohms when above the liquid to about 2000 ohms when immersed.

A recovery system using one inch diameter pipe is used to recover the gas evaporated from the liquid helium. The use of pipe of smaller diameter causes a build up of pressure in the cryostat in the event of the magnet being driven normal.

Liquid helium is excluded from the microwave run when a resonant cavity is used, by placing a thin metal tube, closed at one end, around the waveguide system. The open end of this tube is kept above the surface of the helium, and good thermal contact is maintained by helium gas in the waveguide. The reason for excluding the helium from the waveguide system is because the dielectric constant of liquid helium is sufficiently large to shift the resonant frequency of the cavity outside the operating range of the klystron. At Q-band or when using a shorted waveguide the helium is allowed to fill the waveguide since it is not lossy at microwave frequencies.

6.13 Spectrometer Operation and Low Temperature Techniques

To operate the 4mm spectrometer the superconducting magnet is first pre-cooled in liquid nitrogen if it is to be used. The klystron mode is displayed on the oscilloscope and the cavity tuned to resonance at the centre of the mode without a sample. The sample is mounted in the cavity and aligned and oriented if necessary using a high power stereoscopic microscope. The liquid nitrogen is blown out of the cryostat by pressurising the inside with helium gas and the waveguide flushed out with helium gas. The waveguide is then covered with the metal tube and lowered into the cryostat. The cold gas in the cryostat is used to pre-cool the waveguide. The microwave bridge is then connected to the waveguide run and the cavity mode displayed. The cavity mode is observed as the whole cryostat is cooled since reflections from the oversize waveguide tend to obscure the resonance as the system is cooled.

Helium is syphoned into the cryostat slowly until the magnet coil becomes superconducting. This normally takes 800ccs of liquid and is taken to indicate the moment when the cryostat and its contents have reached 4.2^{o}K. The helium is then syphoned in very rapidly until between 2 and 6 litres of helium have been collected.

When the system has been allowed to settle the klystron reflector modulation is removed and the klystron frequency tuned to that of the cavity. Because of the hysteresis effects observed in millimeter wave klystrons this involves a combination of mechanical and electronic tuning. When the klystron frequency has been adjusted the 60KHz signal

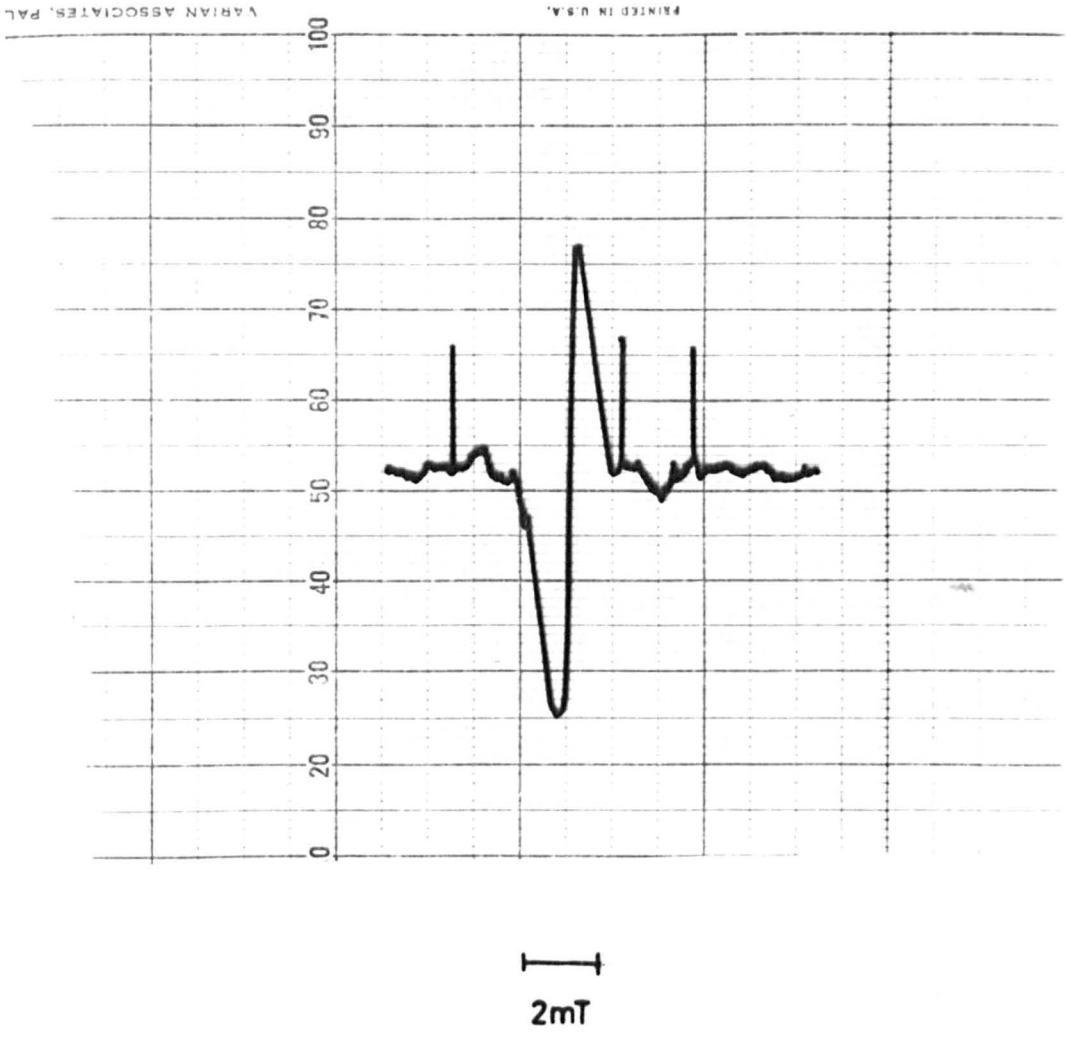

Fig 6-16 SIGNAL FROM PHOSPHOROUS DOPED SILICON
4×10^{12} SPINS

is applied to the klystron reflector and the A.F.C. loop closed. The bridge is then mismatched to bias the detector and the spectrometer operated in the usual manner.

To operate the 2mm spectrometer the klystron is adjusted to give its maximum power output and applied to the harmonic generator. The 2mm bridge is then adjusted.

6.14 Determination of Spectrometer Sensitivity

The sensitivity of the spectrometer was determined by observing the electron resonance signal at 70GHz from a small sample of phosphorous doped silicon containing a known number of free spins. The sample used contained 4×10^{12} spins and was run at $4.2^{o}K$ with a power of less than 5 milliwatts. The signal obtained is shown in Figure 6.16, from which it can be inferred that the overall minimum number of detectable free spins will be 2×10^{10} per unit linewidth for an integrating time of 1 second. The minimum number of spins which can be detected using the shorted waveguide technique is 7×10^{13}.

The figures for the sensitivity can be compared with the theoretical figures obtained from the formula given in Chapter II using a noise figure for the crystal detector supplied by the manufacturer. The filling factor for this calculation was estimated from the known volume of the sample. The minimum detectable number of spins calculated in this way for the same conditions as obtain in the experimental verification is 4.3×10^{9} per unit linewidth. The theoretical figure for the shorted waveguide sample holder is 5×10^{13} spins per unit linewidth.

The width of the signal shown in Figure 6.16 illustrates an interesting application of high frequency e.s.r. spectroscopy. At 35GHz the width is of the order of 3×10^{-4} Teslas (3 gauss) and shows only a small increase from the value obtained at X-band. However, doubling the microwave frequency to 70GHz has shown a very significant increase in linewidth to 11×10^{-4} Teslas. Such measurements should give interesting information on the nature of the line broadening mechanism.

References

Faulkner, E.A. and Harding, D.W., J.S.I. 43 97, 1966.

Van Meier, G., Zeit fur Physik 6 466, 1964.

Poole, C.P., Ph.D. Thesis, University of Maryland, 1958.

Pound, R.V., R.S.I. 17 490, 1946.

Pound, R.V., Proc. I.R.E. 35 1405, 1947.

Robinson, F.N.H., "Noise in Electrical Circuits", Oxford, 1962.

Robinson, F.N.H., J.S.I. 42 653, 1965.

Torrey, H.C. and Whitmer, C.A., "Crystal Rectifiers", McGraw Hill, 1948.

Zimmerer, R.W., R.S.I. 30 1052, 1959.

CHAPTER VII

EXPERIMENTAL RESULTS AND DISCUSSION

7.1 Introduction

The first measurements of this research programme made on myoglobin were made on pastes using the shorted waveguide technique. The interesting g-value obtained for the paste at 4mm wavelengths prompted accurate measurements of the g-value at K and Q-band frequencies. The single crystal measurements were initially carried out at fixed orientations and unexpected results prompted the construction of a cavity in which the crystal orientation could be varied. The general operation of the 4mm spectrometer has been described in Chapter VI and so in this chapter, only special precautions necessary for measurements on myoglobin pastes and single crystals will be described.

All attempts to obtain signals from either pastes or single crystals at 2mm wavelengths failed. This is undoubtedly a fault of the low sensitivity of the 2mm spectrometer, and can possibly be remedied in the future.

7.2 Measurements on Myoglobin Pastes

The paste was prepared by mixing some ammonium sulphate cake of myoglobin with a small amount of phosphate buffer solution at pH 7. The myoglobin extracted from the Sperm Whale is most conveniently stored in this salted form (Kendrew and Parrish 1956) and although it must be purified before crystallisation, the ammonium sulphate cake is adequate

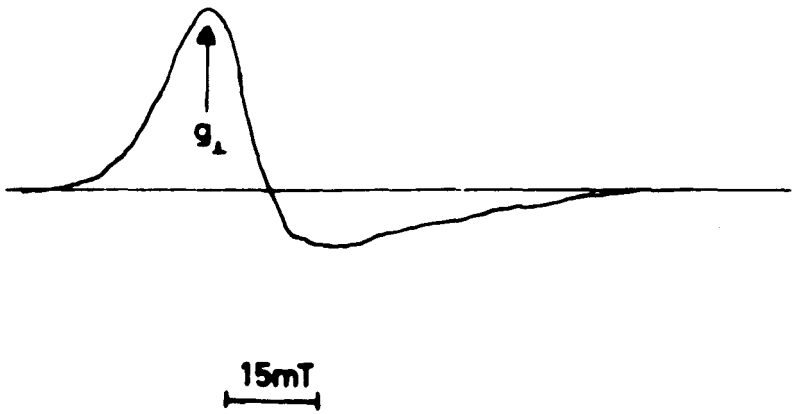

Fig 7·1 SIGNAL FROM MYOGLOBIN PASTE AT 33·6 GHz

for measurements on the pastes. Large signals are visible from the impurities but they are invariably much narrower than the myoglobin signal and occur at magnetic fields near the value for a g factor near the free spin value. On making measurements on a polycrystalline or powdered sample it must be remembered that the observed resonance signal is the envelope of all the possible resonances averaged over all the possible orientations. Sands (1955) has shown that the derivative of the absorption curve has peaks corresponding to the principal g-values. In a purely axial crystalline field this would correspond to two peaks at $g_{\parallel}$ and $g_{\perp}$. If there are three principal g-values then three peaks will occur, unless the linewidth is such as to obscure them. An account of Sands' treatment is given in Appendix 1. Figure 7.1 shows the derivative of part of the absorption curve from acid metmyoglobin paste showing where the value of $g_{\perp}$ is measured.

The g-values in the paste were measured at K, Q and 4mm frequencies. The K and Q band measurements were made on conventional electron spin resonance spectrometers using electromagnets. The 4mm measurements were made using the superconducting magnet at $4.2^{\circ}K$. The other values were made at $77^{\circ}K$. The g-values observed showed a variation in $g_{\perp}$ with frequency, but the value of $g_{\parallel}$ remained constant at 2.00. The measured values are given in Table 7.1.

TABLE 7.1

Band	Frequency	g -value
K	24.1 GHz	5.942 ± .008
Q	33.7 GHz	5.932 ± .002
4mm	69.5 GHz	5.860 ± .006

The larger error on the K over the Q band measurement arises because a 4 inch electromagnet was used for this measurement. In order to obtain the necessary magnetic field with a magnet gap large enough to admit a dewar, highly coned pole pieces were needed, resulting in a very inhomogeneous magnetic field. In all three cases the g-value was measured by comparing the resonance field with that for a standard sample of D.P.P.H. The magnetic fields were measured by the methods described in Chapter VI, and when an electromagnet was used the field values were corrected for inhomogeneities in the magnetic field.

No peaks due to anisotropy in $g_\perp$ were observed. This is probably due to the fact that the line is sufficiently broad to obscure the expected anisotropy. From an estimate of the width of the observed line a limit on the anisotropy in $g_\perp$ can be set. One would expect to detect a variation in the value of $g_\perp$ if its maximum value was greater than 5.96 and its minimum less than 5.85 at Q band. The value measured is a mean value for $g_\perp$ (i.e. the average value of g_x and g_y) and the implication of these values will be discussed further, later in this chapter.

7.3 Measurements on Myoglobin Single Crystals

7.3.1 Preparation of myoglobin single crystals

Sperm Whale myoglobin is now available commercially in a salt free, freeze dried form. With one or two exceptions, it was not found possible to grow single crystals from this freeze dried protein, and in no cases were large crystals prepared. This is probably due to the freeze drying process damaging the protein or removing some essential water from it. Consequently, samples of myoglobin were obtained from the manufacturer after the extraction process but before freeze drying. These samples were in the form of an ammonium sulphate cake, as described by Kendrew and Parrish (1956).

Crystals were grown from this cake using the method outlined in Chapter IV. Approximately 1 gram of myoglobin cake was dissolved in 2ml of distilled, de-ionised water. Ordinary distilled water was found to contain considerable amounts of paramagnetic impurities, and ordinary de-ionised water still contains biological contaminants which caused a growth of fungus on the protein solutions. The solution of myoglobin was enclosed in a small amount of dialysis tube, and dialysed against distilled de-ionised water until salt free. This process was carried out at about $4^{o}C$ and took about three days, the salt content being checked by measuring the conductivity of the water. The dialysis considerably dilutes the protein solution but this does not appear to affect the crystallisation. After dialysis the solution was added to clean 5ml specimen jars, and small amounts of a 2M solution of ammonium sulphate were added until the

protein solution appeared very slightly turbid. The ammonium sulphate was purified by re-crystallisation several times to remove traces of impurities. The pH of each specimen jar was adjusted to between 6.4 and 6.6 by addition of ammonium sulphate or phosphate buffer solution made from equal pastes of sodium di-hydrogen orthophosphate (NaH_2PO_4) and di-potassium hydrogen orthophosphate (K_2HPO_4) dissolved in purified water. Crystallisation took place after 3 days at 20°C. The pH values at which crystallisation was carried out were determined experimentally and proved to be the values at which the largest crystals were formed. Large crystals usually take several weeks to grow. The need for the extra precautions with regard to the purity of the water and ammonium sulphate was due to the high sensitivity of the 4mm spectrometer. Large signals observed from the impurities in the ammonium sulphate solutions were often sufficient to saturate the electronic detection system and occasionally upset the automatic frequency control circuit. The precautions mentioned above were usually sufficient to eliminate all traces of impurities.

7.3.2 g-value measurements at 70GHz

The g-values were measured as a function of orientation about each of the three crystal axes. No accurate frequency measuring equipment for use at 70GHz was available and so g-values were measured by comparison of resonance fields with a standard sample of D.P.P.H. This made the use of the superconducting magnet essential and so angular variations from any one run were limited to about 65°.

Unfortunately this meant that the g-values along any pair of axes could not be measured on the same run.

The crystals were mounted in the cavity visually using a high power stereoscopic microscope. Using the cross wires in the eyepiece it was possible to orientate the crystals visually to within a few degrees. The crystals were held in position with a small amount of silicon grease, but there was no absolute guarantee that the orientation remained constant whilst the crystal and apparatus were cooled to 4.2°K. Fortunately the electron resonance spectrum gives a check on the orientation in certain circumstances. At any random orientation one observes two resonance lines with different g-values, one from each of the molecules in the unit cell. With the magnetic field parallel to a crystal axis, the two molecules in the unit cell are equivalent and the signals occur at the same g-value. This gives an unambiguous check on the orientation with respect to the b axis but unfortunately the two molecules in the unit cell are also equivalent when the magnetic field is anywhere in the ac* plane. It is thus possible to measure the g-value accurately along the b axis but not along the a and c* axis.

The g-values were measured by rotating about each of the axes in turn, and in the case of the a and c* axes the mean of several sweeps with different crystals was taken on the assumption that any misorientation would be averaged out. Several measurements were also made about the b axis to determine the most symmetrical one with respect to the g-value variation for the signals from the two molecules of the unit cell.

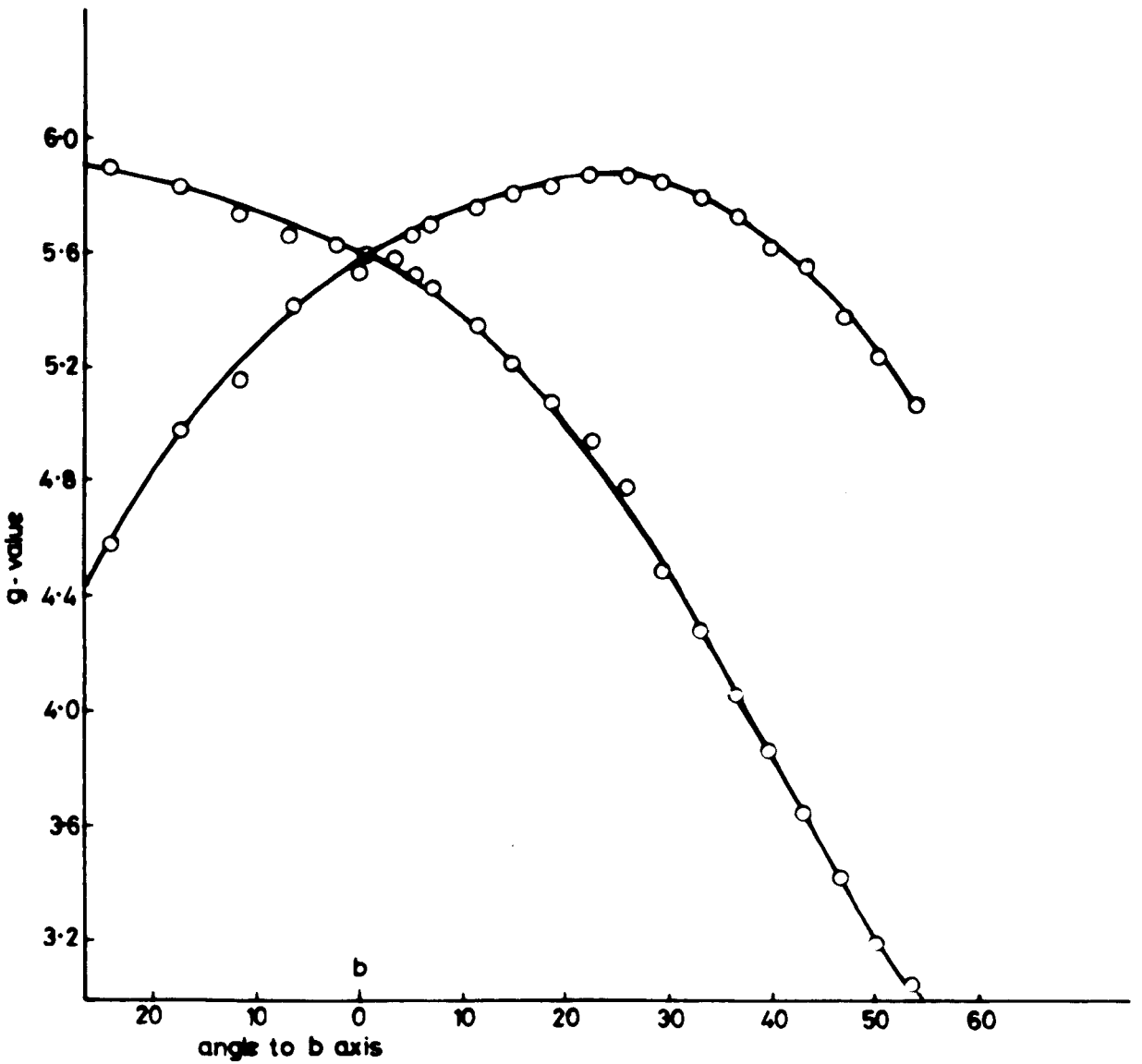

Fig 7·2 g-Value variation about the b axis in the ab plane

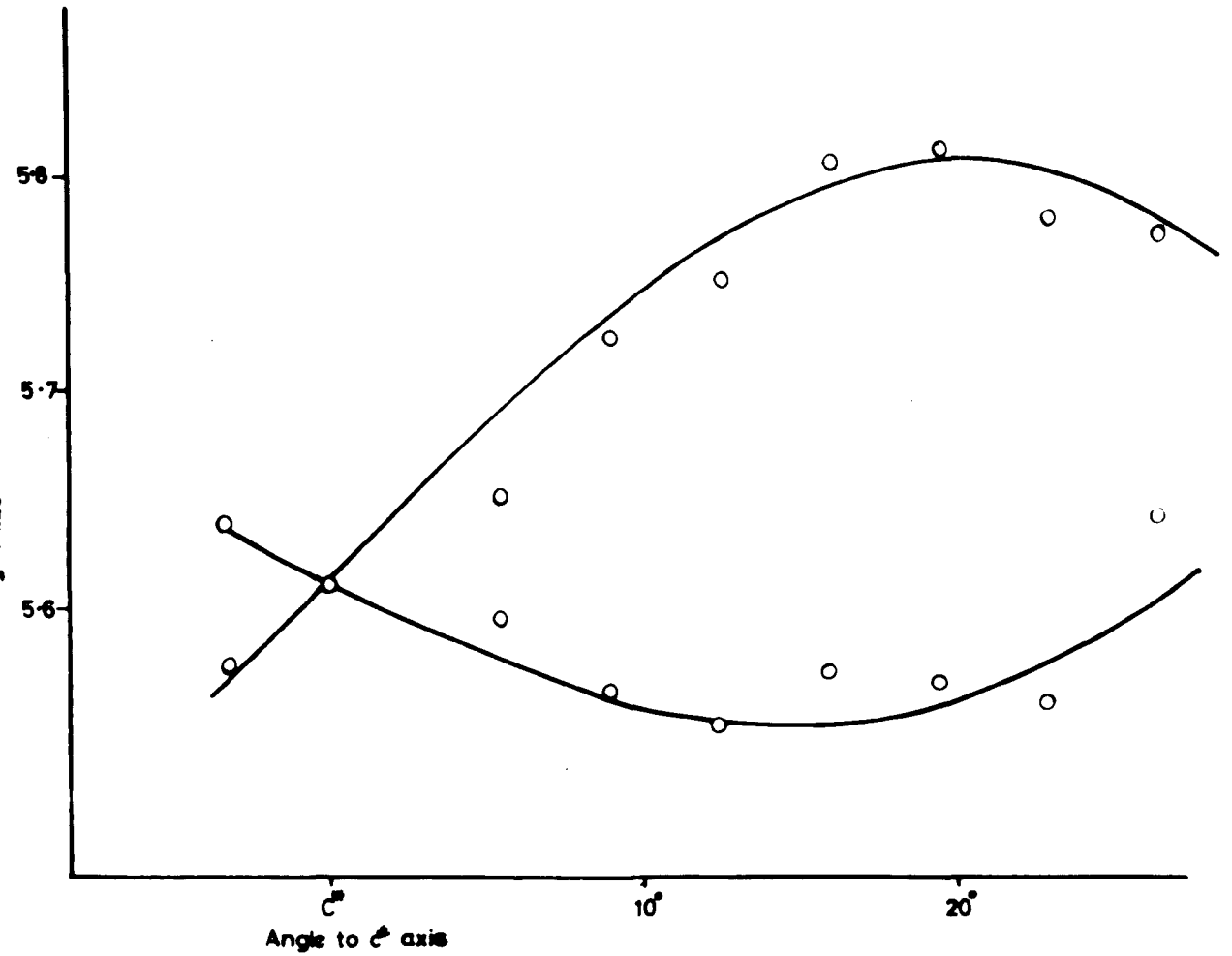

Fig 7·3 g-VALUE VARIATION ABOUT THE C^* AXIS IN THE bc^* PLANE

Using the best rotation about the b and c* axes it was possible to determine the maximum g-value in two crystal planes at fairly accurately known positions. The g-value variations in these two planes are shown in Figures 7.2 amd 7.3, and the g-values along the three axes are given in Table 7.2.

TABLE 7.2

axis	g-value
a	3.11 ± .03
b	5.525 ± .002
c*	5.61 ± .02

The magnetic fields were measured by the method described in Chapter VI using many field markers to each sweep. To overcome any random error in the marking of the chart, a graph of calibration points against distance along the chart paper was plotted for each separate spectrum. The field values at the centre of the derivative of the absorption curve could then be obtained by measuring the distance along the chart paper and reading off the field value from the calibration graph. When used with the electro-magnet this method overcomes the non-linearity due to saturation.

The principal source of error in all these measurements is in orientation of the crystal within the cavity. Since the b axis is uniquely defined, the g-value in this direction is known most accurately

The errors in the g-values along the a and c* axes are taken from the scatter on the values from many runs on different crystals, neglecting any which were so assymetrical as to obviously indicate a large movement of the crystal. In all cases the error in measuring the magnetic field was negligible, but an error is introduced due to the broad lines, especially the line observed along the a axis. However, the maximum error from this source is still well within the error introduced by misorientation. The variation of linewidth with orientation will be discussed in the next section.

The normal method of computing the principal g-values is to measure the directions and values of the minimum and maximum g-values in each crystal plane and to use the method of Schonland (1959). It is not possible to compute the directions of the principal g-values or their orientations by using simply the information available from the g-values along the three axes. However, if use is made of the previous electron spin resonance and X-ray measurements some idea of the directions and values of the principal g-values can be obtained. If we assume that the z axis lies along the haem normal and the g-value in this direction, g_z, is 2.00, then it is possible to calculate the directions and magnitudes of the other principal g-values using equation 3.3, and standard methods of co-ordinate geometry. This assumption is justified by the very good agreement between previous electron resonance studies and X-ray measurements and by the value of 2.00 obtained for g_z from the pastes. From equation 3.3 it can be seen that the g-values in the

haem plane will fit the equation

$$g_x^2\cos^2\phi + g_y^2\sin^2\phi = g_{90,\phi}^2 \qquad 7.2$$

where $g_{\theta,\phi}$ is a g-value in the direction defined by θ and ϕ in a set of cylindrical axes, whose axis is the haem normal. In any plane containing the haem normal the value of $g_{\theta,\phi}$ will be given by

$$g_z^2\cos^2\theta + g_{90,\phi}^2\sin^2\theta = g_{\theta,\phi}^2 \qquad 7.3$$

Hence, from a knowledge of the g-value at any angle to the haem normal (i.e. along the three axes) it is possible to calculate the g-value in the haem plane ($g_{90,\phi}$). Each of the values along the axes will give a value of $g_{90,\phi}$, and the direction to which this corresponds can be easily calculated. It is thus possible to eliminate all the unknowns in equation 7.2 and calculate the values of g_x and g_y and their directions. Two more g-values in the haem plane, corresponding to the maximum values in the ab and bc* planes can be used to check these figures, but due to orientation problems these are less reliable.

Using this method the principal g-values and their directions were calculated from the available experimental data, and are given in Table 7.3.

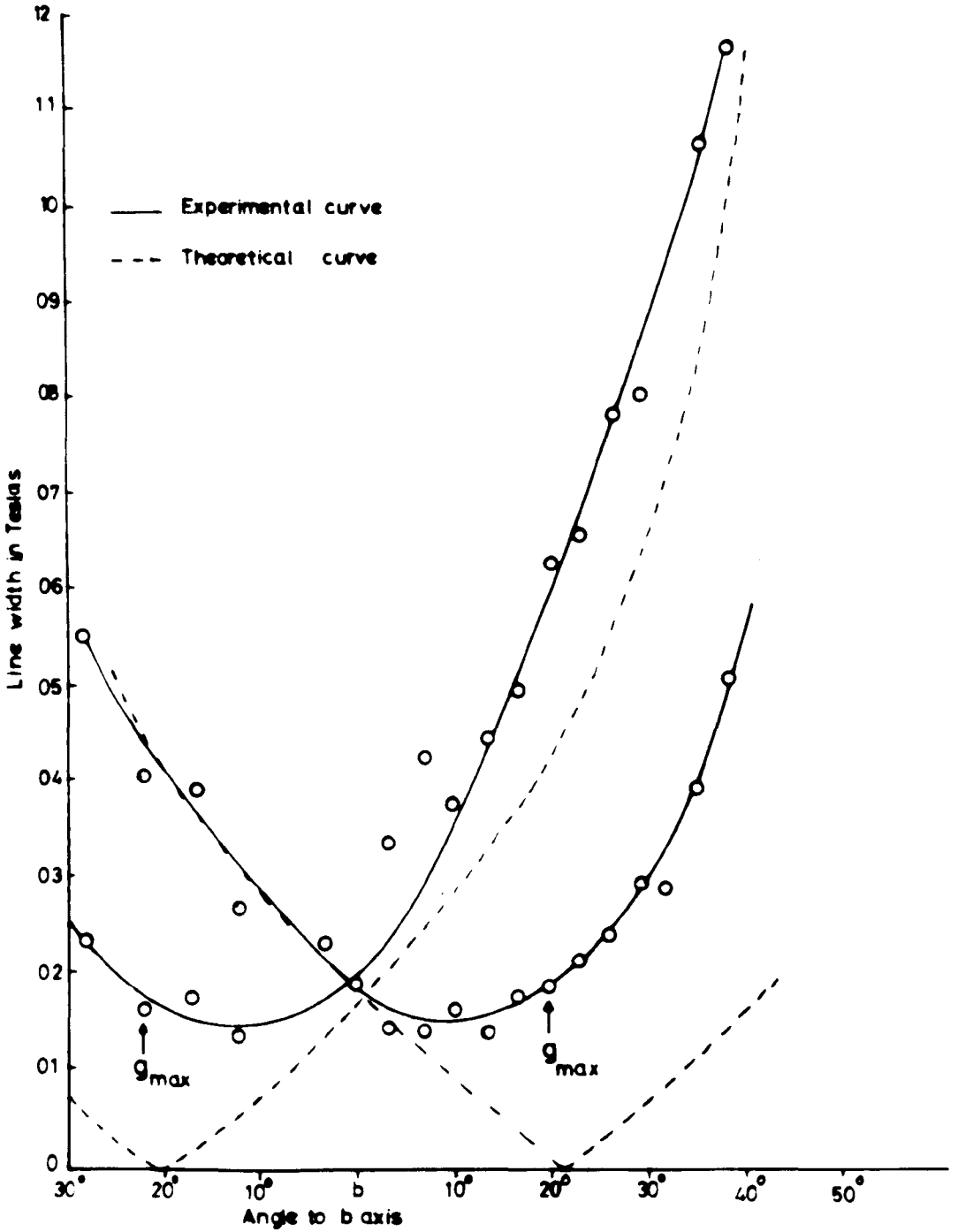

Fig 7·4 LINE WIDTH VARIATION IN THE ab PLANE

TABLE 7.3

		α	β	γ
g_z	2.00	27°	111°	73°
g_x	5.84	101°	75°	20°
g_y	5.93	66°	26°	99°

where α, β and γ are the angles with the ab and c* axes respectively.

Unfortunately the errors in these values will be large (~ 4%) because of the large errors in the g-values along the a and c* axes. The values calculated using the other two values of $g_{90,\phi}$ agree well with these figures indicating that the error is probably much less.

7.3.3 Measurements of line widths

The variation of the electron spin resonance linewidth as a function of orientation in the ab plane was determined from the best run in this plane. The linewidths were measured between the turning points on the derivative of the absorption curve using the magnetic field markers, and a calibration graph as described for the g-value measurements. The variation of linewidth as a function of orientation about the b axis is shown in Figure 7.4. The linewidths in the bc* plane show remarkable variation with orientation, but do not appear to fit any definite pattern whatsoever.

7.4 Theoretical Interpretation and Discussion

7.4.1 g-values

The effective g-values determined by these measurements can be fitted to a Spin Hamiltonian of the form described in Chapter III, vis:-

$$= D(S_z^2 - \tfrac{1}{3}S(S+1)) + g_x\beta H_x + g_y\beta H_y + g_z\beta H_z + E(S_x^2 - S_y^2)$$

The energy matrix from this Hamiltonian can be diagonalised numerically on a computer or by approximation methods. The computer diagonalisation is much more satisfactory and has been used in most of this work. If one neglects the term in $E(S_x^2 - S_y^2)$, which introduces the rhombic distortion, and assumes an axial symmetry the equation derived by perturbation theory in Chapter III (equation 3.5) can be used to determine approximate values for $g_\perp$ and D, using the results at any two frequencies. The values of D and $g_\perp$ are given by

$$g_\perp = \frac{g_\perp^{eff}(1)}{3} \cdot \frac{1}{\alpha}\left(\frac{\alpha - \delta}{1 - \delta}\right)$$

$$|2D| = g_\perp\beta\left[\frac{2(H_2^2 - H_1^2)}{1 - \alpha}\right]^{\frac{1}{2}}$$

$$\text{where } \alpha = \frac{g_\perp^{eff}(1)}{g_\perp^{eff}(2)} \quad \text{and} \quad \delta = \left(\frac{H_1}{H_2}\right)^2$$

and the figures (1) and (2) refer to the frequencies at which the measurements were taken. Using these equations and the data from the pastes one obtains:

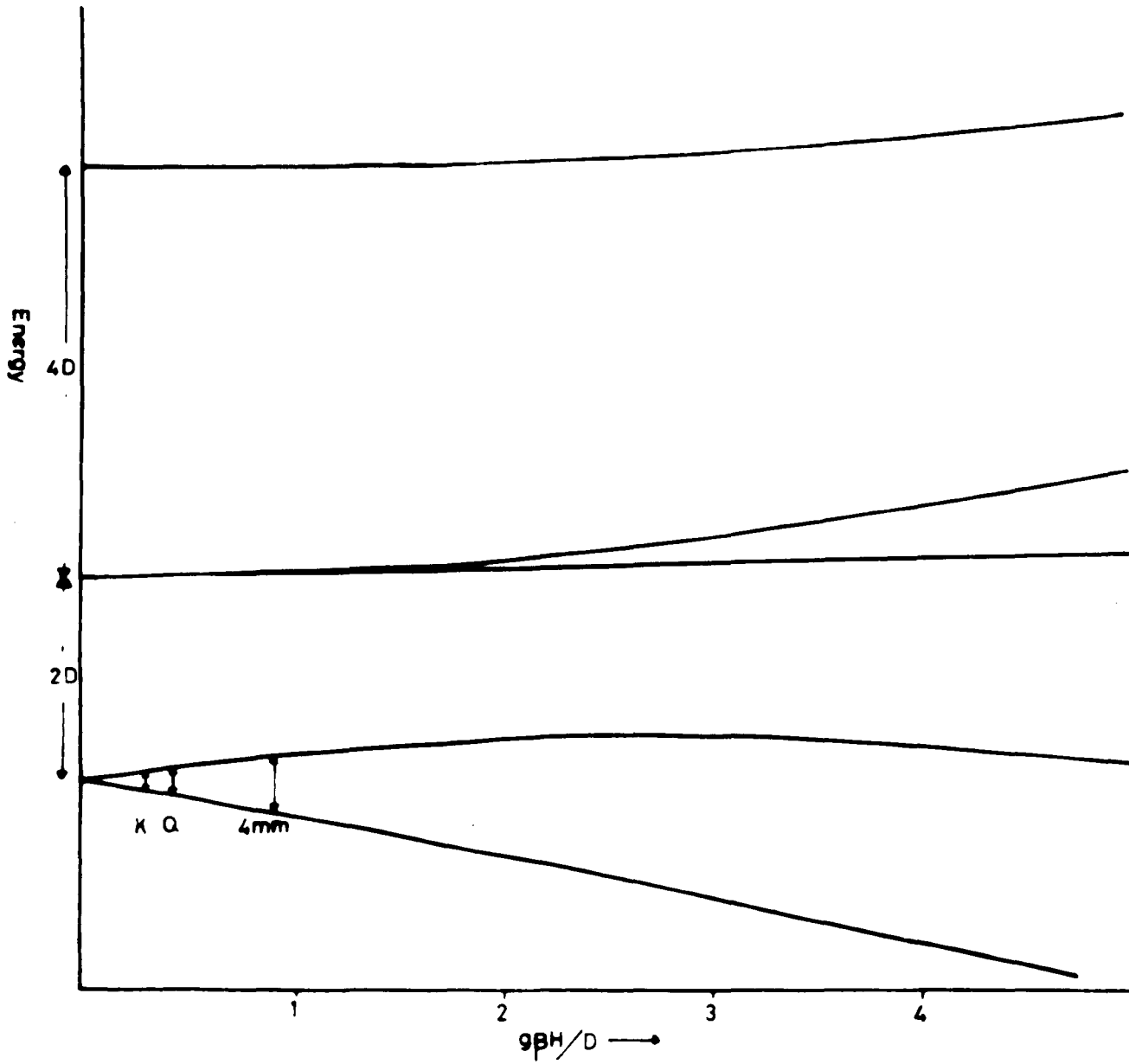

Fig 7·5 ENERGY LEVEL DIAGRAM FOR Fe^{3+} IN AN AXIAL CRYSTAL FIELD H⊥Z

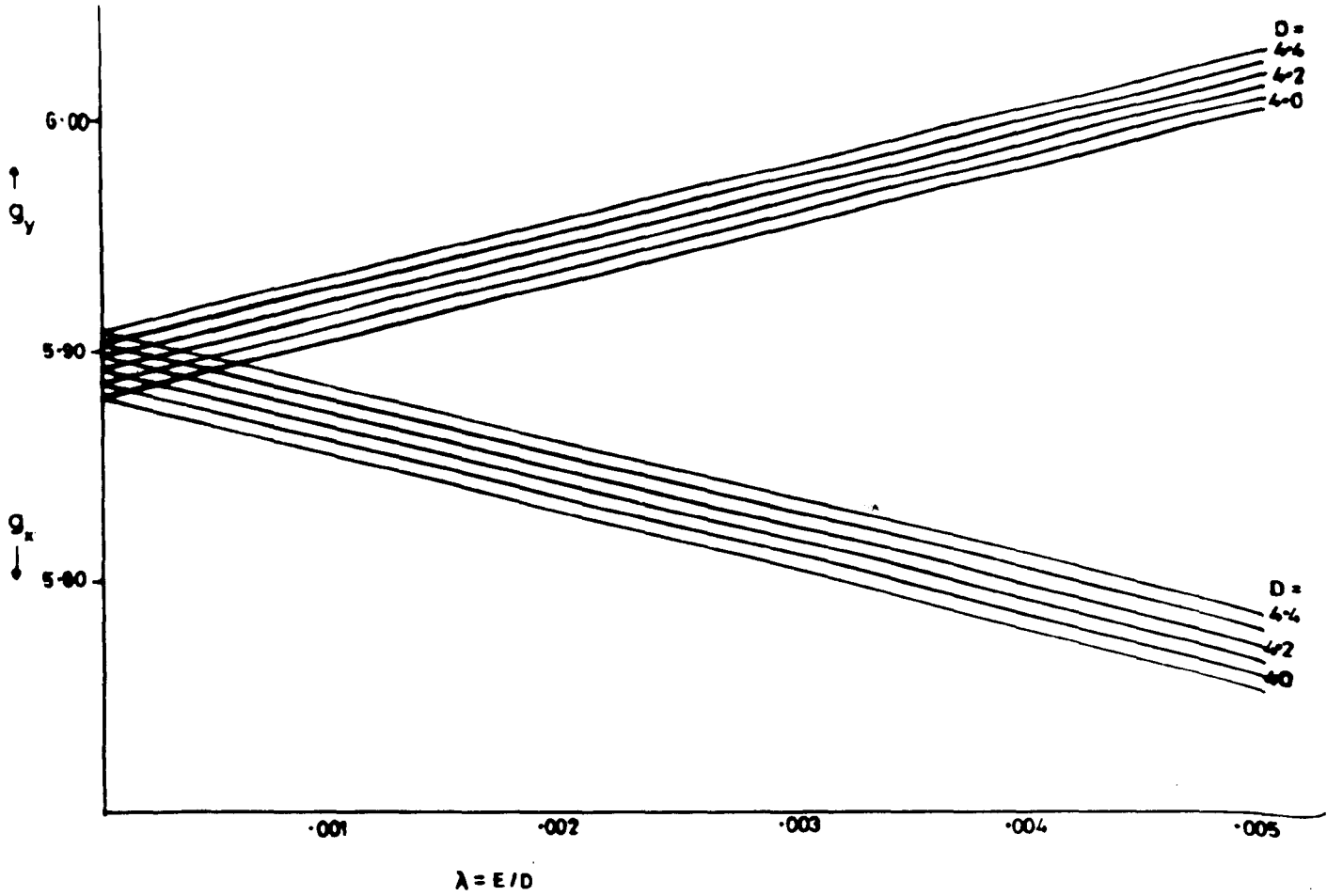

Fig 7·6 g_x & g_y AS A FUNCTION OF E/D

$$g_{\perp} = 1.99 \pm .01$$

$$|2D| = 8.4 \pm .6 cm^{-1}$$

The large error in D arises because of the very small change of $g_{\perp}^{eff}$ with frequency.

The energy level diagram for the purely axial symmetry is shown in Figure 7.5 as a function of magnetic field for the field perpendicular to the axis of symmetry. The transitions observed are indicated by the arrows.

The value of $g_{\perp}^{eff}$ measured in the paste is a true mean of the values g_x^{eff} and g_y^{eff} obtained when the rhombic term is included, provided the value of E is small. The eigenvalues of the rhombic Hamiltonian are best expressed in terms of D and $\lambda = E/D$. This Hamiltonian was diagonalised on a computer for a range of values of D about that obtained for the paste and for a range of values of λ. The variation of g_x^{eff} and g_y^{eff} as a function of λ and D is shown in Figure 7.6. From Figure 7.6 one can see that g_x and g_y increase and decrease linearly with λ at the same rate and that the difference between g_x and g_y is very sensitive to small changes in λ. The g-values can also be seen to be insensitive to changes in D. This situation only holds for very small values of λ, and does not hold when E becomes of the same order as D.

The values of g_x and g_y obtained in the single crystals can be used, with the aid of Figure 7.6 to determine values of D and E, and the approximate values obtained this way are given below.

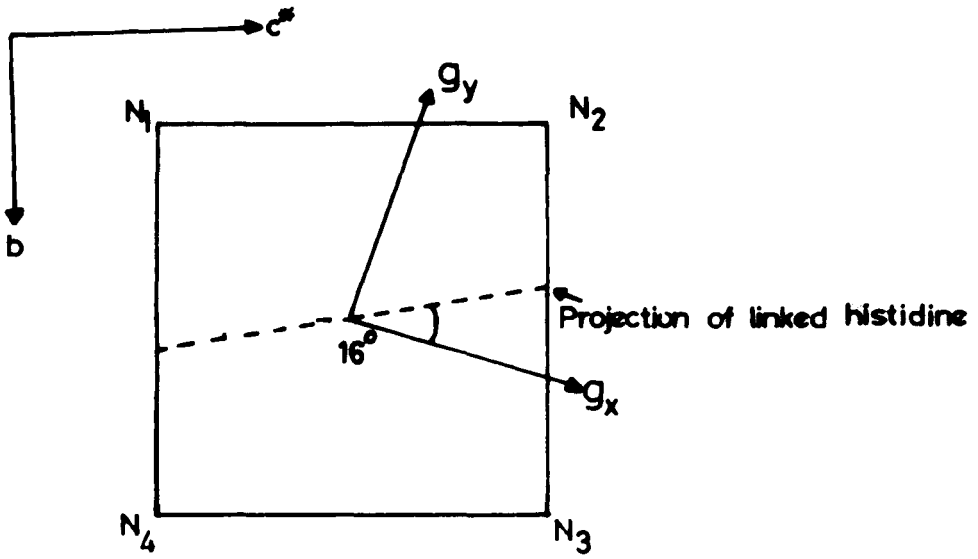

Fig 7·7 THE DIRECTION OF g_x, g_y IN THE HAEM PLANE

$$D = 3.9 \pm .8 cm^{-1}$$

and $$E = .002 \pm .0005 cm^{-1}$$

There is obviously some discrepancy here in the values of D obtained from paste and single crystals. It may be accounted for in an incorrect value of $g_{\perp}$ used in the computation of the data for Figure 7.5, or more likely the very large errors obtained in deriving the values of g_x^{eff} and g_y^{eff} from the values along the crystal axes.

The directions of the principal g-values in the haem plane can be compared with the directions obtained for the Azide derivative, using the X-ray co-ordinates for the atoms of the haem plane. The directions are shown in Figure 7.7. In this case the direction of g_x makes an angle of 14° with the projection of the plane of the linked histidine on to the haem plane. The orientation of the linked histidine ring was originally used by Griffith to explain the g-value variation in the azide derivative (Griffith 1957), but later measurements (Helcké, Ingram and Slade 1968) have shown that this is not quite the case. The orientation of the principal g-values obtained here is within a few degrees of that obtained for the azide. No mechanism to explain the situation in the azide has yet been given. One would expect the principal g-values to be along some principal bond direction, but so far no one appears to have suggested a detailed account of the molecular orbitals in myoglobin, although treatments of the ferric ion in porphorin compounds have been given (Ohno, Tanabe and Sasaki 1962).

The surroundings of the ferric ion in myoglobin are no doubt complicated by the fact that the haem plane is enclosed within a large portion of the protein molecule. X-ray studies of another haem compound, the synthetic oxygen carrier chloro-haemin (Koenig 1965) have indicated that the iron atom is displaced out of the haem plane. If this situation occurred in myoglobin and was accompanied by very small movements of the nitrogen atoms the peculiar symmetry could possibly be explained. The occurrence of the very small rhombic term would probably need only a small distortion of the haem plane which would possibly be outside the resolution of the X-ray analysis.

7.4.2 Line widths

The linewidth variation shown in Figure 7.4 has been compared with equation 4.1, which was used to describe the linewidth variation at Q-band frequencies. A plot of equation 4.1 is shown in Figure 7.4 along with the experimental values, and it can be seen that the g-value variation provides a reasonable fit at angles removed from the haem plane. The discrepancy near the haem plane is marked, and two points are particularly noticeable. Firstly the minimum linewidth does not coincide with the maximum g-value as would be expected from the simple theory. Secondly the deviation of the minimum linewidth from zero, which was previously attributed to residual line broadening mechanisms, has increased in proportion to the increase in frequency.

A scatter in the azimuthal angle and the variation in $g_\perp$ was used to explain the linewidth variation in the azide derivative with considerable success. The same mechanism would only explain this variation if the scatter was as high as 50°, due to the very small anisotropy in $g_\perp$. Helcké observed a strange variation in linewidth in the haem plane and in order to explain these results it must be assumed that this variation is frequency dependent. If the linewidth in the haem plane obeyed an approximately sinusoidal variation which was also very dependent on frequency it might be possible to explain this peculiar occurrence of the minimum linewidth as the sum of the two effects. The mechanism for such a frequency dependent broadening and for the frequency dependence of the so called "residual broadening" remains obscure, since all the normally encountered broadening mechanisms are frequency independent with the exception of g-value variational mechanisms. As has been observed previously, there is no temperature dependence of the linewidth at Q-band or 4mm down to 4.2°K.

7.5 Summary and Conclusions

Measurements at 4mm have given values of the parameters in the Hamiltonian and the directions of the principal g-values. The 4mm measurement on the pastes has given a more accurate estimate of the zero field splitting than was previously available, and indicates where direct transitions may be observed.

In view of the values obtained for the zero field splitting it is not surprising that no transitions were obtained between separated

Kramer's doublets. It might be expected, for instance, that at certain orientations a transition would be observed between the highest level of the lowest doublet, and the lowest level of the first excited doublet. However, in the magnetic field required the population of the lowest of these two levels is reduced from its value in zero field by a factor of about 23 at $4.2^{o}K$, in accordance with the Boltzmann distribution. At $20^{o}K$, however, the factor is 1.2. In addition because of the selection rules this transition would only be allowed with a reduced transition probability at orientations removed from the principal axis. At such orientations the divergence of the higher doublets would be changing at an even greater rate with orientation than the lower ones, giving a still broader line. It is unlikely that even the very high sensitivity of the 4mm spectrometer would be able to detect a signal under these conditions. The problem might possibly be partially solved by raising the sample temperature. Apparatus to enable higher temperature measurements to be made, whilst still retaining the use of the superconducting magnet, is in the process of being assembled.

Estimates of the zero field splittings in some haem-proteins have recently been made by two quite independent methods. Lang and Marshal (1966) have used the technique of Mossbauer spectroscopy to estimate a value of $14cm^{-1}$ for the zero field splittings in Haemoglobin fluoride. The measurements also reveal a significant difference between the acid met and fluoride derivatives, which was not apparent in the early E.S.R. studies. Tasaki, Otsuka and Kotani (1967) have estimated

the values of the D parameter for acid metmyoglobin and myoglobin fluoride to be $10cm^{-1}$ and $7cm^{-1}$ respectively. This implies that the zero field splittings (2D) are $20cm^{-1}$ and $14cm^{-1}$ respectively, although it is possible that D has been taken to be numerically equal to the zero field splitting. In the former case their value agrees well with the Mossbauer measurement for the fluoride but not with the 4mm measurements for the acid met. In the latter case the acid met value is fairly close to the value reported here but the value for the fluoride is well removed from the value obtained in the Mossbauer measurements. Comparing this work with other publications by one of the authors (Kotani 1966) it would seem that the numerical value D has been taken to represent the zero field splitting. The value of the splitting derived from susceptibility measurements is then in reasonable agreement with the value derived here.

The investigations of the linewidth variation at 4mm have given some remarkable experimental results which still need to be explained, and suggest many further investigations.

The development of the 4mm spectrometer has provided a new sensitive tool to the field of electron spin resonance which has enabled some interesting effects in the myoglobin molecule to be observed, and the technique obviously lends itself to development in order to obtain further information which is not available at lower frequencies.
The experiments with various fabrication techniques and detection systems indicate that a spectrometer operating at 2mm wavelengths with similar sensitivity is a feasible proposition.

7.6 Suggestions for Further Work

There is still a certain amount of development work to be carried out on the millimeter spectrometers and particularly on the two millimeter spectrometer. The use of a Golay detector and some method of coupling power into the cell will undoubtedly enable this spectrometer to be developed into a sensitive and accurate instrument. The power could most probably be transmitted to the Golay cell by using a horn and a lens system to focus the radiation onto the Golay window. The millimeter power available for this spectrometer could be increased by using either a varactor diode as a harmonic generator or a 2mm vacuum tube generator, and the sensitivity could be improved further by using a resonant cavity if one could be fabricated.

Two developments are really necessary to the 4mm spectrometer before this investigation can proceed any further. Firstly the rotation mechanism needs to be improved to allow rotation about a much larger angle, and if possible to give two degrees of freedom to allow accurate orientation. This might become possible as the technology of superconducting magnets develops to such an extent as to allow a sufficiently homogeneous high field to be obtained from a pair of Helmholtz coils. This would permit one axis of rotation by rotating the magnetic field and another by a modification of the present method. In addition, the preliminary estimates of the zero field splitting have indicated that it will be necessary to make measurements at higher temperatures, possibly $20^{o}K$ or $77^{o}K$. The cryogenic system must therefore be developed to allow

the use of the superconducting magnet, and yet raise the temperature of the sample above that of the helium. A long metal insert dewar has recently been obtained which fits down the centre of the present cryostat. With this accessory it should be possible to raise the temperature of the sample to something in the region of 100°K or higher. With the aid of a heating coil and sensitive thermocouple it should be possible to control the temperature of the sample to within a few degrees Kelvin, and to enable the temperature dependence of the E.S.R. signals to be measured. In the absence of any direct transitions the temperature dependence of the E.S.R. signal should give another check on the zero field splittings derived from the g-value variation.

A more accurate measurement of the zero field splittings in myoglobin still needs to be made, as does a more accurate measurement of the principal g-values, in order to determine accurately the extent of the rhombic distortion. The obvious discrepancy between E.S.R., Mossbauer and susceptibility determinations of the zero field splitting still needs to be resolved, and a careful study of the whole range of high spin derivatives may clarify the stiuation.

In addition there remains the interesting but unexplained frequency dependent contribution to the linewidth. Initially, a careful measurement of the linewidth variation in the haem plane over as large a range of frequencies as possible may give some indication of the nature of this broadening mechanism.

References

Griffith, J.S., Nature, Lond. 180 30, 1957.

Kendrew, J.C. and Parrish, R.G., Proc. Roy. Soc. A238 305, 1956.

Koenig, D.F., Acta. Cryst. 18 663, 1965.

Lang, G. and Marshal, W., Proc. Phys. Soc. 87 3, 1966.

Kotani, M. and Morinoto, H., Proc. 2nd Int. Conf. on Magnetic Resonance in Biological Systems, Stockholm, 1966.

Ohono, K., Tanabe, Y. and Sasaki, F., Proc. Stockholm conference on quantum chemistry, 1962.

Sands, R.H., Phys. Rev. 99 1222, 1955.

Schonland, D.S., Proc. Phys. Soc. 73 788, 1959.

Tasaki, A., Otsuka, J. and Kotani, M., Biochim. Biophys. Acta 140 284, 1967.

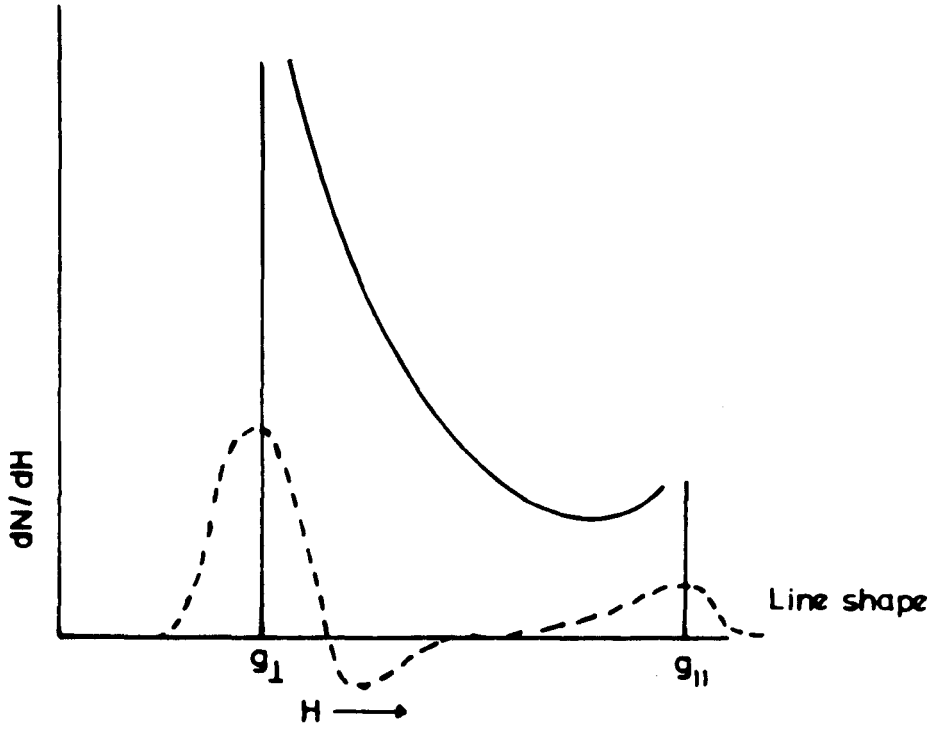

Fig A1 $g_{||}$ & $g_\perp$ in a paste

APPENDIX

Calculation of Envelope Shape for Powder Spectrum

In a myoglobin paste all orientations of the crystalline field symmetry axis in the haem plane are equally probable. One must, therefore, sum over all the orientations. The energy of each orientation transition is given by

$$(1) \qquad h\nu = g\beta H$$

The g-value can, however, be split into a parallel and a perpendicular component to the applied magnetic field. Equation (1) then may be written in the following form:

$$(2) \qquad h\nu = \beta H(g_{\parallel}^2 \, \mathrm{Cos}^2\theta + g_{\perp}^2 \mathrm{Sin}^2\theta)^{\frac{1}{2}}$$

where θ is the angle between the applied magnetic field and the axis of symmetry of the crystalline electric field. (In the axial symmetry case $g_z = g_{\parallel}$, $g_x = g_y = g_{\perp}$).

The number of spins having for their environment an electric field symmetry axis at an orientation with respect to the applied magnetic field between θ and $\theta + d\theta$ is given by:

$$(3) \qquad dN = (N_o/2)\mathrm{Sin}\theta d\theta$$

where N_o = total number of spins.

Using the trigonometric identity $\mathrm{Sin}^2\theta = 1 - \mathrm{Cos}^2\theta$ equation (2) becomes

$$(4) \quad h\nu = \beta H(g_\perp^2 + (g_{||}^2 - g_\perp^2)\mathrm{Cos}^2\theta)^{\frac{1}{2}}$$

Dividing and multiplying equation (4) by $g_\perp$ yields:

$$(5) \quad h\nu = \beta H g_\perp \left[1 + \frac{g_{||}^2 - g_\perp^2}{g_\perp^2} \mathrm{Cos}^2\theta \right]^{\frac{1}{2}}$$

Dividing both sides by $g_o\beta$ gives:

$$(6) \quad \frac{h\nu}{g_o\beta} = H_o = \frac{Hg_\perp}{g_o} \left[1 + \frac{(g_{||}^2 - g_\perp^2)}{g_\perp^2} \mathrm{Cos}^2\theta \right]^{\frac{1}{2}}$$

Substituting the following identities

$$(7) \quad \frac{(g_{||}^2 - g_\perp^2)}{g_\perp^2} = \frac{\Delta g^2}{g_\perp^2}$$

$$(8) \quad x = \mathrm{Cos}\ \theta$$

into equation (6)

$$(9) \quad H_o = \frac{Hg_\perp}{g_o}(1 + \Delta g^2/g_\perp^2\, x^2)^{\frac{1}{2}}$$

Solving equation (9) for H yields:

$$(10) \quad H = \frac{H_o g_o}{g_\perp} (1 + \Delta g^2/g_\perp^2\, x^2)^{-\frac{1}{2}}$$

Taking the derivative of x with respect to θ in equation (8) yields:

$$(12) \quad dx = -\mathrm{Sin}\theta d\theta$$

Substituting (8) into (3) gives:

$$(13) \quad dN = -N_o/2dx$$

The change in spin concentration per change in field can be written as follows:

$$(14) \quad \frac{dN}{dH} = \frac{dN}{dx}\,\frac{dx}{dH}$$

Substituting equation (13) and equation (11) into equation (14):

$$(15) \quad \frac{dN}{dH} = \frac{\frac{N_o}{2}\, g_\perp^3 (1 + \Delta g^2/g_\perp^2\, x^2)^{3/2}}{H_o g_o \Delta g^2\, x}$$

Solving equation (10) for x and placing this value into equation (15) yields:

$$(16) \quad \frac{dN}{dH} = \frac{N_o}{2}\,\frac{H_o^2 g_o^2}{H^3}\,(g_\parallel^2 - g_\perp^2)\left[(2H_o/H)^2 - g_\perp^2\right]^{-\frac{1}{2}}$$

This equation is identical to Sands' equation when g_o is given a value of 2.0. Plotting dN/dH versus H will result in a spectrum as shown in Figure A1. The inclusion of a line shape function into this calculation produces a characteristic line shape as shown in the figure.